

DTIC FILE COPY

20

CLEARED  
FOR OPEN PUBLICATION

NOV 3 1989 12

OFFICE OF NAVAL RESEARCH DIRECTORATE FOR FREEDOM OF INFORMATION  
AND SECURITY REVIEW (OASD-PA)  
DEPARTMENT OF DEFENSE

FINAL REPORT

AUGUST, 1989

CONTRACT N00014-(84K-0423)

Task No. NR (243-049)

"Diffusion and Defect Characterization Studies of  
Mercury Cadmium Telluride"

Principal Investigator: D. A. Stevenson

Department of Materials Science and Engineering  
Stanford University  
Stanford, CA 94305

Sponsored by Defense Advanced Research Projects Agency  
(DOD)

Defense Sciences Office  
DARPA Order #5019  
Issued by Office of Naval Research  
SFRCNO. N00014-84K-0423

DTIC  
ELECTE  
NOV 09 1989

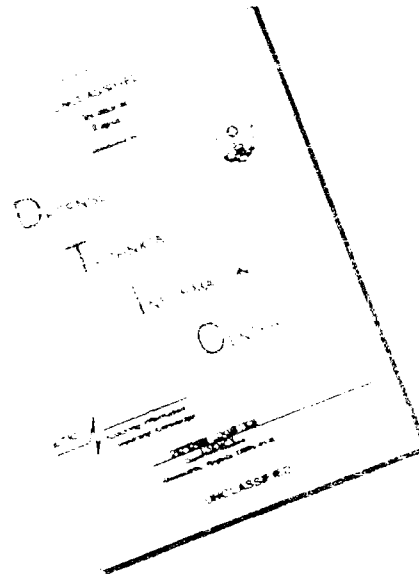
APPROVED FOR PUBLICATION  
DISTRIBUTION: U

89 11 08 009 1894681

~~89 11 27 063~~

AD-A214 655

# DISCLAIMER NOTICE



THIS DOCUMENT IS BEST  
QUALITY AVAILABLE. THE COPY  
FURNISHED TO DTIC CONTAINED  
A SIGNIFICANT NUMBER OF  
PAGES WHICH DO NOT  
REPRODUCE LEGIBLY.

## REPORT DOCUMENTATION PAGE

1a REPORT SECURITY CLASSIFICATION Unclassified			1b RESTRICTIVE MARKINGS		
2a SECURITY CLASSIFICATION AUTHORITY Unclassified			3 DISTRIBUTION/AVAILABILITY OF REPORT  Unlimited		
2b DECLASSIFICATION/DOWNGRADING SCHEDULE					
4 PERFORMING ORGANIZATION REPORT NUMBER(S)  N00014-(84K-0423)			5 MONITORING ORGANIZATION REPORT NUMBER(S)		
6a NAME OF PERFORMING ORGANIZATION  Stanford University		6b OFFICE SYMBOL (If applicable)		7a NAME OF MONITORING ORGANIZATION  Stanford University	
6c ADDRESS (City, State, and ZIP Code) Dept. of Mat. Sci. & Engr. Stanford University Stanford, CA 94305-2205			7b ADDRESS (City, State, and ZIP Code) Dept. Mat. Sci. & Engr. Stanford, CA 94305		
8a NAME OF FUNDING/SPONSORING ORGANIZATION DARPA		8b OFFICE SYMBOL (If applicable)		9. PROCUREMENT INSTRUMENT IDENTIFICATION NUMBER  N00014-(84K-0423)	
8c ADDRESS (City, State, and ZIP Code) 1400 Wilson Boulevard Arlington, Virginia 22209			10. SOURCE OF FUNDING NUMBERS		
			PROGRAM ELEMENT NO. 62301E	PROJECT NO. yd14049	TASK NO. 243-049
			WORK UNIT ACCESSION NO 01-03		
11 TITLE (Include Security Classification) Diffusion Defect Characterization Studies of Mercury Cadmium Telluride					
12 PERSONAL AUTHOR(S) Professor David A. Stevenson					
13a TYPE OF REPORT Final		13b TIME COVERED FROM 2/1/84 TO 4/30/89		14 DATE OF REPORT (Year, Month, Day) 9/18/89	
15 PAGE COUNT 128					
16 SUPPLEMENTARY NOTATION					
17 COSATI CODES			18 SUBJECT TERMS (Continue on reverse if necessary and identify by block number)		
FIELD	GROUP	SUB-GROUP			
19 ABSTRACT (Continue on reverse if necessary and identify by block number) This final report provides an overview of the major activities for our research program on the topic of diffusion and defect chemistry of mercury cadmium telluride (MCT; $Hg_{1-x}Cd_xTe$ ). In this study, we have measured tracer self-diffusion and interdiffusion coefficients in the MCT system. This provides a basis for proposed defect models for this system. A theoretical analysis based on the thermodynamics of diffusion led to new equations for interrelating the diffusion quantities in pseudobinary systems, such as MCT. This analysis is consistent with our experimental information on diffusion in MCT. Epitaxial growth studies are also discussed. The isothermal vapor phase growth method was particularly emphasized in the present study. The kinetics were investigated and a mechanism proposed, based on the kinetic studies and phase equilibria information that is available in the literature. There are also a number of other topics that are described: a novel growth method to prepared graded compositions; a new novel isothermal liquid phase growth method; an electrochemical method for measuring thermochemical quantities for the key binary compounds; and a study of the surface morphology for liquid phase epitaxial MCT. An overview					
20 DISTRIBUTION/AVAILABILITY OF ABSTRACT <input checked="" type="checkbox"/> UNCLASSIFIED/UNLIMITED <input type="checkbox"/> SAME AS RPT <input type="checkbox"/> DTIC USERS			21 ABSTRACT SECURITY CLASSIFICATION Unclassified		
22a NAME OF RESPONSIBLE INDIVIDUAL Professor D. A. Stevenson			22b TELEPHONE (Include Area Code) (415) 723-4251		22c OFFICE SYMBOL

19. Abstract continued

of these topics is given in the main body of the report and more details are provided in the Appendices.

## ABSTRACT

This final report provides an overview of the major activities for our research program on the topic of diffusion and defect chemistry of mercury cadmium telluride (MCT;  $\text{Hg}_{1-x}\text{Cd}_x\text{Te}$ ). In this study, we have measured tracer self-diffusion and interdiffusion coefficients in the MCT system. This provides a basis for proposed defect models for this system. A theoretical analysis based on the thermodynamics of diffusion led to new equations for interrelating the diffusion quantities in pseudobinary systems, such as MCT. This analysis is consistent with our experimental information on diffusion in MCT. Epitaxial growth studies are also discussed. The isothermal vapor phase growth method was particularly emphasized in the present study. The kinetics were investigated and a mechanism proposed, based on the kinetic studies and phase equilibria information that is available in the literature. There are also a number of other topics that are described: a novel growth method to prepared graded compositions; a new novel isothermal liquid phase growth method; an electrochemical methods for measuring thermochemical quantities for the key binary compounds; and a study of the surface morphology for liquid phase epitaxial MCT. An overview of these topics is given in the main body of the report and more details are provided in Appendices.

Accession For	
NTIS GRA&I	<input checked="" type="checkbox"/>
DTIC TAB	<input type="checkbox"/>
Unannounced	<input type="checkbox"/>
Justification	<i>per</i>
By	
Distribution/	
Availability Codes	
Dist	Avail and/or Special
<i>A-1</i>	

## I. INTRODUCTION AND SYNOPSIS

In this program, we have investigated several topics concerning growth and diffusion phenomena in mercury cadmium telluride ( $\text{Hg}_x\text{Cd}_{1-x}\text{Te}$ ; MCT). The growth studies have emphasized the isothermal vapor phase method (ISOVPE) of growth for MCT. We have elucidated the mechanism of growth for this process, based on thermodynamic and phase information in the literature, and have added several refinements to the growth process, including methods for controlling surface composition and surface morphology. In addition, we have developed a new isothermal liquid phase epitaxial growth method and have utilized an electrochemical method to measure the thermochemical properties of the major compounds in the MCT system.

Both tracer self-diffusion and interdiffusion measurements were made in MCT. Self-diffusion studies were made for all three components as a function of the mercury overpressure. One objective of the self-diffusion measurements was to establish the diffusion mechanism and to reveal the defect chemistry of MCT. Another objective was to relate the interdiffusion coefficients to the self-diffusion coefficients. In order to accomplish the later task, a new theoretical expression was derived that is valid for pseudobinary systems. The interdiffusion coefficients were determined by two methods: a direct junction couple between CdTe and HgTe, and an analysis of the growth kinetics in ISOVPE. In the junction couple interdiffusion experiments, Marker experiments were made to investigate the Kirkendall effect in this system.

Our work has resulted in a number of significant contributions for understanding the MCT system. These contributions have been described in detail in two Ph.D. theses (J. G. Fleming and M. F. S. Tang), four patent disclosures, fourteen publications, three manuscripts currently under review, and three manuscripts in preparation. A list of these publications is given in the bibliography.

In this final report, we provide the highlights of each of these contributions. More detail is provided in the Appendixes, which consists of copies of journal articles that are in print or presently under review.

## **II. MAJOR ACCOMPLISHMENTS**

### **A. The Mechanism of Growth for the Isothermal Vapor Phase Epitaxial Growth of MCT**

The isothermal vapor phase epitaxial growth of MCT (ISOVPE) consists of a closed ampule growth system, with a HgTe or a MCT powder source, and a CdTe substrate. The method has been studied for many years and has many attractive features; it is simple to implement, it is close to equilibrium growth, the surface morphology can be excellent, and purification can be implemented by the vapor phase transport step. Prior to our work, there was no clear description of the mechanism of growth. We have developed a model for the growth mechanism, based on our experimental studies of the kinetics of growth, as well as previous studies of growth kinetics and the studies of solid-liquid-vapor phase equilibria. The growth is a combination of transport of  $\text{Te}_2$  and Hg from the source to the CdTe substrate and interdiffusion between Hg and Cd in the growing layer. The basic driving force is a tellurium chemical potential gradient between the source and substrate, which is related to the dependence of the tellurium chemical potential on the  $x$  value (CdTe fraction in MCT). The initial growth regime obeys linear kinetics and the  $\text{Te}_2$  vapor transport is the rate limiting process. At a later stage, parabolic kinetics are obeyed, corresponding to a diffusion limited growth regime. For most of the growth schedules, the majority of the growth occurs under diffusion controlled kinetics. Further details of the growth procedure and the growth mechanism is provided in Appendix A.

### **B. Control of the Surface Composition of Isothermal Vapor Phase Epitaxial Mercury Cadmium Telluride**

In the previous studies of the ISOVPE method, the control of the surface composition was achieved by a very accurate schedule of time and temperature for the growth. We developed a method of fixing the surface composition by using a solid-liquid-vapor source in equilibrium with the desired surface composition. For sufficiently long growth times and for  $x$  values in the range of 0.2 to 0.7, good

control of the surface composition is achieved. Further details of this method are provided in Appendix B.

### **C. The Effect of Orientation on the Surface Morphology of Mercury Cadmium Telluride Grown by LPE and VPE**

There are advantages in layer morphology and uniformity of doping from terrace-free layers. We have studied the influence of substrate orientation on the surface morphology for both LPE and ISOVPE growth. Lenticular {111} CdTe substrates were formed using a simple grinding jig. MCT layers were grown using a tilting LPE method, or our ISOVPE method. By measuring the radius of curvature of the substrate and the size of the terrace free regime, one can calculate the critical misorientation for the development of terraces. This was found to be on the order of  $0.2 \pm 0.1^\circ$ . Further details of this study are given in Appendix C.

### **D. Cooling Rate Dependence of the Morphology of $\text{Hg}_{0.80}\text{Cd}_{0.20}\text{Te}$ Liquid Phase Epitaxial Layers.**

A related study of surface morphology was made, namely the influence of cooling rate on the morphology of LPE MCT layers. LPE layers were grown on CdTe substrates at  $500^\circ\text{C}$  at various cooling rates. The width of terraces was inversely proportional to the cooling rate. The result is explained by the increase in constitutional supercooling with increasing cooling rate. Further details are given in Appendix D.

### **E. Interdiffusion in Mercury Cadmium Telluride Evaluated from Vapor Phase Growth Kinetics**

As was indicated in section II. A, after an initial vapor phase transport limited regime, the growth kinetics of MCT is diffusion limited. We have developed a method of determining the interdiffusion coefficients in MCT by an analysis of the ISOVPE growth profiles. Because the interdiffusion coefficient increases substantially with decreasing  $x$  value, the interdiffusion process reaches a quasi-steady state in the concentration regime from  $x=0.1$  to  $x=0.7$ . Using a simple geometric analysis of the profiles in this composition regime, interdiffusion coefficients were obtained over the temperature range from  $450$  to  $700^\circ\text{C}$ . Our results are in good agreement with previous studies of interdiffusion. The method offers



advantages in simplicity and the ability to control the defect chemistry of MCT during measurement. Further details of this study are given in Appendix E.

#### **F. Isothermal Liquid Phase Epitaxial Growth of Mercury Cadmium Telluride**

As was mentioned in section II A, the ISOVPE method offers simplicity and also the possibility of purification during the vapor transport step. An advantage of LPE is the favorable segregation coefficient of many impurities between the liquid solvent and the growing layer. We have developed an isothermal liquid phase epitaxial growth method (ISOLPE) to take advantage of the simplicity of the isothermal process and the purification of the liquid solvent process. Epilayers were grown by a mercury or tellurium-rich solvent at 500°C. Growth is initiated by the deposition of HgTe onto the substrate. Cadmium then diffuses from the substrate to the surface, thus increasing the  $x$  value and reducing the tellurium pressure at the surface to a value below that of the source. This maintains the chemical potential gradient between source and growing layer and leads to further HgTe deposition. Interdiffusion coefficients were calculated from the growth profiles using the methods described in section II. E. Further details of the ISOLPE process are given in Appendix F.

#### **G. Vickers Hardness of MCT Epilayers Grown by Isothermal Vapor Phase Epitaxy**

The hardness of compound semiconductor alloy systems is a quantity of practical and theoretical interest. The hardness relates to the ease of plastic deformation and the ease with which dislocations are introduced during such processes as crystal growth, wafer slicing, and surface polishing. In addition, the mechanical properties are related to fundamental atomic properties by theory. To provide more information on MCT, we employed a novel variation of our ISOVPE process, in which the substrate is oriented normal to the source. With appropriate growth times, a MCT layer is grown with a graded composition along the surface of the layer. Epilayer thicknesses of 100-200  $\mu\text{m}$  were deposited with  $x$  values ranging from 0.1 to 0.7. Vickers hardness measurements were made over the composition range with hardness values varying from 33 to 75  $\text{kg/mm}^2$ . These values are in good agreement with hardness values in the literature

which were measured on individual bulk specimens. Our method is particularly effective since a single oriented layer of varying composition is measured, rather than separately prepared samples of different orientation. Further details of the hardness studies are given in Appendix G.

#### **H. The Determination of the Free Energy of Formation of Binary Tellurides Using Lithium Coulometric Titration Techniques**

A low temperature electrochemical coulometric titration technique using Li was developed and used to determine the Gibbs free energies of formation of binary telluride compounds. The approach is based on the metal/lithium/tellurium phase diagram and relies upon the rapid diffusion of Li in these systems. The Gibbs free energy of formation of  $\text{Li}_2\text{Te}$  was determined by electrochemically titrating Li into pure Te until a 2 phase  $\text{Li}_2\text{Te}/\text{Te}$  mixture was formed. With this information, the Gibbs free energies of formation of  $\text{HgTe}$ ,  $\text{CdTe}$ , and  $\text{ZnTe}$  were determined from the measured Li electrochemical potential found in appropriate metal/telluride/ $\text{Li}_2\text{Te}$  Gibbs tie triangle regions. Suitable analysis of the data gave room temperature values for the free energies of formation for  $\text{CdTe}$ ,  $\text{ZnTe}$ , and  $\text{HgTe}$  of  $-23.2 \pm 0.6$ ,  $-26.4 \pm 0.9$  and  $-6.8 \pm 1.1$  kcal, respectively, in good agreement with the literature. Further details of the determination of the free energies of formation of binary tellurides using electrochemical coulometric techniques are given in Appendix H.

#### **I. Interdiffusion Behavior in $\text{HgTe}$ - $\text{CdTe}$ Junctions**

The interdiffusion kinetics in the  $\text{HgTe}$ - $\text{CdTe}$  system relate to a number of practical processes: the homogenization of solid state recrystallized samples (a major method for preparing MCT); the conversion of MCT from p to n-type by annealing in a Hg ambient; the stability of junctions, such as LPE layers on  $\text{CdTe}$  substrates; and the stability of superlattices. Prior to our work, the interdiffusion coefficients ( $D$ ) were determined for MCT only at higher temperatures, whereas there is interest in the stability of junctions at growth temperatures for MBE and MOCVD. We have measured  $D$  from 600 to 300°C for  $\text{HgTe}$ - $\text{CdTe}$  diffusion couples. The influence of binary composition, temperature, and Hg overpressure on the diffusion coefficient was established. Significant differences were

found in the behavior of  $D$  in two temperature regimes. At higher temperatures ( $T > 450^{\circ}\text{C}$ ),  $D$  is a strong function of composition and temperature and is insensitive to the Hg overpressure. At lower temperatures ( $T < 450^{\circ}\text{C}$ ), the following trends are observed with decreasing temperature: (i) the activation energy decreases, (ii)  $D$  is less dependent on  $x$  (the mole fraction of CdTe), and (iii)  $D$  depends on Hg overpressure. Based on an analysis of our interdiffusion information, a dual mechanism is proposed for diffusion at higher temperatures ( $T > 450^{\circ}\text{C}$ ), with a vacancy mechanism and an interstitial mechanism dominating at low and high  $x$  value regions, respectively, and an interstitial mechanism predominating at lower temperatures. The proposed model is confirmed by electrical property, tracer diffusion and theoretical studies, and provides a basis for predicting the interdiffusion behavior at even lower temperatures. Further details of the interdiffusion study are given in Appendix I.

#### J. Tracer Self-Diffusion in Mercury Cadmium Telluride; Diffusion Mechanisms

The tracer self-diffusion coefficients are fundamental quantities that provide insight into diffusion mechanisms, provide information on the dominant defect chemistry of compound semiconductors, and are used to calculate the interdiffusion coefficient from fundamental diffusion theory. The diffusion coefficients for the three components in the MCT system ( $x = 0.2$ ) were studied by tracer techniques. There are two branches in the tracer diffusion profiles for each component. Tellurium diffuses much more slowly than either metal species, and the fast component of Te is related to chemical diffusion for attaining equilibrium stoichiometry and does not appear in preannealed samples. The two components for each metal both appear after preannealing and are related to the lattice diffusion. The following mechanisms were proposed for the diffusion of the three components: Te diffuses by interstitials; Hg diffuses by vacancies and interstitials proceeding in parallel; and Cd diffuses by vacancies and interstitial proceeding in series. Further details of self-diffusion and diffusion mechanisms are given in Appendix J.

## K. The Relation Between Tracer Self-Diffusion Coefficients and Interdiffusion Coefficients

We have measured both self-diffusion coefficients for all the components, and the interdiffusion coefficient as a function of composition in the MCT system. For binary systems, there is a fundamental equation, known as the Darken Equation, that relates these two quantities. We found, however, that this relationship is not obeyed in the MCT system. This is not surprising, since MCT is a pseudobinary system. We have derived a general relationship between self-diffusion coefficients and the interdiffusion coefficient by incorporating the thermodynamic constraints for a pseudobinary system. Although our motivation for deriving this relationship was to correlate diffusion quantities in the MCT system, it is completely general and may be applied to any pseudobinary system. The general equation has two important limiting forms for a compound with two atoms on one sublattice (Hg and Cd, in MCT) and one atom on the other sublattice (Te in MCT). If Te were to diffuse much faster than Cd or Hg, the general equation approaches the Darken Equation as a limit. (In this case, one could consider the diffusion species as HgTe and CdTe). For the other extreme, with Te much less mobile than Cd or Hg, the general equation approaches a Nernst-Planck type of equation. For MCT, we have concluded that the fast components in the self-diffusion profiles are true self-diffusion coefficients and they are related to the interdiffusion coefficient by a Nernst-Planck type of equation, with a thermodynamic factor calculated from available thermodynamic data. The slow components of the metal species in the tracer diffusion profile are the intrinsic diffusion coefficients and they are related to the interdiffusion coefficient by a Darken equation. The MCT system exhibits modest positive deviation from ideality, with a thermodynamic factor less than one. This indicates a positive mixing enthalpy of HgTe and CdTe and is consistent with the observed results that the intrinsic diffusion coefficient of the metal species is smaller than the self-diffusion coefficients. Further details of our analysis of the thermodynamics of diffusion and the relationship between self-diffusion and interdiffusion coefficients in MCT are given in Appendix K.

## III. SUMMARY AND ACKNOWLEDGMENT

During the course of this research program, we have made substantial contributions to the understanding of the growth and defect structure of MCT. Our contributions have both fundamental

and practical implications to the future of this important compound semiconductor. We are grateful for the generous sponsorship of this program. We are also grateful for the interaction we had with many researchers in this field. It is impossible to make a detailed description of this interaction, but we particularly wish to express our appreciation for the strong and helpful interaction with the following people: Drs. Margaret Brown (Grumman Space Systems, formerly with Rockwell International), Arden Sher and Marcy Berding (SRI International), Ken Zanio and Robert Kay (Ford Aerospace and Communications Corporation), John Tregilgas, Herb Schaake, Luigi Colombo, and Carlos Castro (Texas Instruments), Mitra Sen and Tse Tung (SBRC), Richard Reynolds and Jim Murphy (DARPA), and Hermann Schmalzried (University of Hanover)

#### IV. PAPERS PUBLISHED AND SUBMITTED FOR PUBLICATION

1. "Interdiffusion in  $\text{Hg}_{1-x}\text{Cd}_x\text{Te}$ , Evaluated from Vapor Phase Growth Kinetics", Phys. Stat. Sol. (a) 105, 77 (1987) (J. Fleming and D. A. Stevenson).
2. "Isothermal Vapor Phase Epitaxy of Mercury Cadmium Telluride", J. of Crystal Growth, 82 621-627 (1987) (J. G. Fleming and D. A. Stevenson).
3. "Isothermal Liquid Phase Epitaxial Growth of Mercury Cadmium Telluride", J. Electrochem. Soc., Vol. 134 No. 5, 1225-1227, (1987), (J. G. Fleming and D. A. Stevenson).
4. "The Effect of Orientation on the Surface Morphology of Mercury Cadmium Telluride Grown by LPE and VPE", (J. G. Fleming and D. A. Stevenson). Submitted to J. of Crystal Growth.
5. "Control of Surface Composition of Isothermal Vapor Phase Epitaxial Mercury Cadmium Telluride". (J. G. Fleming and D. A. Stevenson). J. of Vac. Sci. and Tech. A(5) 3383 (1987).
6. "Cooling Rate Dependence of the Morphology of  $\text{Hg}_{0.8}\text{Cd}_{0.2}\text{Te}$  Liquid Phase Epitaxial Layers", (S. H. Suh and D. A. Stevenson). J. Vac. Sci. & Tech. A6 (1), (1988).
7. "Interdiffusion and the Related Defect Mechanisms in the  $\text{HgTe-CdTe}$  System", (M.F.S. Tang and D. A. Stevenson), J. Vac. Sci. Tech. A.5 (5), 3161 (1987).

8. "Interdiffusion Behavior of HgTe-CdTe Junctions", Appl. Phys. Lett. 50 (18), 1272 (1987) (M.F.S. Tang and D. A. Stevenson).
9. "Vickers Hardness of  $\text{Hg}_{1-x}\text{Cd}_x\text{Te}$  Epilayers Grown by Isothermal Vapor Phase Epitaxy", (J. G. Fleming, L. J. Farthing and D. A. Stevenson), J. of Crystal Growth, 86, pp. 506-510 (1988).
10. "Diffusion Studies in the  $\text{Hg}_{1-x}\text{Cd}_x\text{Te}$  System", (M.F.S. Tang and D. A. Stevenson) Accepted, J. of Vac. Sci. and Technol. A7, 1989.
11. "Mechanisms of Component Diffusion in Mercury Cadmium Telluride", M.F.S Tang and D. A. Stevenson, J. Vac. Sci. Technol. A7, 1989.
12. "Hardness and Elastic Modulus Measurements in CdTe and ZnTe Thin Films and Bulk Samples and ZnTe-CdTe Superlattices", L.J. Farthing, T.P. Weihs, D.W. Kisker, J.J. Krajewski, M.F.S Tang and D. A. Stevenson, Proceedings of the MRS Symposium, Boston, 1988.
13. "The Relationship Between Component Self-diffusion Coefficients and Interdiffusion Coefficient for Pseudobinary Systems," M.-F. S. Tang and D. A. Stevenson, submitted to J. of Chem. Phys., 1989.
14. "Growth and Characterization of ISOVPE Mercury Cadmium Telluride", S.B. Lee, L.K. Magel, M.F.S. Tang and D.A. Stevenson, submitted to MCT Workshop, San Diego, October 1989.
15. "Diffusion and Hardness Studies in Mercury Zinc Telluride", S. Fang, L.J. Farthing, M.F.S. Tang and D.A. Stevenson, submitted to MCT Workshop, San Diego, October 1989.
16. "Review of Defects in Mercury Cadmium Telluride," K.S. Chou and D.A. Stevenson, Chinese Journal of Materials Science 21 No. 2, pp. 93-109, 1989.

## ISOTHERMAL VAPOR PHASE EPITAXY OF MERCURY CADMIUM TELLURIDE

J.G. FLEMING and D.A. STEVENSON

*Materials Science and Engineering Department, Stanford University, Stanford, California 94305, USA*

Received 28 July 1986

A model is presented for the thermodynamic and the kinetic basis of isothermal vapor phase epitaxy (ISOVPE) of mercury cadmium telluride. Growth is the result of a combination of transport of  $\text{Te}_2$  and Hg from the source to the substrate and interdiffusion between Hg and Cd in the growing layer. Using a Te-rich mercury cadmium telluride source, it is possible to fix the surface composition of the growing layer. The observed effects of time, source to substrate spacing, temperature, and mercury overpressure are explained using the model.

### 1. Introduction

Mercury cadmium telluride ( $\text{Hg}_{1-x}\text{Cd}_x\text{Te}$ ) epilayers are of great interest for use in infrared detectors. Isothermal vapor phase epitaxy (ISOVPE) of this material has been studied since the 1960's [1-15]. The technique has a number of advantages: simplicity, good surface quality, and ease of scale up. One disadvantage is that it produced only graded junctions. Although many growth trends have been reported in the literature, the relevant pressure-temperature diagrams and basic thermodynamic data for the  $\text{HgTe}$ - $\text{CdTe}$  solid solutions have only recently been determined [16-18]. This information is essential to an understanding of the growth process. The objective of the present study is to confirm and supplement the existing information on the growth kinetics and to analyze the process in terms of thermodynamic driving forces and kinetic models in the light of this information. A better understanding of the growth mechanism should provide a basis for improving the growth technique and lend insight into the properties of the material itself.

A major problem in analyzing the mechanism of growth is the large number of variables involved. These include: growth temperature, mercury overpressure, source composition, substrate orientation, source to substrate spacing, and the growth time. To simplify the problem, we have

investigated one variable at a time while keeping the others fixed. An analysis of our results and those in the literature has enabled us to develop a theory which qualitatively explains the observed trends of this growth process.

### 2. Experimental

The general growth geometry is shown in fig. 1. A relatively large source-to-substrate spacing was used since previous workers had shown that growth is a strong function of spacing for small spacings [1,15]. A large spacing minimizes variations due to slightly different spacings. The (111)  $\text{CdTe}$  substrates were etched for 30 seconds in a 4% bromine-methanol solution just prior to growth.

Our source consisted of a mixture of solid mercury cadmium telluride of a given fraction  $\text{CdTe}$  (including pure  $\text{HgTe}$ ) and an equilibrium Te-rich liquid with a ratio of solid to liquid  $\sim 9/1$ . The liquid composition was taken from the LPE melt compositions reported by Harman [19]. Thus, at the growth temperature, this source consists of three phases: solid, liquid and vapor. Large amounts of source were made up by annealing the elements at  $650^\circ\text{C}$  for 16 h, quenching the ampoule in water, and powdering and sintering the resulting material at  $500^\circ\text{C}$  for 30 min to ensure homogeneity. The amount of source used per growth was  $\sim 1-1.5$  g.

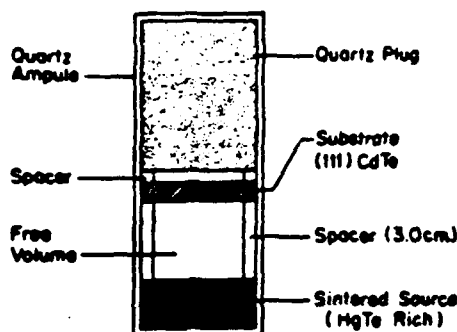


Fig. 1. The experimental geometry used throughout this work. Before growth, and immediately after the substrates were etched, the ampoules were evacuated to  $\sim 10^{-5}$  Torr and sealed.

After growth, the cross section composition profiles were determined using electron probe microanalysis by suitably mounting, sectioning, polishing, and coating the samples. In some experiments, the position of the original substrate surface was established by alumina markers placed on the surface by dipping the substrates into a slurry of  $0.3 \mu\text{m}$  diameter alumina particles in acetone and then air drying the surface. After growth, this produces a fine line of particles and defects which can be highlighted by a 30 s Polisar 2 etch.

### 3. The thermodynamic driving force

Fig. 2 gives a composition versus distance plot with the position of the original substrate surface indicated and clearly shows that material has been added to the CdTe substrate. The metal to non-metal ratio is maintained throughout the solid indicating that deposition occurs stoichiometrically. Even though the process is isothermal, there is a chemical gradient driving force for this deposition. Tung et al. [17], in their paper on the pressure-temperature diagrams of mercury cadmium telluride, present values for the entropy and enthalpy of CdTe and HgTe in the solid solution. The calculated free energies of HgTe ( $G_{\text{HgTe}} = H_{\text{HgTe}} - TS_{\text{HgTe}}$ ) and CdTe at  $550^\circ\text{C}$  versus  $x$  (where  $x$  is the fraction of CdTe in  $\text{Hg}_{1-x}\text{Cd}_x\text{Te}$ ) are given in figs. 3 and 4. These graphs show that the total free energy of the

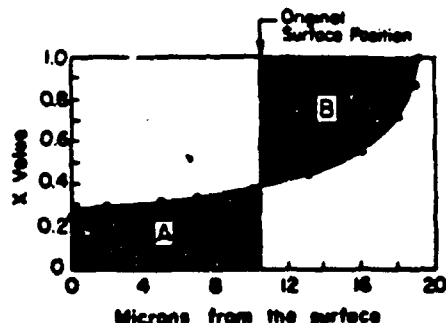


Fig. 2. A plot of a typical composition profile. The growth time was 16 h at a temperature of  $550^\circ\text{C}$ , and the source was in equilibrium with Te-rich  $\text{Hg}_{0.5}\text{Cd}_{0.5}\text{Te}$ . The position of the original substrate surface, observed by alumina markers placed on the surface before growth is also shown. Area A is approximately equal to area B, which is directly proportional to the amount of Cd which has "diffused" (interdiffused with Hg) out of the substrate; indicating that the cadmium in the film originates from the CdTe substrate.

system decreases upon alloying HgTe-rich and CdTe-rich material, as expected for stable solid solutions. This is the thermodynamic driving force for isothermal vapor phase growth. However, this does not provide information on the kinetics or mechanism of the growth process, which are of major practical interest.

### 4. The source of Cd

A key question in the growth mechanism is the source and transport mechanism of the Cd in the growing MCT layers; does the Cd come from the source or the substrate or both? We propose that all the Cd in the layer comes from the substrate by Hg and Cd interdiffusion. Area B of fig. 2 corre-

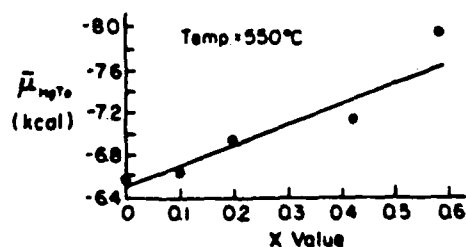


Fig. 3. The free energy of formation of HgTe in  $\text{Hg}_{1-x}\text{Cd}_x\text{Te}$  versus composition at  $550^\circ\text{C}$ . The relevant data are taken from Tung et al. [17].



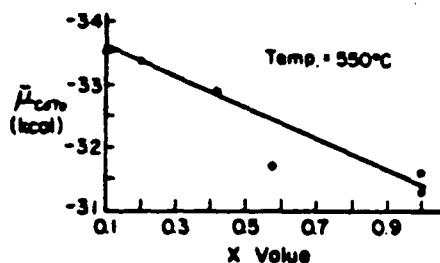


Fig. 4. The free energy of formation of CdTe in  $\text{Hg}_{1-x}\text{Cd}_x\text{Te}$  versus composition at 550°C. The relevant data are taken from Tung et al [17].

sponds to the amount of Cd transported from the substrate and is roughly equal to area A, which corresponds to the amount of Cd present in the  $\text{HgCdTe}$  outside the original substrate surface. (These areas are directly proportional to the amount of Cd since the lattice parameter of MCT solid solutions changes only slightly with composition.) A further analysis of 27 samples grown under a variety of conditions show that, on the average, area B is 15% larger than area A. This discrepancy is at least partially due to a systematic error in the microprobe profiles which occurs in the region where the profiles are changing rapidly. The error arises from the finite beam size, and beam spreading within the sample which effectively increases the layer transition region, thereby increasing area B. Another possible reason is a Kirkendall effect moving the alumina markers away from the position of the original CdTe surface towards the vapor-solid interface. The Kirkendall effect in this system was reported by Leute and Stratmann [20]. Furthermore, the partial pressure of Cd in the system is very low [16,17] and the transport of Cd from the substrate to the source is expected to be small; thus, to a good approximation, we may consider the growth as consisting of vapor transport of  $\text{HgTe}$  only, with interdiffusion taking place between CdTe and  $\text{HgTe}$  to form the  $\text{HgCdTe}$  layer.

### 5. HgTe transport

Insight into the transport of  $\text{HgTe}$  is provided by the pressure-temperature diagrams of this sys-

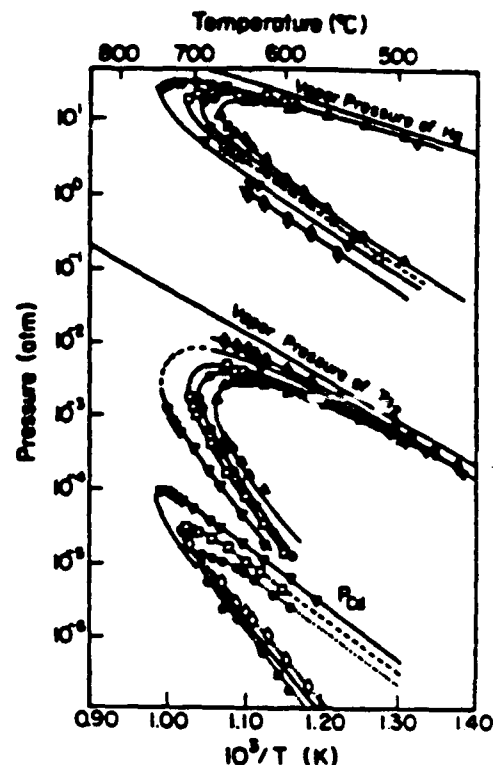


Fig. 5. The pressure-temperature diagrams for  $\text{Hg}_{1-x}\text{Cd}_x\text{Te}$  determined by Tung et al. [17]. Closed and open symbols represent experimental and calculated values respectively. Since the material is a ternary, each composition exists over a different range of partial pressures: ( $\Delta$ ,  $\Delta$ ) for  $x = 0$ ; ( $\bullet$ ,  $\circ$ ) for  $x = 0.094$  and  $x = 0.108$ ; ( $\blacksquare$ ,  $\square$ ) for  $x = 0.194$ ; ( $\nabla$ ,  $\nabla$ ) for  $x = 0.416$ ; ( $\diamond$ ,  $\diamond$ ) for  $x = 0.581$ .

tem [17]. These are given in fig. 5 and show that, at all temperatures and compositions, the partial pressure of Hg is dominant. Since the mercury partial pressure is so large, it should be unaffected by the relatively slow growth process and remain constant throughout the ampoule. Svob et al. in their study of the growth process [14,15] maintain that the mercury pressure in the growth system changes with time. However, the sources used in their studies,  $\text{HgTe}$ -annealed to Hg-rich conditions with added free Hg, were different than ours. In accord with the Gibbs phase rule, the three phase equilibrium source used in the present study provided constant component partial pressures over the source at a constant temperature and a

fixed composition of solid in the source. The overall composition of the source is not appreciably altered since the source is very much larger than the layer grown. Furthermore, the amount of change in the mercury partial pressure, reported by Svob et al. [14,15] to be due to vacancy formation, is in disagreement with studies on the width of stability of the mercury cadmium telluride system [21].

Because the  $\text{Te}_2$  pressure is much smaller than the Hg pressure,  $\text{Te}_2$  transport from source to substrate is expected to be rate limiting, at least in the early stages of growth. Fig. 6 shows the variation in the  $\text{Te}_2$  partial pressure with fraction CdTe in the mercury cadmium telluride for the conditions of growth: constant growth temperature and Hg pressure. This graph indicates that there is a gradient in  $\text{Te}_2$  partial pressure between the source and the substrate; during growth,  $\text{Te}_2$  vapor is transported down this partial pressure gradient from the HgTe-rich source to substrate surface where it supersaturates the vapor and deposits HgTe. Fig. 6 also establishes that it is not possible to grow material with a lower fraction CdTe than the source since this would require Te transport up a partial pressure gradient. Another view of the driving force is provided by noting that the mercury vapor pressure is fixed by the three phase Te-rich source and in, accord with the Hg-Cd-Te pressure-temperature diagram (fig. 5), material with higher HgTe fractions is not stable in this environment and therefore cannot form.

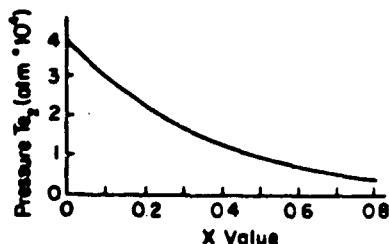


Fig. 6. The variation of tellurium partial pressure with composition for the conditions of isothermal vapor phase growth, constant temperature and mercury pressure. A temperature of 550°C and mercury pressure of 1 atm are used as an example. The tellurium partial pressure was determined from the entropy and enthalpy data given by Tung et al. [17].

## 6. The effect of source composition

The source consists of a solid-liquid-vapor mixture in equilibrium with the desired MCT composition. Further details of this type of source are described elsewhere [22]. The source was prepared by mixing solid HgCdTe of the desired composition with its equilibrium Te rich liquid in a 9/1 molar ratio. At temperature, the solid-liquid mixture vaporizes to supply the third phase. As has already been mentioned, in accord with the Gibbs Phase Rule for a three component system such as HgCdTe, three phases will correspond to two degrees of freedom. Thus, specifying the temperature and the solid composition will fix all of the intensive properties of the system. In practice the solid composition of the source is fixed as long as the amount of HgTe deposited is small with respect to the amount of HgTe in the source.

Both Becla et al. [8] and Kay [11] have reported that the layer surface composition and thickness depend on the fraction of Te-rich melt in the source. This should not be the case from purely thermodynamic considerations. However, these two authors report different findings; in one case the surface CdTe fraction reportedly increases with increasing Te fraction [8], while the opposite trend is reported for the other study [11]. Purely thermodynamic arguments may not apply for the initial stages of growth when the source and substrate surface are well displaced from equilibrium, but should apply for the stages of growth when the growing layer surface composition is close to the source composition. In this analysis we will only consider this near equilibrium condition.

## 7. The effect of growth time

Fig. 6 illustrates that there is a gradient in the  $\text{Te}_2$  partial pressure favoring transport as long as the fraction of CdTe in the source is less than that at the growing surface. As growth proceeds, interdiffusion between Hg and Cd maintains this gradient. Fig. 7 shows a plot of the log of the amount of HgTe transported versus log time. Initially, the layer are thin enough that Cd and Hg can quickly interdiffuse and growth is limited by

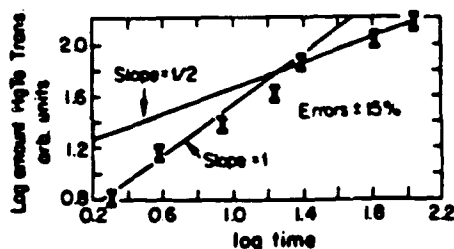


Fig. 7. A plot of the log of the amount of HgTe transported versus log time (hours) for samples grown at 550°C from a Te-rich HgTe source. As time increases, growth becomes diffusion limited as evidenced by the  $1/2$  slope.

transport of  $\text{Te}_2$  from the source to the substrate. This vapor transport limitation gives rise to the initial linear portion of the curve. This initial linear dependence has been observed in the literature [5,11,12]. For longer times, the layer thickness and growth is limited by interdiffusion of Cd and Hg increasing the fraction of CdTe at the growing surface. In this regime, growth follows the  $t^{1/2}$  dependence expected for a diffusion limited process; this  $t^{1/2}$  dependence has been observed in other studies [1-8, 12-15]. As the thickness of the growing layer increases, the composition of the surface approaches that of the source. Eventually, growth is purely diffusion limited and the surface composition becomes essentially the same as that of the source.

#### 8. The effect of temperature

Fig. 8 shows the effect of changing the growth temperature while keeping all other variables fixed. As the growth temperature is lowered, the surface composition approaches that of the source and the layers are thinner. The observed interdiffusion activation energy is  $\sim 2$  eV [23,24]. The activation energy governing the  $\text{Te}_2$  partial pressure under Te-rich conditions can be deduced from the equation given by Schwartz et al. and is on the order of 1.2 eV [16]. Thus, growth will be strongly temperature dependent, with the interdiffusion process being primarily affected. Lowering the temperature produces thinner layers with lower surface fractions of CdTe which is consistent with a rela-

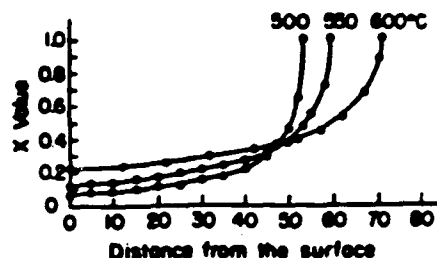


Fig. 8. The effect of growth temperature on layers grown from Te-rich HgTe for a time of 24 h. As the temperature is increased, the interdiffusion coefficient increases, leading to thicker layers with higher surface  $x$  values.

tively lower interdiffusion rate as compared to the HgTe vapor transport rate.

#### 9. The effect of the substrate polarity and source-to-substrate spacing

The effect of CdTe (111) surface polarity was addressed for this process by simultaneously depositing on both the A and B faces. This was achieved by orientating the substrate as shown in fig. 9. To within experimental error, no effect on either surface composition or thickness was observed. This is expected since these experiments were performed in the diffusion limited regime and interdiffusion will be unaffected by the surface polarity. However, there may be an effect at shorter times when growth is transport limited. The surface

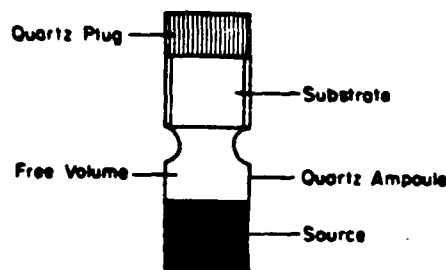


Fig. 9. The experimental geometry used to investigate the effect of the source to substrate spacing and (111) substrate polarity on growth. The substrate is oriented vertically with respect to the source so that different points on the substrate are different distances from the source and the A (Cd) and B (Te) faces are both exposed to the same environment.

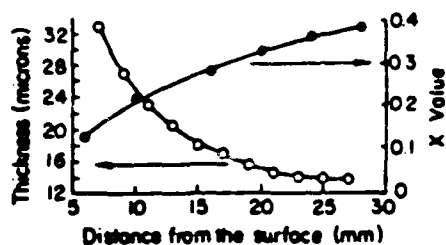


Fig. 10. The effect of source to substrate spacing (horizontal axis) on layer thickness (left-hand side vertical axis) and surface composition (right-hand side vertical axis). The source used was Te-rich HgTe, the temperature was 550°C and the growth time 16 h.

morphology of the layers was found to vary between the A and B faces. While both surfaces were macroscopically smooth, the A face had a more pronounced microscopic surface terrace structure.

The same experimental geometry was also used to determine the influence of source to substrate spacing and the results are given in fig. 10. Similar trends on the effect of source to substrate spacing were reported by Svob et al. [15] from a study of separate growth runs. From the present study, we see that increasing the source to substrate spacing increases the surface CdTe fraction and decreases the layer thickness. An explanation of this behavior is that as the source to substrate spacing increases, the flux of  $\text{Te}_2$  should decrease since the  $\text{Te}_2$  potential gradient will decrease, reducing the amount of HgTe deposited. This experiment is complicated by the possibility of  $\text{Te}_2$  depletion resulting from deposition occurring on parts of the substrate which are closer to the source. However, the fact that there is an observable dependence on distance from the source is evidence that growth is, at least initially, limited by transport of  $\text{Te}_2$  and not a surface reaction of Hg and  $\text{Te}_2$  at the growing surface or interdiffusion, neither of which depends on spacing.

#### 10. The effect of mercury overpressure

Becla et al. [9], Svob et al. [15] and Tufte and Stelzer [4] have investigated the effect of the ambient pressure of Hg on the surface composition

grown. In these studies, the Hg partial pressure was controlled by either a two zone technique [9] or by adding a fixed amount of Hg to the growth ampoule [4,15]. This work has shown that increasing the mercury partial pressure results in layers which are thinner and have higher surface fractions of CdTe. Increasing the partial pressure of the Hg will have several effects on growth. The partial pressure of  $\text{Te}_2$  over both the source and the substrate will decrease in accord with the equilibrium constant,  $P_{\text{Te}_2} = K/(P_{\text{Hg}})^2$ . The mobility of the  $\text{Te}_2$  in the vapor will also decrease inversely as the total pressure increases. Both these effects would give rise to the higher CdTe fractions and thinner layers observed at higher Hg pressures. The Hg pressure might influence the interdiffusion coefficient, although, previous studies [20] have shown that interdiffusion is relatively insensitive to this parameter. Furthermore, if the dominant effect of increasing the mercury overpressure was to lower the interdiffusion coefficient, then the surface composition of the layers should approach that of the source, while the opposite is the case.

Another effect comes into play when the mercury pressure falls below the minimum value for which HgTe is stable. In this case only CdTe rich material will be stable. The minimum mercury partial pressure for which mercury cadmium telluride of a certain composition is stable is given by the pressure-temperature diagrams for the system. By accurate control of the mercury partial pressure, for example using a two zone system, it is possible to set a lower limit of CdTe at the surface of the layer. This effect has been observed in the work of Becla et al. [9].

#### 11. Summary

Isothermal vapor phase growth is the result of two processes: transport of  $\text{Te}_2$  and Hg (though only the transport of  $\text{Te}_2$  is limiting) from source to substrate and interdiffusion between Hg and Cd within the growing layer. At short times, growth is limited by the transport of  $\text{Te}_2$  while at longer times growth is diffusion limited. Eventually, growth becomes entirely diffusion limited and the

surface composition becomes essentially equal to that of the source. The time it takes for this to occur is greater for material with lower CdTe fractions, higher temperatures, higher mercury overpressures and greater source to substrate spacings. Increasing the Hg overpressure decreases both the partial pressure and the mobility of  $\text{Te}_2$  vapor. If the mercury overpressure is sufficiently low, then the lower limit of the CdTe fraction in the layer is determined by the materials' lower limit of mercury partial pressure stability.

#### Acknowledgements

The authors thank Dr. R. Kay and Dr. K. Zanio of Ford Aerospace for helpful discussions and Dr. Margaret Brown of Rockwell International for helpful discussions and for supplying CdTe substrates. One of the authors, J.G. Fleming, gratefully acknowledges the support of an ONR fellowship. This work was funded by DARPA through the Office of Naval Research, Contract No. N00014-84K-0423.

#### References

- [1] G. Cohen-Solal, Y. Marfaing, F. Bailly and M. Robert, *Comput. Rend. (Paris)* 261 (1965) 931.
- [2] Y. Marfaing, G. Cohen-Solal and F. Bailly, in: *Crystal Growth*, Ed. H.S. Peiser (Pergamon, Oxford, 1967) p. 549.
- [3] G.S. Almasi and A.C. Smith, *J. Appl. Phys.* 39 (1968) 233.
- [4] O.N. Tufte and E.L. Stetzer, *J. Appl. Phys.* 40 (1969) 4559.
- [5] L.A. Bovina, V.P. Meshcheryakova, V.I. Stafeyev and E.S. Bania, *Soviet Phys.-Semicond.* 7 (1973) 25.
- [6] J.M. Pawlikowski and P. Becla, *Phys. Status Solidi (a)* 32 (1975) 639.
- [7] J.M. Pawlikowski, *Thin Solid Films*, 44 (1977) 241.
- [8] P. Becla, J. Lagowski, H.C. Gatos and H. Ruda, *J. Electrochem. Soc.* 128 (1981) 1171.
- [9] P. Becla, J. Lagowski, H.C. Gatos and L. Jedral, *J. Electrochem. Soc.* 129 (1982) 2855.
- [10] P. Becla, J. Lagowski and H.C. Gatos, *J. Electrochem. Soc.* 129 (1982) 1103.
- [11] R.E. Kay, US Patent No. 4,447,470, May 8, 1984.
- [12] Y. Nemirovsky and A. Koptez, *J. Electron. Mater.* 13 (1984) 867.
- [13] P. Becla, P.A. Wolff, R.L. Aggarwal and Y.S. Yuen, *J. Vacuum Sci. Technol. A3* (1985) 119.
- [14] F. Bailly, L. Svob, G. Cohen-Solal and R. Triboulet, *J. Appl. Phys.* 46 (1975) 4244.
- [15] L. Svob, Y. Marfaing, R. Triboulet, F. Bailly and G. Cohen-Solal, *J. Appl. Phys.* 46 (1975) 4251.
- [16] J.P. Schwartz, T. Tung and R.F. Brebrick, *J. Electrochem. Soc.* 128 (1981) 438.
- [17] T. Tung, L. Golonka and R.F. Brebrick, *J. Electrochem. Soc.* 128 (1981) 451.
- [18] C.-H. Su, P.-K. Liao and R.F. Brebrick, *J. Electrochem. Soc.* 132 (1985) 942.
- [19] T.C. Harman, *J. Electron. Mater.* 9 (1980) 945.
- [20] V. Leute and W. Stratmann, *Z. Physik. Chem.* 90 (1974) 172.
- [21] H.F. Schaake, *J. Electron. Mater.* 14 (1985) 513.
- [22] J.G. Fleming and D.A. Stevenson, submitted for publication.
- [23] J.G. Fleming and D.A. Stevenson, submitted for publication.
- [24] K. Zanio and T. Massopust, *J. Electron. Mater.* 15 (1986) 103.

## Appendix B: Control of the surface composition of isothermal vapor phase epitaxial mercury cadmium telluride

J. G. Fleming and D. A. Stevenson

*Department of Materials Science and Engineering, Stanford University, Stanford, California 94305*

(Received 21 July 1986; accepted 21 June 1987)

A method is described for controlling the surface composition of mercury cadmium telluride during isothermal vapor phase epitaxy of mercury cadmium telluride. The method employs a three-phase solid-liquid-vapor source in equilibrium with the desired composition. The thermodynamic and kinetic basis of the method is outlined.

### I. INTRODUCTION

Isothermal vapor phase epitaxy (ISOVPE) of mercury cadmium telluride ( $\text{Hg}_{1-x}\text{Cd}_x\text{Te}$ ) has been studied since the 1960s.<sup>1-16</sup> Since the band gap of the material is governed by the composition, ranging from 1.6 eV for CdTe to  $-0.3$  eV for HgTe, the control of composition is a major practical concern. The isothermal growth technique produces relatively flat composition profiles near the surface due to the way the interdiffusion coefficient varies with composition.<sup>17</sup> The composition of this plateau region is determined by that of the surface of the layer; therefore, controlling the surface composition is critical. The desired surface composition may be obtained by either equilibrium or nonequilibrium methods. In nonequilibrium techniques, the surface composition of the layers changes continuously with time, requiring that the process be terminated after a fixed time. These methods rely on the fact that the surface composition changes relatively slowly with time through the composition range of interest, 0.3–0.2 mole fraction CdTe. However, using equilibrium methods, the surface composition remains at the desired value after an initial transient. In practice, equilibrium techniques rely on controlling the mercury partial pressure<sup>9</sup> or the composition of the source.<sup>3,16</sup> In this paper, only the latter method will be considered, along with a description of the thermodynamic basis for this approach.

### II. EXPERIMENTAL APPROACH

The experimental geometry used is shown in Fig. 1. The sources consist of  $\sim 90\%$  solid mercury cadmium telluride of the desired composition and  $\sim 10\%$  of a tellurium-rich liquid which is in equilibrium with that solid at the growth temperature. The liquid composition was determined from the liquid phase epitaxy data of Harman.<sup>18</sup> Batches of source material were made by reacting the components in a sealed quartz ampoule at  $650^\circ\text{C}$  for 16 h and then quenching the ampoule in water. The source material was then powdered and sintered for 30 min at  $500^\circ\text{C}$  in order to ensure homogeneity. After growth, the layers were mounted in epoxy, cross sectioned, polished, coated, and analyzed by electron probe microanalysis.

The basis for this method is given by the Gibbs phase rule and basic concepts of ternary phase equilibria. As described above, the source consists of an equilibrium solid-liquid mixture, with the solid of the desired CdTe mole fraction.

The source in the closed ampoule at a specified annealing temperature will vaporize and develop partial pressures of the components that are in equilibrium with the solid-liquid mixture. Upon vaporization in the ampoule, the amounts of solid and liquid phases may change slightly, but their compositions will not change. Applying the Gibbs phase rule ( $F = C + 2 - P$ ) for this ternary system, the number of components  $C$  are 3 and the number of phases  $P$  are 3 (solid, liquid, and vapor). The variance  $F$  of the system is 2 and specifying the temperature and the solid composition fixes the chemical potentials of all three of the components in the source. If a relatively small amount of source is consumed during growth, then there will be a small shift in the relative amounts of the phases but not in the chemical potentials of the components. This will be the case for a relatively large amount of source compared to the substrate for long growth times, in which case the entire grown layer will eventually convert to the composition very close to the solid phase in the source. For typical amounts of source for normal growth times, only a small amount of the source is consumed by the growth process and the chemical potentials in the source remain constant. Therefore, the surface composition of the growing layer will tend to approach that of the solid phase in the source. Details of the growth mechanism and the relevant solid-liquid-vapor equilibrium are given in Ref. 16 and further discussion of the basis for the present method is given in Sec. III.

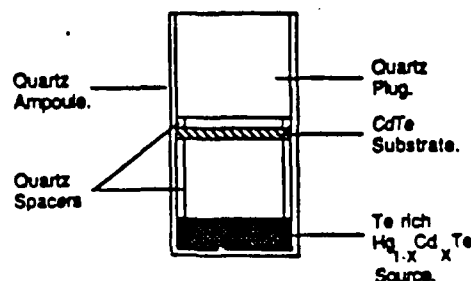


FIG. 1. The experimental geometry used to investigate the effect of the source composition. Just after the substrate was etched, the ampoule was assembled, evacuated to  $\sim 10^{-5}$  Torr, and sealed. The source-to-substrate spacing was 3 cm. Growth was performed in the isothermal zone of a sodium heat pipe.

### III. RESULTS AND DISCUSSION

The results of growths performed under the same conditions (550 °C and 24 h) but with different source compositions are given in Fig. 2. For sources with fractions of CdTe greater than 0.2, the surface of the sample is the same as that of the mercury cadmium telluride in the source. The thermodynamic basis of this behavior is illustrated by the Hg-Cd-Te Gibbs triangle, shown schematically in Fig. 3. Initially, the overall composition of the source is at point A, which is in equilibrium with mercury cadmium telluride of composition C and a tellurium-rich liquid. If we add a piece of CdTe to the system, the overall composition of the entire system is moved towards CdTe to point B, which is in equilibrium with a solid of composition D and a tellurium-rich liquid. When the amount deposited on the substrate is small compared to the source, then the source composition will not change significantly during growth. Furthermore, for longer times and thicker films, the interdiffusion process is slow compared to the rate of vapor transport and the surface composition of the growth layer closely approaches that of the source.

The Cd vapor pressure is very low, especially under tellurium-rich conditions of growth in the present study.<sup>19</sup> As a consequence, there is a negligible transport of Cd through the vapor; the Cd in the grown layer results from the diffusion from the substrate.<sup>16</sup> The role of Cd in the source is to control the Hg and Te<sub>2</sub> partial pressures to values corresponding to equilibrium with Hg<sub>1-x</sub>Cd<sub>x</sub>Te of the desired composition under tellurium-rich conditions, in accord with the Gibbs phase rule and the pressure-temperature diagram for Hg<sub>1-x</sub>Cd<sub>x</sub>Te.

The system approaches its equilibrium composition through the growth of the mercury cadmium telluride layer on the substrate. Growth proceeds by the deposition of HgTe, which is limited by Te<sub>2</sub> vapor transport from source to substrate and interdiffusion between Hg and Cd in the growing layer.<sup>16</sup> It is this interdiffusion which maintains a gradient in the tellurium chemical potential between the source and the substrate surface. Initially the layer is thin so that interdiffusion quickly changes the surface composition so that growth is limited by tellurium transport and the fraction of CdTe at the surface of the growing layer is greater than that of the solid Hg<sub>1-x</sub>Cd<sub>x</sub>Te in the source. However,

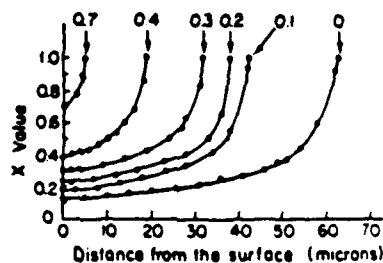


FIG. 2. Composition profiles of samples grown under the same conditions (550 °C and 24 h) but with different source compositions (shown on top). Notice that for material grown from sources with fractions of CdTe greater than 0.2, the surface compositions are the same as the solid in the source.

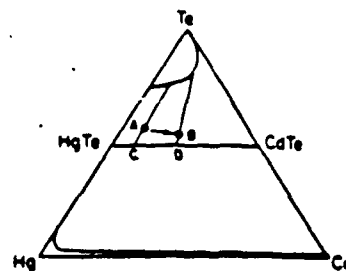


FIG. 3. A schematic of the Hg-Cd-Te phase diagram at the growth temperature. Initially the source is at position A, in equilibrium with mercury cadmium telluride of composition C. If the source is in communication with a piece of CdTe (the substrate), the overall composition of the system is moved to point B. Since the source is large compared to the film which is grown, the overall composition of the system is only perturbed slightly by the presence of the substrate.

as the layer thickens, the interdiffusion process becomes rate limiting. Once this has occurred, the source and substrate surface are essentially in equilibrium so that the composition at the surface of the layer closely approaches that of the solid in the source.

Factors which increase the rate at which HgTe is deposited relative to the amount of interdiffusion between Hg and Cd allow the surface to approach equilibrium more rapidly. Since growth of material with lower fractions of CdTe requires relatively more HgTe deposition per Cd diffusing to the surface, and since the interdiffusion coefficient at the surface of these layers is greater (the interdiffusion coefficient increases over three orders of magnitude as the composition changes from CdTe to HgTe<sup>17,20,21</sup>), the nonequilibrium transient time is longer in this composition range. With material grown from higher  $x$  value sources, the layers have thickened sufficiently relative to the interdiffusion coefficient of the material at the surface, so that the surface of the layer is essentially in equilibrium with the source, and the surface composition will be constant with time. Thus the composition of the source sets a lower limit on the composition of the mercury cadmium telluride formed.

The present method has the advantage that the desired surface composition does not change with time once it has been established and the method is easy to implement. Another method for fixing the surface composition is by control of the mercury partial pressure to sufficiently low levels so that only material with the desired, or higher, fractions of CdTe are stable. Evidence for this can be seen in the work of Becla.<sup>9</sup> However, this method is somewhat more complicated since it requires the use of a two-zone system to control the mercury overpressure.

### IV. SUMMARY

A solid-liquid-vapor source is described which allows accurate control of the component chemical potentials, the theoretical basis for this being the Gibbs phase rule. There exists an initial transient during growth in which the composition of the sample surface is not in equilibrium with the source due to interdiffusion within the growing layer. This transient period is longer for layers grown with lower  $x$  values, greater source-to-substrate spacings, and higher temperatures.

## ACKNOWLEDGMENTS

We thank Dr. Margaret Brown of Grumman Corporate Research Center for helpful discussions and for supplying some of the CdTe substrates used in this work. This project was sponsored by DARPA through the Office of Naval Research, Contract No. N00014-84K-0423. One of the authors, J. G. Fleming, gratefully acknowledges the support of an Office of Naval Research Fellowship.

<sup>1</sup>G. Cohen-Solal, Y. Marfaing, F. Bailly, and M. Robot, *C. R. Acad. Sci.* 261, 931 (1965).

<sup>2</sup>Y. Marfaing, G. Cohen-Solal, and F. Bailly, *J. Phys. Chem. Solids Suppl.* 1, 549 (1967).

<sup>3</sup>G. S. Almasi and A. C. Smith, *J. Appl. Phys.* 39, 233 (1968).

<sup>4</sup>O. N. Tufte and E. L. Stelzer, *J. Appl. Phys.* 40, 4559 (1969).

<sup>5</sup>L. A. Bovina, V. P. Meshcheryakova, V. I. Stafcev, and E. S. Banin, *Sov. Phys. Semicond.* 7, 26 (1973).

<sup>6</sup>J. M. Pawlikowski and P. Becla, *Phys. Status Solidi A* 32, 639 (1975).

<sup>7</sup>J. M. Pawlikowski, *Thin Solid Films* 44, 241 (1977).

<sup>8</sup>P. Becla, J. Lagowski, H. C. Gatos, and H. Ruda, *J. Electrochem. Soc.* 128, 1171 (1981).

<sup>9</sup>P. Becla, J. Lagowski, H. C. Gatos, and L. Jedral, *J. Electrochem. Soc.* 129, 2855 (1982).

<sup>10</sup>P. Becla, J. Lagowski, and H. C. Gatos, *J. Electrochem. Soc.* 129, 1103 (1982).

<sup>11</sup>R. E. Kay, U. S. Patent No. 4 447 470 (8 May 1984).

<sup>12</sup>Y. Nemirovsky and A. Kepten, *J. Electron. Mater.* 13, 867 (1984).

<sup>13</sup>P. Becla, P. A. Wolf, R. L. Aggarwal, and Y. S. Yuen, *J. Vac. Sci. Technol. A* 3, 119 (1985).

<sup>14</sup>F. Bailly, L. Svob, G. Cohen-Solal, and R. Triboulet, *J. Appl. Phys.* 46, 4244 (1975).

<sup>15</sup>L. Svob, Y. Marfaing, R. Triboulet, F. Bailly, and G. Cohen-Solal, *J. Appl. Phys.* 46, 4251 (1975).

<sup>16</sup>J. G. Fleming and D. A. Stevenson, *J. Cryst. Growth* 82, 621 (1987).

<sup>17</sup>J. G. Fleming and D. A. Stevenson (submitted for publication).

<sup>18</sup>T. C. Harman, *J. Electron. Mater.* 9, 945 (1980).

<sup>19</sup>T. Tung, L. Golonka, and R. F. Brebrick, *J. Electrochem. Soc.* 128, 451 (1981).

<sup>20</sup>V. Leute, H. M. Schmidtke, W. Stratmann, and W. Winking, *Phys. Status Solidi A* 67, 183 (1981).

<sup>21</sup>M. S. F. Tang and D. A. Stevenson, *Appl. Phys. Lett.* 50, 1272 (1987).



## THE EFFECT OF ORIENTATION ON THE SURFACE MORPHOLOGY OF MERCURY CADMIUM TELLURIDE GROWN BY LPE AND VPE.

J.G.Fleming and D.A.Stevenson.

*Department of Materials Science and Engineering. Stanford University, Stanford CA. 94305.*

The influence of substrate orientation on the morphology of liquid phase and vapor phase epitaxial films of mercury cadmium telluride was studied using spherically shaped {111} CdTe and CdZnTe substrates. A smooth terrace-free central region was observed, with terrace formation occurring for misorientations of greater than  $0.2^\circ \pm 0.1^\circ$  from the {111} orientation. The interpretation of these results and the practical implications are discussed.

### 1. Introduction.

Mercury cadmium telluride is an important material for infrared detectors in the long wavelength regime. The material exists as a pseudobinary series of continuous solid solutions between HgTe, with a "band gap" -0.3 eV, to CdTe, with a band gap of 1.6 eV.[1]. However, the material has properties which make it difficult to produce (see for example, Ref. [2]): high mercury pressures at growth and processing temperatures, poor mechanical properties, retrograde Te solubility, high diffusion coefficients, and the difficulty of specifying the thermodynamic state of a ternary system.

Due to its importance and the difficulties in preparing material with the desired properties, many growth techniques have been developed. The most important epitaxial technique is currently

liquid phase epitaxy (LPE), which has been developed for both Te [3-9] and Hg [10,11] melts. Another technique which has been extensively investigated is the isothermal vapor phase epitaxial technique (ISOVPE) [12-20] which takes advantage of the relatively high component vapor pressures and the high interdiffusion coefficient. The surface morphology of the layers grown by liquid phase epitaxy has been reported by many investigators [4-8]. In general, it consists of a wavy terraced structure like that shown in Fig. 1. Some workers have reported on the effect of orientation on morphology [6,7].

Many of the effects known to be important in Si and GaAs growth have not yet been investigated for the mercury cadmium telluride system. The surface morphology of III-V compound semiconductors produced by LPE and other growth techniques has been investigated by many workers. (See, for example, Ref. 21 and references therein.) In these systems it was found that for substrate orientations deviating only slightly from the low index plane,  $\{111\}$  or  $\{100\}$ , there exists a growth regime in which very flat, uniform layers are produced. However, when the substrate misorientation deviates further, a terraced surface morphology develops. The terrace-free structures have advantages which will be outlined in later sections. Bauser and Strunk [21] have investigated the effect of substrate orientation on the surface morphology of LPE GaAs layers using a spherically shaped substrate. Similar work on mercury cadmium telluride has also recently been published [7]. The advantage of this type of experiment is that a continuous range of orientations can be investigated under the same growth conditions

in a single experiment. It was the objective of our study to perform similar experiments on the LPE and ISOVPE growth of mercury cadmium telluride to determine if there is a similar terrace-free regime in this system and, if so, the critical misorientation for the change from terrace-free to terraced growth.

## 2. Experimental.

Lenticular substrates were formed using the simple jig shown in Fig. 2. The rough shape is patterned using a portion of a round bottomed flask. The substrate material was {111} CdTe, both A (Cd) and B (Te) faces, for ISOVPE and {111}  $\text{Cd}_{0.955}\text{Zn}_{0.045}\text{Te}$ , A face, for the LPE growths. The substrates were attached to an aluminum shaft by yellow wax. The shaft in turn was held radially to the the lowest portion of the arc of the flask. Rough forming was achieved by placing a slurry of 400 grit SiC in ethylene glycol in the round bottomed flask, putting the substrate in contact with the flask/slurry, and manually turning the aluminum shaft. Once the basic shape has been obtained, the shaft is removed from the slurry and the substrate surface hand finished using 600 grit paper, followed by 0.2 micron  $\text{Al}_2\text{O}_3$  with 2% bromine in ethylene glycol. Just before growth, the substrates were etched for 2 minutes in a 4% Br in methanol solution. The resulting radius of curvature was determined by optically measuring the change in focus with lateral deviation from the center of the substrate. The results obtained for two samples are presented in Table 1 and give an indication of the technique's reproducibility.

Epitaxial layers were grown on the resulting substrates by either the LPE or ISOVPE techniques. A closed ampoule tilting LPE method ~~was~~ used, with the melt composition taken from the data of Harman [3] for a temperature of 500°C and a solid composition of 20% CdTe in the mercury cadmium telluride. The melt was prepared by annealing the elements in a sealed quartz ampoule at 600°C, for 12 hours. The ampoule was then quenched, opened and the source broken up for use. The same melt was not used more than twice. The ISOVPE layer that forms on the substrate as the melt is heated was removed by slightly melting back the substrate. Growth was then initiated by cooling at 0.3°C/min for 33 minutes. Some of the samples underwent a slight melt back at the end of growth prior to removal of the melt from the substrate.

ISOVPE layers were grown using a tellurium-rich mercury cadmium tellurium source which allows us to fix the surface composition of the layers [20]. The source to substrate spacing was ~ 2 cm. and growth was performed in the constant temperature zone of a sodium heat pipe at temperatures of 500, 550 and 600°C. After growth, the surface morphology of the layers was observed using an optical microscope.

### 3. Results. -

Optical micrographs of the surface of layers grown by ISOVPE and LPE reveal a distinct terrace-free region which is flat compared to either the original radius of curvature or the terraced region, Fig. 3. The black spots on the LPE samples are retained melt, which was a problem throughout this work due, in part, to the small size of

the substrates. The density of the pyramid structures in Fig. 3a is on the order of the  $1.5 \cdot 10^5$  per  $\text{cm}^2$ . These features are only visible when the sample is tilted slightly. The center of these terrace-free regions is assumed to be exactly perpendicular to the  $\{111\}$  direction. The critical misorientation at which the surface morphology changes from terrace-free to terraced is readily calculated from the radius of curvature of the sample and the diameter of the terrace-free area. Table 2 gives pertinent data for a number of ISOVPE and LPE runs. The critical degree of misorientation is found to range from  $0.32^\circ$  to  $0.15^\circ$ ; the error in the technique is estimated to be  $\pm 0.1^\circ$ . Notice also that the terraces in the ISOVPE material are not as wide and therefore also lower than those found in the LPE material.

#### 4. Discussion.

The existence of distinctly different layer morphologies with different deviations from the low index growth plane closely parallels the results of experiments in the III-V semiconductors (see for example [21]). In these studies, the different morphologies were related to different growth mechanisms. In work on LPE GaAs, a one-to-one correspondence between pyramids on the central facet and dislocations has been established [21-24]. Although no similar work was done in this study, the density of pyramid structures seen on the facet in Fig. 3a,  $\sim 1.5 \cdot 10^5/\text{cm}^2$ , is of the same order of magnitude as the expected dislocation density, and the terrace-free growth probably proceeds by growth on dislocations which exit the free surface. On the other hand, terrace growth occurs by the

movement of terraces across the surface and by the movement of smaller steps between the terraces [21]. The terraces arise from the coalescence of monoatomic steps which are initially present as a result of the original deviation from the {111} caused by the spherical substrate shape. Bauser and Strunk [21] also observed a further terrace-free region at misorientations greater than those for terrace-free growth. However, a similar region was not observed in our work, possibly because the range of misorientations on our samples was not large enough to observe this effect.

In the III-V compounds, it has been shown that there are a number of advantages to growth in the terrace-free regime, some or all of which may apply to the mercury cadmium telluride system. The layer morphology in the terrace-free region of both systems is very flat and uniform, which offers advantages in device fabrication. Also, it has been shown in work on the III-V compounds that the terraced structure effects the distribution of dopants and impurities in the layer. For example, experiments have shown that melt impurities tend to segregate to the riser portion of the terrace and consequently preferentially deposit in these regions [21,24-27]. Since the terrace free region consists of monomolecular steps, this is not a problem in this regime. While impurity segregation was not investigated in our work, it seems probable that the same effect occurs in the mercury cadmium telluride system.

In this work this angle between terrace-free and terraced growth is calculated to be  $0.2^\circ \pm 0.1^\circ$ . This value seems to be relatively unaffected by the experimental parameters outlined in Table 2 and is close to that found during the LPE growth of GaAs,

0.1° [21] but is not in good agreement with the value of 0.5° reported in [7] and this disagreement may reflect the influence of some other experimental variable. Rode [28] determined this critical misorientation using a mathematical model that treats the misorientation steps as linear disruptions to the surface reconstruction which introduced surface strain.

#### **4. Summary.**

A terrace-free growth regime has been identified for the LPE and the ISOVPE growth of mercury cadmium telluride, in agreement with the results of more complete studies on the growth of III-V compound semiconductors. The critical misorientation is found to be on the order of  $0.2^\circ \pm 0.1^\circ$ . Assuming that the system behaves similarly to the III-V compounds, there should be advantages in layer morphology and uniformity of doping in growth from the terrace-free regime. However, growth in this regime does require accurate substrate orientation.

#### **Acknowledgements.**

Helpful discussions with Prof. W. Tiller of Stanford University are gratefully acknowledged. Thanks to Drs. Margaret Brown of Rockwell International and Carlos Castro of Texas Instruments for supplying the substrates used in this work. This project is sponsored by DARPA through the Office of Naval Research, contract no. N00014-84K-0423. One of the authors, J.G.Fleming, gratefully acknowledges the support of an Office of Naval Research Fellowship.

## References.

- [1] J.L.Schmit. J. Crystal Growth 65 (1983) 249.
- [2] W.F.H. Micklethwaite in "Semiconductors and Semimetals." Vol.18. ed. by R.K.Willardson, 1981 Academic Press. pp47.
- [3] T.C.Harman. J. Electronic Materials. 19 (1980) 945.
- [4] M.Chu and C.C.Wang, J. Appl. Phys. 51 (1980) 2255.
- [5] K.Nagahama, R.Ohkata, K.Nishitani and T.Murotani. J. Electronic Materials 13 (1984) 67.
- [6] D.D.Edwall, E.R.Gertner and W.E.Tennant. J. Appl. Phys. 55 (1984) 1453.
- [7] C.F.Wan, D.F.Weirauch, E.G.Bylander and C.A.Castro. J. Electronic Materials.15 (1986) 151.
- [8] C.C.Wang, S.H.Shin, M.Chu, M.Lanir and A.H.B.Vanderwyck. J. Electrochem. Soc. 127 (1980) 175.
- [9] J.A.Mroczkowski and H.R.Vydyanath. J. Electrochem. Soc. 128 (1981) 655.
- [10] J.L.Schmit, R.J.Hager and R.A.Wood. J. Crystal Growth. 56 (1982) 485.
- [11] P.E.Herning J. Electronic Materials. 13 (1984) 1.
- [12] M.H.Kalisher J. Crystal Growth. 70 (1984) 365.
- [13] P.Becla, J.Lagowski and H.C.Gatos. J. Electrochem. Soc. 129 (1982) 1103.
- [14] P.Becla, J.Lagowski, H.C.Gatos and H.Ruda. J. Electrochem. Soc. 128 (1981) 1171.
- [15] Y. Marfaing, F. Bailly, Massy, and G. Cohen-Solal. US Patent#3472685 Oct. 14, 1969.
- [16] O.N.Tufte and E.L.Stelzer. J. Appl. Phys. 40 (1969) 4559.
- [17] Y.Marfaing, G.Cohen-Solal and F.Bailly. J. Phys. Chem. Solids. Suppl. 1 (1967) 549.
- [18] J.M.Pawlikowski. Thin Solid Films 44 (1977) 241.
- [19] L.A.Bovina, V.P.Meshcheryakova, V.I.Stafeev and E.S.Banin. Soviet Physics-Semiconductors. 7 (1973) 26.
- [20] S.H.Shin, E.R.Gertner, J.G.Pasko and W.E.Tennant. J. Appl. Phys. 57 (1985) 4721.
- [21] J.G.Fleming and D.A.Stevenson. to be submitted.
- [22] E.Bauser and H.P.Strunk. J. Crystal Growth. 69 (1984) 561.
- [23] E.Bauser and H.Strunk, Thin Solid Films. 93 (1982) 185.
- [24] E.Bauser and W.Hagen. J. Crystal Growth. 50 (1980) 771.
- [25] E.Bauser and H.Strunk. J. Crystal Growth. 51 (1981) 362.
- [26] B.Fischer, E.Bauser, P.A.Sullivan and D.L.Rode. Appl. Phys. Lett. 33 (1978) 78.
- [27] T.Kajimura, K.Aiki and J. Umeda. Appl. Phys. Lett. 30 (1977) 526.



- [28] T.Nishinaga, T.Kazuno, T.Tanbo, J.Koide, K.Pak, T.Nakamura and  
Y.Yasuda. J. Crystal Growth. 65 (1983) 607.
- [29] D.L.Rode. Phys.Stat.Sol. (a) 32 (1975) 425.

### Table Captions.

Table 1. Measured radii of curvature for two lenticular substrates at 1 mm. ~~and~~ 2 mm. away from the highest point on each sample. Two values are given at each distance, one averaged from the "north-south" directions, the other from the "east-west" directions. The radius of curvature of the pattern was 8.75 cm.

Table 2. The results and growth parameters of a series of LPE and ISOVPE experiments. The LPE layers were grown on  $\text{Cd}_{0.945}\text{Zn}_{0.055}\text{Te}$  and the ISOVPE layers were grown on CdTe.

Table 1.

Sample	Radius at 1mm	Radius at 2mm
1	<del>6.7</del> cm. 8.7 cm.	8.5 cm. 7.4 cm.
2	8.3 cm. 4.2 cm.	7.5 cm. 10.3 cm.

Table 1. Measured radii of curvature for two samples at 1mm and 2mm away from the highest points on the sample. Each has two values one from the "north-south" direction, the other from the "east-west" direction. The radius of curvature of the original pattern was 8.75 cm.

Table 2

LPE on Cd Zn Te. (4.5% ZnTe).  
VPE on CdTe

Method	X Value	Critical Angle	Thickness	Temp.	Cooling Rate.	Face
LPE	0.2	0.25 +0.1°	~10 micron.	500°C	0.3°C/min.	A
LPE	0.2	0.25° "	~10 micron	500°C	0.3°C/min.	A
VPE	0.25	0.30° "	~200 micron	600°C		A
VPE	0.3	0.15° "	~12 micron	500°C		A
VPE	0.2	0.25° "	~60 micron	550°C		B
VPE	0.2	0.15° "	~60 micron	550°C		B
VPE	0.2	0.15° "	~60 micron	550°C		B

## Figure Captions.

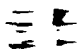
 Fig. 1. Optical micrographs of the terraced surface morphology commonly found on layers grown by LPE.

Fig. 2. The jig used to form the lenticular substrates. The sample is held by yellow wax at the end of an aluminum shaft which is rotated by hand. A slurry of 400 grit SiC in ethylene glycol was used to rough form the surface. The substrates were then hand finished with 600 grit SiC followed by 0.2 micron  $\text{Al}_2\text{O}_3$  in a 2% Br/ethylene glycol solution. Just before growth the layers were etched for 2 minutes in a 4% Br/methanol solution.

Fig. 3. Optical micrographs of ISOVPE and LPE layers grown on the lenticular substrates. a) An ISOVPE layer 200 microns thick grown at 600°C. b-d) LPE layers grown on the A (Cd) face of  $\text{Cd}_{0.955}\text{Zn}_{0.045}$  at 500°C using a cooling rate of 0.3°C/min; the layers are ~10 microns thick.



Fig. 1. Optical micrographs of the terraced surface morphology commonly found on layers grown by LPE.

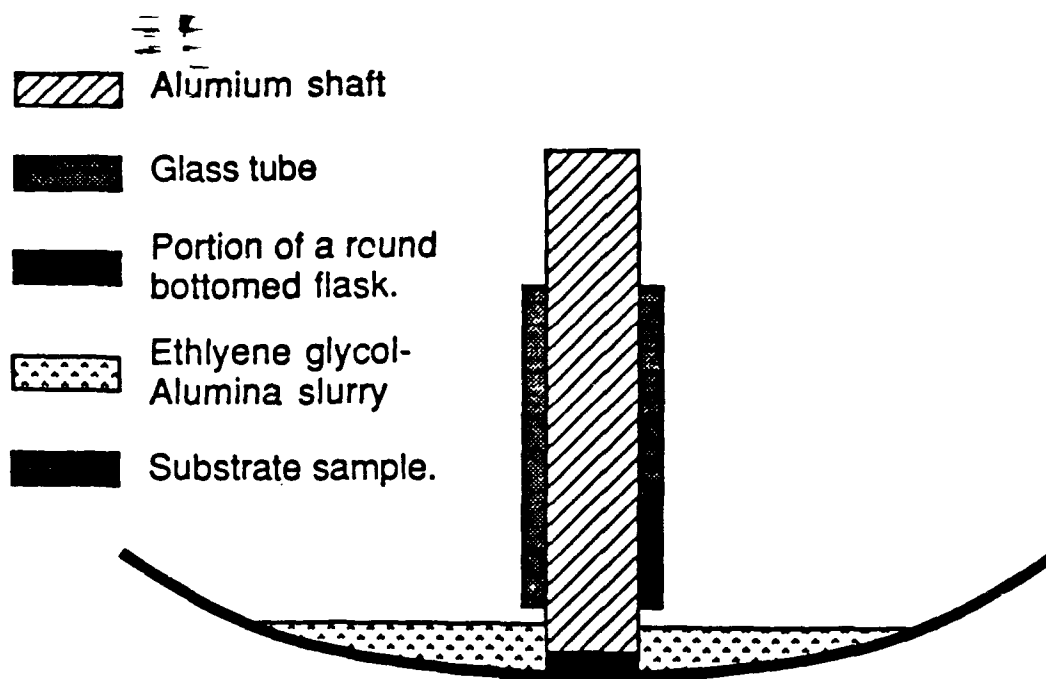


Fig. 2. The jig used to form the lenticular substrates. The sample is held by yellow wax at the end of an aluminum shaft which is rotated by hand. A slurry of 400 grit SiC in ethylene glycol was used to rough form the surface. The substrates were then hand finished with 600 grit SiC followed by 0.2 micron  $\text{Al}_2\text{O}_3$  in a 2% Br/ethylene glycol solution. Just before growth the layers were etched for 2 minutes in a 4% Br/methanol solution.

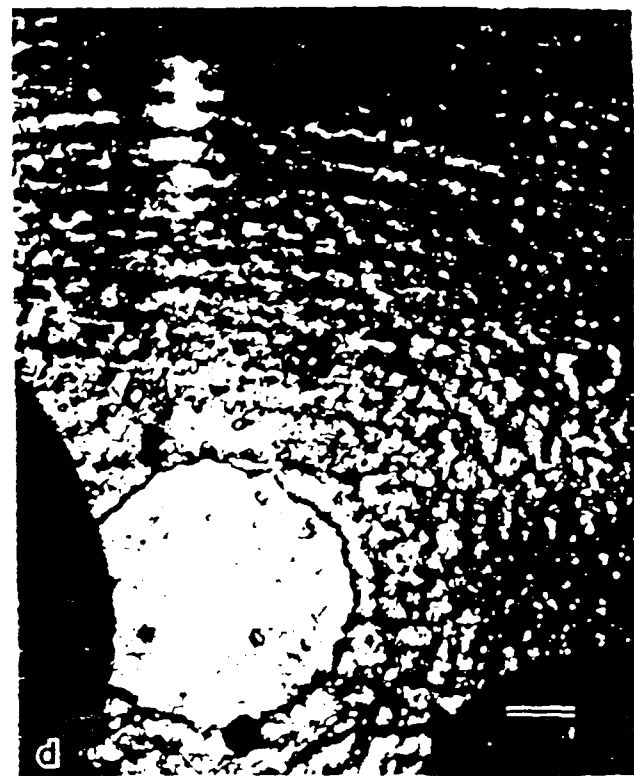


Fig. 3. Optical micrographs of ISOVPE and LPE layers grown on the lenticular substrates. a) An ISOVPE layer 200 microns thick grown at 600°C. b-d) LPE layers grown on the A (Cd) face of  $\text{Cd}_{0.955}\text{Zn}_{0.045}$  at 500°C using a cooling rate of 0.3°C/min; the layers are ~10 microns thick.



## Appendix D:

# Cooling rate dependence of the morphology of $\text{Hg}_{0.80}\text{Cd}_{0.20}\text{Te}$ liquid phase epitaxial layer

S. H. Suh<sup>a)</sup> and D. A. Stevenson

Department of Materials Science and Engineering, Stanford University, Stanford, California 94305

(Received 3 June 1986; accepted 19 September 1987)

$\text{Hg}_{0.80}\text{Cd}_{0.20}\text{Te}$  liquid phase epitaxial layers were grown at 502 °C on CdTe substrates. The cooling rate was varied from 0.15 to 1.32 °C/min, and the terrace surface morphologies were evaluated for all the liquid phase epitaxial (LPE) layers. The width of terraces was inversely proportional to the cooling rate. This result is explained by the increase in constitutional supercooling with increasing cooling rate. Composition of the LPE layer was uniform up to the surface except at the interface region. The composition profile did not depend on the cooling rate.

## I. INTRODUCTION

Mercury cadmium telluride,  $\text{Hg}_{1-x}\text{Cd}_x\text{Te}$ , is an important material for the fabrication of advanced photovoltaic and photoconductive devices. The quench and annealing (QA) solid-state recrystallization method has been most extensively used to produce this material; however, only small-diameter crystals are obtained by this method because of the high Hg pressures involved. Furthermore, the crystals are not oriented. In order to obtain  $\text{Hg}_{1-x}\text{Cd}_x\text{Te}$  of large dimensions and good composition uniformity, attention has been given to the liquid phase epitaxial (LPE) growth technique.<sup>1-6</sup>

One of the major problems with the LPE process is the difficulty in obtaining good surface morphology of the LPE layers. There have been only a few studies on the morphology of  $\text{Hg}_{1-x}\text{Cd}_x\text{Te}$  LPE layers. Wang *et al.*<sup>2</sup> reported terrace substructure of LPE layers grown on (111) Cd surface of CdTe substrates and the formation of voids in LPE layers on the (111) Te surface. Edwall *et al.*<sup>3</sup> reported that surface morphology of the LPE layers depends on the orientation of the CdTe substrates as well as on the crystalline quality of the substrate.

However, there have been no studies reported on the cooling rate dependence of the morphology of  $\text{Hg}_{1-x}\text{Cd}_x\text{Te}$  LPE layers. The cooling rate plays a major role in determining the cell spacing in cellular solidification<sup>7</sup>; thus, we would expect a cooling rate dependence of the surface morphology for the liquid phase growth of  $\text{Hg}_{1-x}\text{Cd}_x\text{Te}$ . This paper reports the cooling rate dependence of the surface morphology of  $\text{Hg}_{0.80}\text{Cd}_{0.20}\text{Te}$  grown on CdTe substrates.

## II. LPE FILM GROWTH PROCEDURES AND ANALYSIS

LPE film growth was accomplished by a tipping technique. Figure 1 shows a quartz ampule which contains a melt, graphite substrate holder, substrate, spacers, and a quartz plug. A composition of the LPE melt ( $\text{Hg}:\text{Cd}:\text{Te} = 18:1.1:80.9$  at. %) was selected from the liquidus and solidus data of Harman,<sup>4</sup> so that a  $\text{Hg}_{0.80}\text{Cd}_{0.20}\text{Te}$  LPE layer could be grown at 502 °C. The LPE melt was obtained by the following procedure: 15 g of the above mixture of Hg, Cd, and Te of "5 nines" purity was placed in a quartz ampule, which was then evacuated, sealed, heated to 600 °C for 24 h, and water cooled to form an ingot.

The dimension of CdTe substrates used was typically

5×15 mm; chem-mechanically polished substrates were supplied by the Rockwell International Science Center. The orientation of all substrates was measured to be 1° off the (111) plane by Laue x-ray diffraction. Substrates were chemically etched with a 5% bromine-methanol solution just prior to growth. The substrate was mounted in the graphite holder so that only the (111) Cd surface was exposed to the melt.

After loading the 15-g melt ingot and the substrate into the 17-mm-i.d. quartz ampule, the quartz ampule was evacuated and sealed. LPE growth was performed in a tilting furnace whose temperature uniformity was better than 0.2 °C in the active zone (75 mm long). The ampule was heated to 502 °C and held at this temperature for 1 h. The furnace was then tilted by 180°, so that the entire substrate was immersed in the melt. To insure that both the substrate and the melt were exactly at the same temperature, the furnace was held at 502 °C for four additional minutes before initiation of the cooling. Different cooling rates from 0.15 to 1.32 °C/min were used. The extent of cooling in order to obtain about the same thicknesses of the LPE layer (20 μm with each cooling rate was calculated by the following equation<sup>8</sup>:

$$d = C \{R_G t\}^{1/2}.$$

Here,  $d$  is the thickness of LPE layer,  $C$  is a material constant,  $R_G$  is the cooling rate, and  $t$  is the growth time. Table I summarizes the cooling rates, extent of cooling, and thickness of LPE layers obtained. When the growth was completed, the furnace was tilted back and the ampule was immedi-

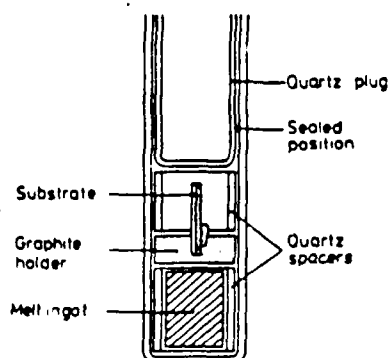


FIG. 1. Quartz ampule for LPE growth of  $\text{Hg}_{1-x}\text{Cd}_x\text{Te}$ .

TABLE I. LPE growth parameters.

Run no.	Cooling rate (°C/min)	Degree of cooling (°C)	Thickness of LPE layer (μm)
513	0.15	4.8	24
803	0.25	5.7	18
919	0.52	7.3	21
805	1.32	10	20

ately removed from the furnace and air cooled.

Surface morphologies of LPE layers were observed by an optical microscope. Cross sections of LPE layers were observed on the (110) cleaved planes which were polished with 0.03-μm alumina powder after grinding with 600-grit paper. Electron microprobe analysis was performed across (110) cleaved planes. The size of the electron beam of ~3 μm limited the resolution of composition versus distance at the interface region to ~3 μm; however, the accuracy of the composition measurement was better than 5%.

### III. RESULTS AND DISCUSSIONS

Figures 2(a)–2(d) show the surface morphology of the  $\text{Hg}_{0.80}\text{Cd}_{0.20}\text{Te}$  LPE layers grown with different cooling rates. Terrace surface morphologies and circular extrusions are seen on all LPE specimens. Results of microprobe analysis indicate that the compositions of circular extrusions are the same as the ones on flat areas. These circular extrusions are believed to arise from either dislocations or defects grown from the substrate and they appear to act as pinning points for the movement of terrace edges.

Terracelike surface morphologies have been reported for GaAs,<sup>9</sup> GaP,<sup>10</sup> and InP<sup>11</sup> as well as for HgCdTe.<sup>2,3</sup> A slight misorientation of substrates from the low-index planes, such as (111) and (110), may cause a terracelike surface morphology. A misoriented substrate contains native steps on the surface which are believed to play an essential role in the formation of terraces. It has been proposed that a grouping of the native steps leads to terraces that are several tens of microns wide.<sup>12</sup>

We propose a different mechanism for the formation of terraces in accord with the following model. There is a strong tendency of a growing front to maintain an exact (111) orientation. On the other hand, all locations on the substrate tend to have the same growth rate, otherwise, there will be a constitutionally supercooled region between two adjacent growing fronts. The breakdown of the growing front into terraces will accommodate these two conditions.

As we have seen in Figs. 2(a)–2(d), the terrace width decreases with cooling rate. The average terrace widths were plotted against the inverse of the cooling rate in Fig. 3, where the bars indicate the standard deviation of the terrace widths. This figure shows an average terrace width inversely proportional to the cooling rate.

Similar results have been reported for GaAs, GaAlAs,<sup>13</sup> and InP.<sup>11</sup> Small and Potemski<sup>13</sup> studied the effect of the growth rate on the terrace width and reported that the terrace widths of GaAs and GaAlAs LPE layers decrease with

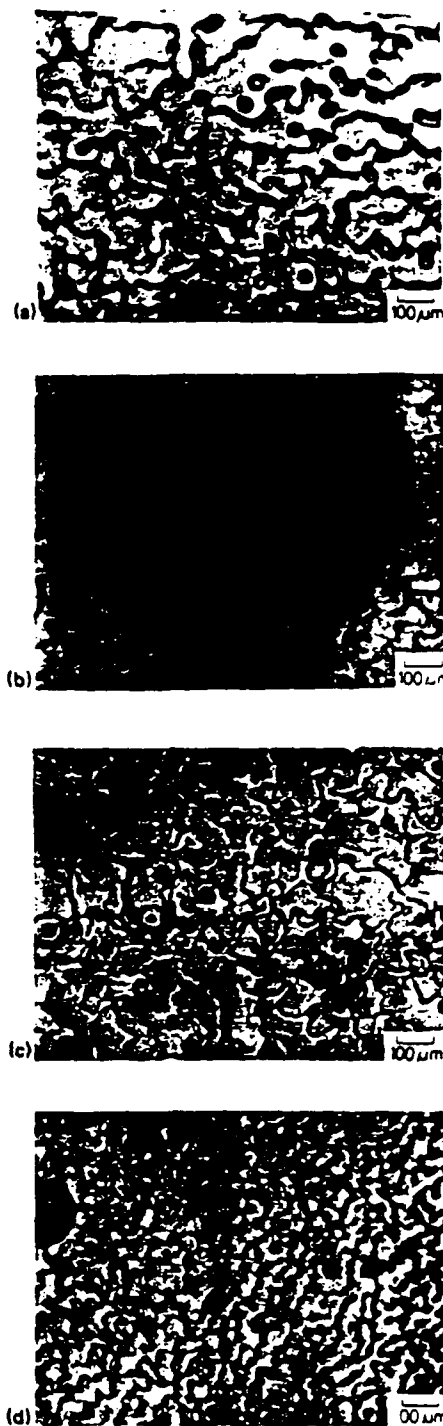


FIG. 2. The surface morphologies of  $\text{Hg}_{0.80}\text{Cd}_{0.20}\text{Te}$  layers grown at different cooling rates: (a) 0.15, (b) 0.25, (c) 0.52, and (d) 1.32 °C/min

increasing growth rate. Pak, Nishinaga, and Uchiyama<sup>11</sup> reported that the terrace width of the InP LPE layers decreases with increasing supersaturation. Since the cooling rate and the growth rate are expected to be approximately proportional to the extent of supercooling,<sup>7</sup> our observations on HgCdTe concern the same phenomena as the result of Small and Potemski on GaAs and GaAlAs and the result of Pak, Nishinaga, and Uchiyama on InP.

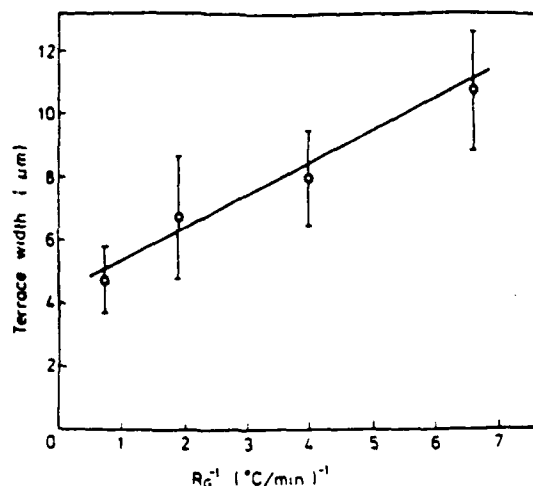


FIG. 3. Dependence of terrace width on the cooling rate  $R_G$ .

Our cooling rate dependence of the terrace width may be explained qualitatively by the model for the development of a cellular morphology upon solidification<sup>7</sup>; the terrace width adjusts in order to reduce constitutional supercooling. If the terrace spacing is sufficiently wide for the development of regions between terraces that are supercooled, then a new terrace will be nucleated (see Fig. 4). Since the concentration difference between points A and B in Fig. 4 is proportional to the cooling rate, the degree of supercooling is roughly proportional to the cooling rate with a terrace width inversely proportional to the cooling rate.

On the other hand, Nishinaga developed a morphological stability theory for supercooled LPE by modifying Mullin and Sererka's interface stability theory.<sup>15</sup> The resulting theory predicts a critical wavelength, i.e., a minimum stable distance between terraces. The critical wavelength is proportional to the interfacial free energy and inversely proportional to the degree of supercooling. There is insufficient evidence at present to establish one of the two models, the constitutional supercooling theory and the morphological stability theory are more appropriate. A well-established theory that correctly predicts the most stable terrace width for varying degrees of supercooling is not yet available.

Figure 5 shows the composition profile of the LPE layers. Uniform composition is maintained up to the surface except at the interface region which is  $\sim 3\text{--}5\text{ }\mu\text{m}$  thick. The composition profile does not depend on the cooling rate. For LPE growth with slider systems which use small amounts of melt, composition profiles showing gradual decrease in the  $X$  value have been reported.<sup>3,5</sup> By contrast, Shaw<sup>16</sup> predicts an increase in the gradient with increasing cooling rate.

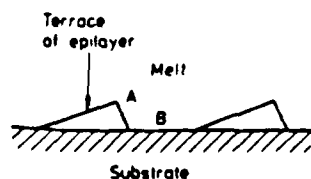


FIG. 4. Schematic description of how terrace width is adjusted.

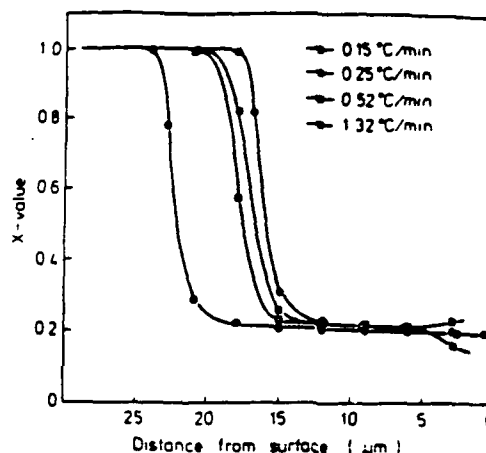


FIG. 5. Composition profile of LPE layers grown with different cooling rates.

#### IV. SUMMARY

The terrace width of  $\text{Hg}_{0.80}\text{Cd}_{0.20}\text{Te}$  LPE layer decreases with increasing cooling rate and is inversely proportional to the cooling rate. This behavior is explained by an increase in the constitutional supercooling with increasing cooling rate. The composition was uniform up to the surface except at the interface region and the composition profile does not depend on the cooling rate.

#### ACKNOWLEDGMENTS

One of the authors (S. H. Suh) acknowledges the financial support from the Korean Science and Engineering Foundation and the Korea Advanced Institute of Science and Technology. The authors thank J. G. Fleming and M. F. S. Tang of Stanford University for valuable discussions, and Dr. M. Brown of the Grumman Corporate Research Center for helpful discussions and for supplying CdTe substrates. The authors acknowledge the role of the Central Facilities at the Center for Materials Research of Stanford University. This work was supported by DARPA, through the Office of Naval Research Contract No. N00014-84K-0423.

<sup>11</sup> On leave from Korea Advanced Institute of Science and Technology, Seoul, Korea.

<sup>12</sup> J. L. Schmit, *J. Cryst. Growth* **65**, 249 (1983).

<sup>13</sup> C. C. Wang, S. H. Shin, M. Chu, M. Lanir, and A. H. B. Vanderwyck, *J. Electrochem. Soc.* **127**, 175 (1980).

<sup>14</sup> D. D. Edwall, E. R. Gertner, and W. E. Tennant, *J. Appl. Phys.* **55**, 1453 (1984).

<sup>15</sup> T. C. Harman, *J. Electron. Mater.* **9**, 945 (1980).

<sup>16</sup> J. A. Mroczkowski and H. R. Vidyant, *J. Electrochem. Soc.* **128**, 655 (1981).

<sup>17</sup> K. Nagahama, R. Ohkata, K. Nishitani, and T. Murotani, *J. Electron. Mater.* **13**, 67 (1984).

<sup>18</sup> M. C. Flemings, *Solidification Processing* (McGraw-Hill, New York, 1974), p. 83.

<sup>19</sup> M. Feng, L. W. Cook, M. M. Tashima, and G. E. Stillman, *J. Electron. Mater.* **9**, 241 (1980).

<sup>20</sup> E. Bauser and H. P. Strunk, *J. Cryst. Growth* **69**, 561 (1984).

- <sup>10</sup>R. H. Saul and D. D. Roccasecca, *J. Appl. Phys.* **44**, 1983 (1983).
- <sup>11</sup>K. Pak, T. Nishinaga, and S. Uchiyama, *Jpn. J. Appl. Phys.* **16**, 949 (1977).
- <sup>12</sup>R. L. Moon, in *Crystal Growth*, edited by B. R. Pamplin (Pergamon, New York, 1980), p. 441.
- <sup>13</sup>M. B. Small and R. M. Potemski, *J. Cryst. Growth* **37**, 163 (1977).
- <sup>14</sup>T. Nishinaga, in *Semiconductor Optoelectronics* edited by A. Herman (Wiley and Polish Scientific, New York, 1980), p. 131.
- <sup>15</sup>W. W. Mullins and R. F. Sekerka, *J. Appl. Phys.* **35**, 444 (1964).
- <sup>16</sup>D. W. Shaw, *J. Cryst. Growth* **62**, 247 (1983).

LIQUID PHASE EPITAXIAL GROWTH OF  $\text{Hg}_{0.8}\text{Cd}_{0.2}\text{Te}$  ON  
 $\text{Cd}_{1-x}\text{Zn}_x\text{Te}$  SUBSTRATES AND THE DEPENDENCE OF THE SURFACE  
MORPHOLOGY ON THE SUBSTRATE ORIENTATION

S. H. Suh\* and D. A. Stevenson

Department of Materials Science and Engineering  
Stanford University, Stanford, CA 94305

\*On leave from the Korea Advanced Institute of Science and  
Technology, Seoul. Korea

Abstract

$\text{Cd}_{1-x}\text{Zn}_x\text{Te}$  ( $x = 0.02$  and  $0.04$ ) single crystals were grown by a vertical Bridgman method and were used as substrates for the liquid phase epitaxial (LPE) growth of  $\text{Hg}_{0.8}\text{Cd}_{0.2}\text{Te}$ . Smooth virtually terrace-free LPE surfaces were obtained by using a substrate with nearly perfect (111) Cd orientation. As the surface orientation of the substrate deviates from (111) Cd, terracing becomes more prevalent. Replacing CdTe with  $\text{Cd}_{1-x}\text{Zn}_x\text{Te}$  does not completely suppress the formation of terraces. The superior quality of the layers grown on  $\text{Cd}_{1-x}\text{Zn}_x\text{Te}$  substrates is probably due to lower dislocation densities and/or better lattice matching of substrates. The microhardness of  $\text{Cd}_{1-x}\text{Zn}_x\text{Te}$  increased with increasing  $x$ -value, being roughly 30% greater for  $x = 0.04$  as compared with  $x = 0$ .

## Introduction

The semiconductor  $\text{Hg}_{1-x}\text{Cd}_x\text{Te}$  is an important material for infrared detectors in the wavelength region of 3-5 and 8-14  $\mu\text{m}$ . Several techniques such as quench/anneal, vapor phase epitaxy growth, MBE, MOCVD, and LPE growth have been used to prepare this material [1]. Recently, the LPE technique has been used to obtain larger sample areas with good compositional uniformity [2-6].

CdTe is the most common substrate for LPE of  $\text{Hg}_{1-x}\text{Cd}_x\text{Te}$  because of the close lattice match between CdTe and  $\text{Hg}_{1-x}\text{Cd}_x\text{Te}$ . Terraces are observed on the LPE surfaces, if the orientation of the substrate surface deviates from the (111) plane [2]. It is known that dislocations are formed at the interface between CdTe substrate and  $\text{Hg}_{1-x}\text{Cd}_x\text{Te}$  LPE layer and are propagated into the epitaxial layer [7]. Bell and Sen [8] used  $\text{Cd}_{1-x}\text{Zn}_x\text{Te}$  as a substrate in order to reduce the dislocation density in the LPE layer and they obtained a good surface morphology of  $\text{Hg}_{0.80}\text{Cd}_{0.20}\text{Te}$  LPE layers with  $\text{Cd}_{0.96}\text{Zn}_{0.04}\text{Te}$  substrates, which have an almost perfect lattice match.

The surface morphology of  $\text{Hg}_{1-x}\text{Cd}_x\text{Te}$  LPE layers depend strongly on the orientation of the substrate [3]. It is not clear in Bell and Sen's paper whether the lattice match, substrate quality, or the orientation plays the major role in improving surface quality. In the present study, we investigate the dependence of the surface morphology on the orientation of  $\text{Cd}_{1-x}\text{Zn}_x\text{Te}$ .

### Growth of $\text{Cd}_{1-x}\text{Zn}_x\text{Te}$ Single Crystals

Two boules of  $\text{Cd}_{1-x}\text{Zn}_x\text{Te}$  crystals with  $x$  values of 0.02 and 0.04 were grown by the vertical Bridgman method. A 25mm I.D. quartz tube was loaded with 200 g of 6 nines grade Cd, Zn, and Te. The quartz tube was sealed after evacuating for 1 hr. at  $10^{-7}$  torr. After homogenizing the melt at  $1160^\circ\text{C}$  for 12 hrs, the furnace was raised at 1 mm/hr., with a temperature gradient at the liquid-solid interface of  $28^\circ\text{C}/\text{cm}$ .

The boule with  $x = 0.04$  consisted of three large grains, with the largest comprising two thirds of the boule. The boule with  $x = 0.02$  was a single crystal except at the bottom. The CdTe-ZnTe pseudo-binary system has a narrow liquidus-solidus region [9], thus, the problems of segregation and constitutional supercooling are not too serious in this system. Electron microprobe analysis shows a variation of about 10% in composition from the bottom to the top of the boules.

Crystals were oriented by a goniometer with the Laue method, so that a (111) plane could be obtained and 2 mm thick slices were cut with an abrasive wire saw. Sliced substrates were chem-mechanically polished for about 1 hr. with 1.5% bromine in ethylene glycol.

### LPE Film Growth

A composition of LPE melt ( $\text{Hg}:\text{Cd}:\text{Te}=18:1.1:81$  a/o) was selected from the liquidus and solidus data of Harman [4] in order to grow a  $\text{Hg}_{0.80}\text{Cd}_{0.20}\text{Te}$  LPE layer at  $502^\circ\text{C}$ . LPE melt ingots of 15 g were obtained by water cooling melts after heating at  $600^\circ\text{C}$  for 24 hrs.

A tipping technique was used for LPE film growth and is described below. Figure 1 shows an ampule of 17 mm I.D. which contains a melt ingot, a graphite holder, a substrate, spacers, and a quartz plug. The quartz ampule was evacuated and sealed at a pressure of  $10^{-7}$  torr. The LPE film growth was performed in a tilting furnace whose temperature uniformity was better than  $\pm 0.25^\circ\text{C}$  for an active zone of 75 mm. Ampules were heated to  $502^\circ\text{C}$  and held at this temperature for 1 hr. The furnace was then tilted  $180^\circ$  to immerse the substrate in the melt. The furnace was cooled down by  $10^\circ\text{C}$  at  $0.25^\circ\text{C}/\text{min}$ , and then the furnace was tilted back and the ampule immediately removed from the furnace.

#### Results and Discussion

Figure 2(a) shows the surface morphology of a  $\text{Hg}_{0.80}\text{Cd}_{0.20}\text{Te}$  LPE layer grown on a  $\text{Cd}_{0.98}\text{Zn}_{0.02}\text{Te}$  substrate with an almost perfect (111) Cd orientation. The surface morphology is featureless, except for two vertical lines and small extrusions accompanied by wave-like short lines. The small extrusions are believed to originate from defects in the substrate. Figure 2(b) is the cross section of the same epitaxial layer; the flat surface also indicates a terrace free surface.

Terrace surface morphology is always observed when we use a CdTe substrate, even when the orientation of the surface is close to (111) Cd [3]. To check whether the excellent surface morphology obtained with the  $\text{Cd}_{0.98}\text{Zn}_{0.02}\text{Te}$  substrate was due to perfect orientation of the substrate or to improved perfection of lattice match caused by the presence of Zn, substrates whose surfaces



were off the (111) Cd orientation by  $2^\circ$  ( $\text{Cd}_{0.98}\text{Zn}_{0.02}$ ) and by  $4^\circ$  ( $\text{Cd}_{0.96}\text{Zn}_{0.04}\text{Te}$ ) were used to grow LPE layers. Figures 3 and 4 show the surface morphologies of the resulting layers. Changes of the surface morphology with the increase of the deviation from the exact (111) Cd orientation are clearly seen. Terraces are observed on LPE layer surfaces grown on the  $2^\circ$  misoriented substrate and, as the misorientation increases to  $4^\circ$ , continuity between adjacent terraces disappears.

These results can be explained as follows. Growth of LPE layers are limited by two factors: every region on the substrate tends to have the same growth speed, and a growing front tends to maintain the exact (111) Cd orientation, as closely as possible. The only way to satisfy these two conditions at the same time is to break down the growing front into small units or terraces. If the misorientation becomes as large as  $4^\circ$ , planes perpendicular to (111) want to maintain their own crystallographic planes, instead of being smoothly connected to adjacent terraces. It is clear that the terrace surface morphology is due to surface misorientation from the exact (111) Cd plane and replacing a CdTe substrate with a  $\text{Cd}_{1-x}\text{Zn}_x\text{Te}$  substrate does not suppress this tendency.

The smooth surfaces obtained with  $\text{Cd}_{1-x}\text{Zn}_x\text{Te}$  substrates are thought to arise partly from reduced lattice strain due to better lattice matching between the substrate and the LPE layer. Lower dislocation densities of the  $\text{Cd}_{1-x}\text{Zn}_x\text{Te}$  substrates also may cause lower densities of extrusions.

Figure 5 shows the composition profile of the LPE layer measured by an electron microprobe. Very uniform composition is maintained up to the surface. The interface region is shown to be about 3  $\mu\text{m}$  in this composition profile.

The easier growth of single crystals of  $\text{Cd}_{1-x}\text{Zn}_x\text{Te}$ , as compared to  $\text{CdTe}$ , and the apparent improvement in surface imperfections may arise from a higher hardness for the ternary alloy, due to solid solution hardening. Sher et al. [10] predicted theoretically the increase of hardness with the increase of  $x$ -value in  $\text{Cd}_{1-x}\text{Zn}_x\text{Te}$ . They suggested that the shorter bond length of  $\text{ZnTe}$  in  $\text{Cd}_{1-x}\text{Zn}_x\text{Te}$  gives rise to a higher dislocation energy and a higher hardness. In order to test this idea, we measured the microhardness of these alloys and of  $\text{CdTe}$ . Table 1 shows the results of microhardness measurements of  $\text{CdTe}$  and  $\text{Cd}_{1-x}\text{Zn}_x\text{Te}$ . Hardness increased by about 30% by replacing  $\text{CdTe}$  of 4% with  $\text{ZnTe}$ .

#### Summary

The development of surface terraces is a natural tendency in liquid phase epitaxy, if substrates are not precisely oriented. For example, the  $\text{Hg}_{1-x}\text{Cd}_x\text{Te}$  LPE layer tries to maintain the exact (111) orientation and terraces develop if the substrate is misoriented. The tendency is observed with  $\text{Cd}_{1-x}\text{Zn}_x\text{Te}$  substrates as well as with  $\text{CdTe}$  substrates. Smooth LPE layers with fewer defects are obtained with  $\text{Cd}_{1-x}\text{Zn}_x\text{Te}$  substrates. Lower dislocation densities and/or better lattice matching contribute to this improvement.

Microhardness of  $\text{Cd}_{1-x}\text{Zn}_x\text{Te}$  increases with increasing  $x$ -value. Thus,  $\text{Cd}_{1-x}\text{Zn}_x\text{Te}$  is more resistant to breakage and developing scratches. The higher microhardness would also be expected to establish lower dislocation densities for  $\text{Cd}_{1-x}\text{Zn}_x\text{Te}$ , as compared to  $\text{CdTe}$ .

#### Acknowledgment

The authors thank Professor R. S. Feigelson and Dr. R. K. Route of Stanford University for advice and facilities for the growth of the  $\text{Cd}_{1-x}\text{Zn}_x\text{Te}$  single crystals and J. G. Fleming and M.F.S. Tang of Stanford University for valuable discussions. One of the authors (S.H. Suh) expresses his appreciation to the Korean Science and Engineering Foundation and Korea Advanced Institute of Science and Technology for fellowship support. This work was supported by DARPA through the Office of Naval Research, contract NO. N00014-84K-0423.

## References

1. J. L. Schmit, J. Crystal Growth 65 (1983) 249.
2. C. D. Wang, S. H. Shin, M. Chu, M. Lanir and A.H.B. Vanderwyck, J. Electrochem. Soc. 127 (1980) 175.
3. D. D. Edwall, E. R. Gertner and W. E. Tennant, J. Appl. Phys. 55 (1984) 1453.
4. T. C. Harman, J. Electron. Mater. 9 (1980) 945.
5. J.A. Mroczkowski and H.R. Vydyanath, J. Electrochem. Soc. 128 (1981) 655.
6. K. Nagahama, R. Ohkata, K. Mishitani and T. Murotani, J. Electron. Mater. 13 (1984) 67.
7. G.R. Woolhouse, H. Kawayoshi and T.J. Magee, "Spatially Distributed Misfit Dislocations in LPE  $\text{Cd}_x\text{Hg}_{1-x}\text{Te}$  ( $0.2 < x < 0.4$ ) Films Grown on CdTe Substrates." AACG 6th Conference on Crystal Growth, Stanford Sierra Camp, CA June 1-4 (1982).
8. S.L. Bell and S. Sen, J. Vac. Sci. Technol. A3 (1985) 112.
9. J. Steininger, A. J. Strauss and R. F. Brebrick, J. Electrochem. 117 (1970) 1305.
10. A. Sher, A. Chen, W. E. Spicer and C. Shih, "Proceedings of 1984 workshop on the Physics and Chemistry of Mercury Cadmium Telluride".

Fig. 1 Quartz ampule for LPE growth of  $\text{Hg}_{1-x}\text{Cd}_x\text{Te}$ .

Fig. 2 (a) The surface morphology of an  $\text{Hg}_{0.80}\text{Cd}_{0.20}\text{Te}$  layer grown on a  $\text{Cd}_{0.98}\text{Zn}_{0.02}\text{Te}$  substrate whose surface is less than  $0.2^\circ$  off (111) (b) The cross section of the above LPE layer.

Fig. 3 The surface morphology of an  $\text{Hg}_{0.80}\text{Cd}_{0.20}\text{Te}$  layer grown on a  $\text{Cd}_{0.98}\text{Zn}_{0.02}\text{Te}$  substrate whose surface is  $2^\circ$  off (111).

Fig. 4 The surface morphology of an  $\text{Hg}_{0.80}\text{Cd}_{0.20}\text{Te}$  layer grown on a  $\text{Cd}_{0.96}\text{Zn}_{0.04}\text{Te}$  substrate whose surface is  $4^\circ$  off (111).

Fig. 5 Composition profile of the LPE layer grown on a  $\text{Cd}_{0.98}\text{Zn}_{0.02}\text{Te}$  substrate.

Table 1 Microhardness of  $\text{Cd}_{1-x}\text{Zn}_x\text{Te}$  and  $\text{CdTe}$  ( $\text{Kg/mm}^2$ )

$\text{CdTe}$	$\text{Cd}_{0.98}\text{Zn}_{0.02}\text{Te}$	$\text{Cd}_{0.96}\text{Zn}_{0.04}\text{Te}$
$46.0 \pm 1.0$	$52.4 \pm 1.2$	$59.4 \pm 3.6$

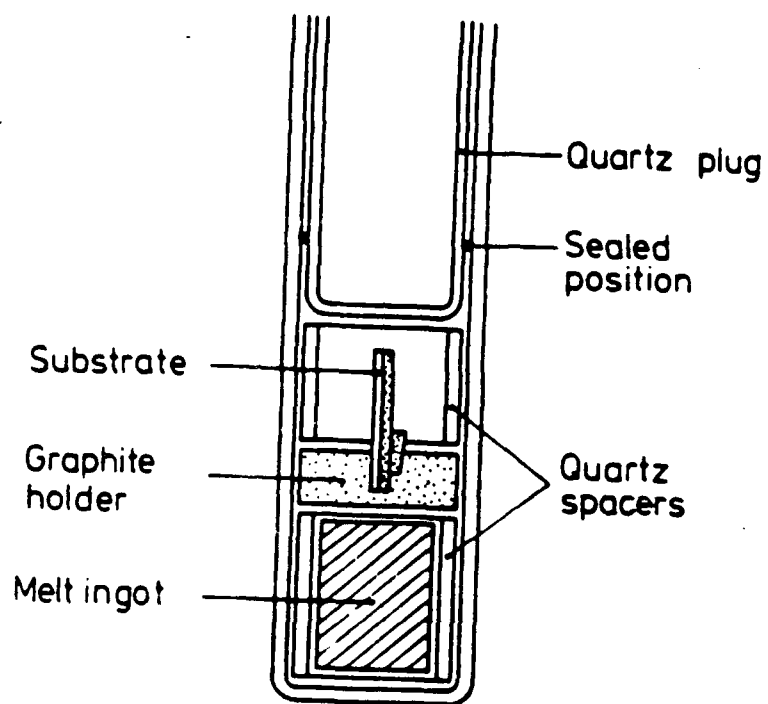


Fig. 1 Quartz ampule for LPE growth of  $\text{Hg}_{1-x}\text{Cd}_x\text{Te}$ .

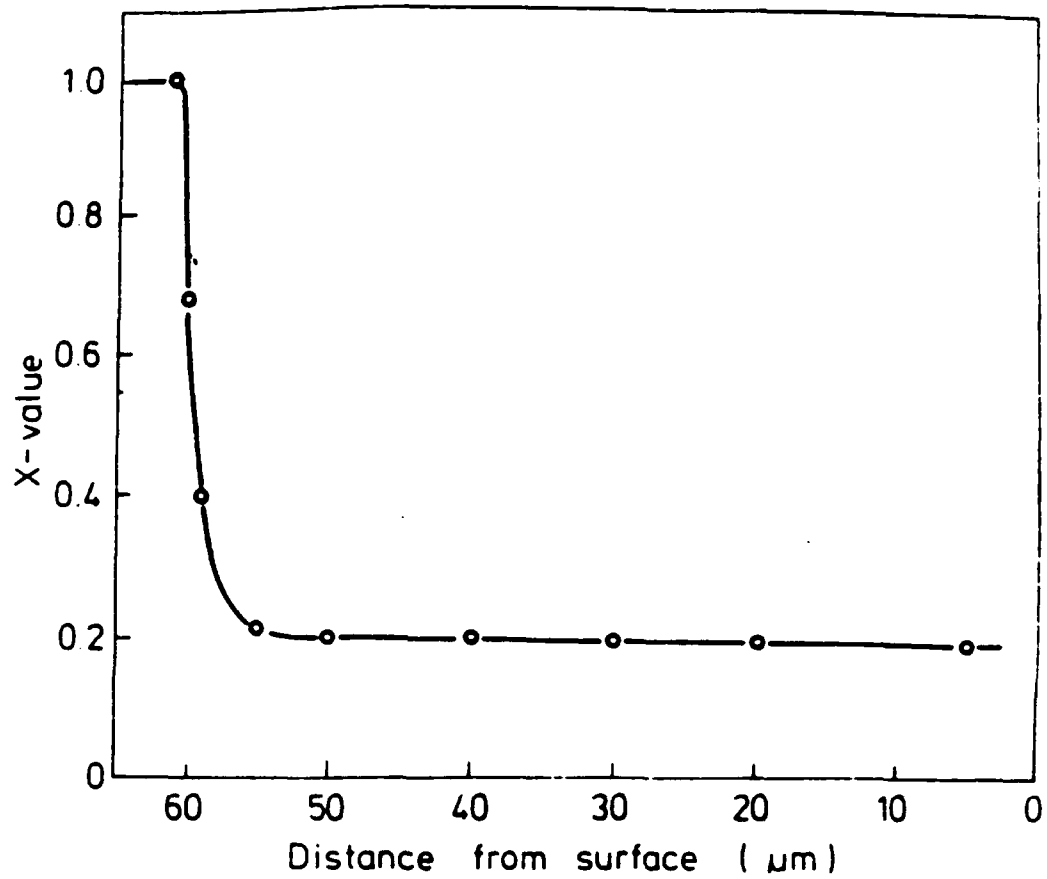


Fig. 5 Composition profile of the LPE layer grown on a  $\text{Cd}_{0.98}\text{Zn}_{0.02}\text{Te}$  substrate.



phys. stat. sol. (a) 105, 77 (1987)

Subject classification: 66.30; 68.55; 58.15

Department of Materials Science and Engineering, Stanford University<sup>1)</sup>

# Interdiffusion in Mercury Cadmium Telluride Evaluated from Vapor Phase Growth Kinetics

By

J. G. FLEMING and D. A. STEVENSON

A method is presented for determining interdiffusion coefficients from the kinetics of isothermal vapor phase epitaxial growth of mercury cadmium telluride ( $\text{Hg}_{1-x}\text{Cd}_x\text{Te}$ ). After an initial transient, growth is interdiffusion limited. Interdiffusion coefficients in the composition range  $x = 0.1$  to  $0.7$  and a temperature range of  $450$  to  $700^\circ\text{C}$  are determined using a simple geometric analysis of the composition profiles obtained in this interdiffusion limited regime. The technique offers advantages in simplicity and added control over the defect nature of the material during the interdiffusion process. The interdiffusion coefficients for the composition and temperature range studied are represented by the following equation:  $D_2(\text{cm}^2/\text{s}) = 300 \exp(-7.53x) \exp(-1.92 \text{ eV}/kT)$ . (Comparison with other studies shows good agreement.)

Es wird eine Methode zur Bestimmung der Interdiffusionskoeffizienten aus der Kinetik des isothermen gasphasen-epitaktischen Wachstums von Quecksilber-Kadmiumtellurid ( $\text{Hg}_{1-x}\text{Cd}_x\text{Te}$ ) angegeben. Nach einer Anlaufphase ist das Wachstum diffusionslimitiert. Diffusionskoeffizienten im Zusammensetzungsbereich  $x = 0.1$  bis  $0.7$  und einem Temperaturbereich von  $450$  bis  $700^\circ\text{C}$  werden mittels einfacher geometrischer Analyse der in diesem Interdiffusionsbereich erhaltenen Konzentrationsprofile bestimmt. Die Technik besitzt durch ihre Einfachheit und unveränderte Verbindungseigenschaften Vorteile. Die Technik ermöglicht die Herstellung von Material mit einer Kontrolle über die Defektnatur des Materials während des Interdiffusionsprozesses. Die Interdiffusionskoeffizienten im untersuchten Zusammensetzungsbereich und Temperaturbereich lassen sich durch die Gleichung  $D_2(\text{cm}^2/\text{s}) = 300 \exp(-7.53x) \exp(-1.92 \text{ eV}/kT)$  darstellen. Ein Vergleich mit anderen Untersuchungen zeigt gute Übereinstimmung.

## 1. Introduction

Mercury cadmium telluride ( $\text{Hg}_{1-x}\text{Cd}_x\text{Te}$ ) is an important infrared detector material used in focal plane arrays and spectroscopic detectors and has potential for use in optical communications. Interdiffusion in this system is of practical concern since it determines the width of the transition region between the substrate and an epitaxially grown layer, the stability of  $\text{HgTe/CdTe}$  superlattice structures, and the rate of homogenization of nonuniform bulk material. There has been generally good agreement between previous studies of interdiffusion in  $\text{Hg}_{1-x}\text{Cd}_x\text{Te}$  using the Boltzmann-Matano analysis [1], even though it is not possible to thermodynamically fix the diffusion host in such a ternary system, as is discussed below.

In this paper we present a method for determining interdiffusion coefficients from isothermal vapor phase epitaxial growth and apply this method to our experimental results. The method gives a closed expression for the interdiffusion coefficient which can be readily manipulated to give a closed expression for the composition profile which results during the isothermal vapor phase growth process, if the surface composition, temperature, and growth time are known.

<sup>1)</sup> Stanford, CA 94305, USA.

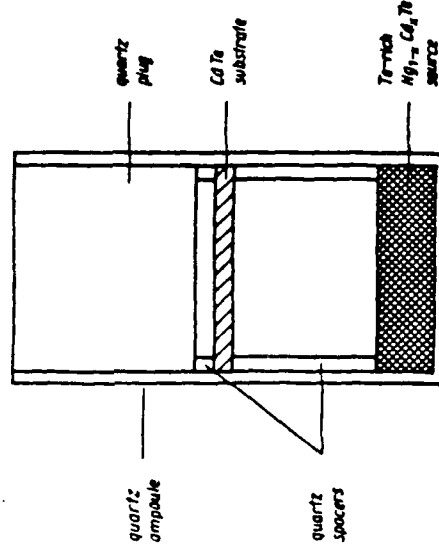


Fig. 1. The general experimental geometry used throughout this work. Before growth, and just after the substrate was etched, the ampoule was evacuated to  $10^{-3}$  to  $10^{-4}$  Torr and sealed.

## 2. The Isothermal Vapor Phase Growth Process

The present method for obtaining interdiffusion information is based on an analysis of the isothermal vapor phase epitaxial technique for growing layers of  $\text{Hg}_{1-x}\text{Cd}_x\text{Te}$ . This growth technique has been used since the 1960's and many observations on the growth kinetics have been reported [3 to 9], but the kinetics and mechanism of the growth process have only recently been analyzed in a fundamental way [10].

A schematic of our growth system is shown in Fig. 1. In our studies, we use a source which fixes the surface composition of the growing layers after an initial transient. This source is a solid-liquid mixture of solid  $\text{Hg}_{1-x}\text{Cd}_x\text{Te}$  of the desired composition and a small amount of an equilibrium Te-rich melt. Such a source establishes a constant chemical potential of all three components in the source throughout the growth run, providing the source is substantially larger than the layer grown. The substrates used were (111)  $\text{CdTe}$ .

Isothermal growth is the result of a two series process: transport of  $\text{Te}_2$  vapor from the source to the substrate surface, where it reacts with ambient  $\text{Hg}$  vapor to deposit  $\text{HgTe}$ ; and interdiffusion between  $\text{Hg}$  and  $\text{Cd}$  in the growing epilayer. The growth kinetics are initially  $\text{Te}_2$  vapor transport limited and then become interdiffusion limited as growth progresses [10]. The interdiffusion limited regime has been observed by many workers [2, 3, 6 to 10]. Since it is possible to grow a  $\text{Hg}_{1-x}\text{Cd}_x\text{Te}$  layer using a pure  $\text{HgTe}$  source, the  $\text{Cd}$  in the layers must come from the substrate. This hypothesis is consistent with the fact that the partial pressure of  $\text{Cd}$  over  $\text{Hg}_{1-x}\text{Cd}_x\text{Te}$  is very much lower than that of the other two components [11, 12], so negligible vapor transport of  $\text{Cd}$  is expected. In fact, if  $\text{Cd}$  vapor transport did take place, it would be from the substrate to the source, since the  $\text{Cd}$  pressure is lower over the source than it is over the substrate.

## 3. Determination of Interdiffusion Coefficients

Critical to any interdiffusion analysis is the selection of a spatial coordinate system and on the present study, the Boltzmann-Matano interface is appropriate. Composition

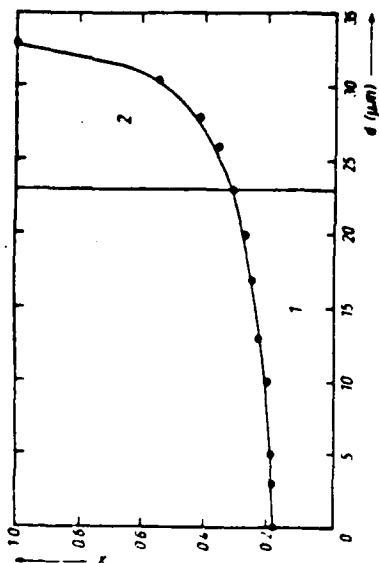


Fig. 2. A plot showing the position of the original substrate surface (observed from the position of alumina markers placed on the substrate before growth). Area 1 roughly equals area 2 and is directly proportional to the amount of Cd which has diffused (interdiffused with Hg) out of the substrate.

profiles of layers grown by the isothermal vapor phase epitaxial technique were determined by electron microprobe analysis and a typical profile is shown in Fig. 2, with the position of the Boltzmann-Matano interface indicated by the vertical line. Area 1, which represents the amount of Cd that has diffused out of the substrate, equals area 2 by conservation of Cd. (There is only a negligible change in the molar volume due to the slight lattice mismatch between CdTe and HgTe.) This plot shows a profile which is roughly rectangular in shape, although nowhere is it actually flat since it results from an interdiffusion process. The nearly rectangular shape of the profile is a result of the strong compositional dependence of the interdiffusion coefficient, as is discussed in the Appendix. Fig. 3 shows the composition profiles of two samples: one grown for 22 h, and the other for 24 h; the profiles have been aligned so that their Boltzmann-Matano interfaces overlap. By conservation of Cd, areas A and B of Fig. 3

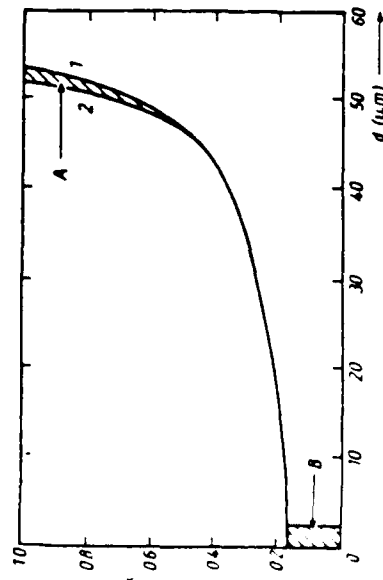


Fig. 3. Two experimentally obtained profiles, one of a sample grown for (1) 24 h and the other for (2) 22 h. The profiles have been aligned so that their Boltzmann-Matano interfaces overlap. By conservation of Cd, areas A and B of Fig. 3

are equal. Area A is directly proportional to the amount of Cd and Hg which have interdiffused through the surface of the growing layer at 22 h. Since we know the amount of material which has interdiffused in a certain period of time, we can determine the interdiffusion coefficient for the composition at the surface of the layer at 22 h from Fick's law for diffusion

$$J \Delta t = \Delta t D_p (dz/dy)_s, \quad (1)$$

where  $J$  is the material flux in the diffusion direction  $y$ ,  $\Delta t$  is the time increment (2 h in this case),  $D_p$  is the interdiffusion coefficient of material at the layer surface,  $z$  is the fraction of CdTe in the formula  $\text{Hg}_{1-x}\text{Cd}_x\text{Te}$ ,  $z^s$  is the composition at the surface of the layer, and  $(dz/dy)_s$  is the concentration gradient at the surface of the layer. The area B of Fig. 3 is directly proportional, through the molar volume, to the moles per unit area which have interdiffused in a time of 2 h. The value of  $D_p$  can therefore be determined using (1), knowing the concentration gradient,  $(dz/dy)_s$ , the time increment,  $\Delta t$ , and the molar volume.

It is notable that the two profiles in Fig. 3 overlap, to within experimental error, up to a composition of  $\approx \text{Hg}_{0.3}\text{Cd}_{0.7}\text{Te}$ . This indicates that a quasi-steady state condition exists throughout this composition range and time interval, and requires that an equal number of moles have interdiffused throughout this composition range. The overlap of the profiles is a result of the strong dependence of the interdiffusion coefficient on composition; a simple mathematical argument for this behavior is given in the Appendix. Interdiffusion coefficients can be calculated for material within this region of overlap using the above analysis and the experimentally determined composition profile with the experimental parameters.

The above analysis requires the accurate determination of two composition profiles which vary only slightly from one another. However, this is difficult to implement experimentally given run to run variations in layer thickness resulting from slightly different growth temperatures, sources to substrate spacing, and substrate quality. It is therefore desirable to develop an analytical technique requiring only a single profile. We develop such a method for interdiffusion limited growth below, using a simplifying assumption about the shape of the composition profile.

Consider two layers grown for times  $t$  and  $t + \Delta t$ , respectively. The layer thickness is given by the following linear/parabolic rate law [10]:

$$Y = Kt^{1/2} + Q \quad (2)$$

and

$$Y + \Delta Y = K(t + \Delta t)^{1/2} + Q, \quad (3)$$

where  $K$  and  $Q$  are constants,  $Y$  is the layer thickness at time  $t$ , and  $Y + \Delta Y$  is the thickness at time  $t + \Delta t$ . Dividing (3) by (2) we have

$$(Y + \Delta Y)/Y = [K(t + \Delta t)^{1/2} + Q]/[Kt^{1/2} + Q]. \quad (4)$$

For long times, growth is interdiffusion limited and the square root term dominates so that

$$(Y + \Delta Y)/Y = (t + \Delta t)^{1/2}/t^{1/2}. \quad (5)$$

For small  $\Delta t$ , one may expand the square root and retain the first two terms

$$(Y + \Delta Y)/Y = 1 + \Delta t/2t \quad (6)$$

so that

$$Y + \Delta Y = Y(1 + \Delta t/2t) \quad (7)$$

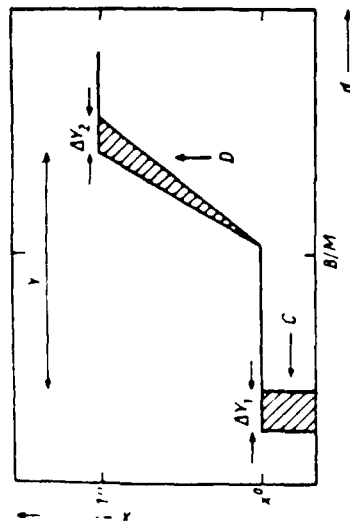


Fig. 4. The approximation used for the profile shape. Two schematic profiles are given, one "grown" for time  $t$  with thickness  $Y$  and the other "grown" for time  $t + \Delta t$  with thickness  $Y + \Delta Y$ . The profiles are aligned so that their Boltzmann-Matano (B/M) interfaces overlap. By conservation of Cd area  $C$  equals area  $D$ .

An approximation for the profile shape is now introduced and is illustrated in Fig. 4. Two schematic profiles are shown, one "grown" for a time  $t$ , the other for a time  $t + \Delta t$ . By conservation of Cd area  $C$  equals area  $D$

$$x^0 \Delta Y_1 = (1 - x^0) \Delta Y_2 / 2 \quad (8)$$

also

$$\Delta Y = \Delta Y_1 + \Delta Y_2 \quad (9)$$

Solving for  $\Delta Y_1$  using (7) to (9)

$$\Delta Y_1 = [(1 - x^0) \Delta t Y / (1 + x^0) 2] \quad (10)$$

The amount of Hg and Cd which has interdiffused per unit area in time  $\Delta t$ ,  $J \Delta t$ , is given by

$$J \Delta t = x^0 \Delta Y_1 / V, \quad (11)$$

where  $V$  is the molar volume. Substituting for  $\Delta Y_1$  from (10) gives

$$J \Delta t = [x^0 (1 - x^0) \Delta t Y / (1 + x^0) 2] \quad (12)$$

The moles of Cd and Hg which have interdiffused in time  $\Delta t$  per unit area can also be expressed using Fick's first law as

$$J \Delta t = \Delta t D_2 (dx/dy)_2 / V. \quad (13)$$

Equating (13) and (12) and solving for  $D_2$

$$D_2 = [x^0 (1 - x^0) Y / (2(1 + x^0) (dx/dy)_2)] \quad (14)$$

#### 4. Results and Discussion

Interdiffusion coefficients can be determined using the above analysis from readily obtainable experimental data. The method is based on a number of assumptions which will now be considered in more detail. The assumption that growth is limited by interdiffusion is good. After an initial transient, a  $t^{1/2}$  dependence of layer thickness on time is observed, as has been reported in the literature [2, 3, 6 to 10]. The approximation of conservation of Cd in the substrate-layer system is valid since the Cd partial pressure is very low. The assumption that the same amount of material interdiffuses over a large composition range is valid for fractions of CdTe in the Hg<sub>1-x</sub>Cd<sub>x</sub>Te layer less than 0.7, as is discussed in the Appendix. The modeling of area B of Fig. 3 as a rectangle is a good approximation since the profile in this region is relatively flat. The modeling of area A as a triangle, however, is less valid. But, the value obtained

for the interdiffusion coefficient is relatively insensitive to the shape of area A for low values of  $x^0$ . For example, if the area is modelled as a rectangle, the value of the interdiffusion coefficient is only changed by a factor of  $(1 + x^0)$ . The actual area is between that of a rectangle or a triangle, so the actual error involved is less than a factor of  $(1 + x^0)$  and is of the order of 10%.

Fig. 5 shows the results of a series of experiments which have been analyzed by the method described above to determine interdiffusion coefficients as a function of temperature and composition. Different symbols represent different growth runs. The necessary data were obtained by electron microprobe analysis. These results can be represented by an equation of the form

$$D_2 (\text{cm}^2/\text{s}) = 300 \exp(-7.53x) \exp(-1.92 \text{ eV}/kT) \quad (15)$$

over the temperature range 450 to 700 °C (for compositions which are solid at these temperatures) and the composition range 0.1 to 0.7 fraction CdTe in the Hg<sub>1-x</sub>Cd<sub>x</sub>Te. Also shown are points determined by Leute et al. [13] for Te rich conditions at 500 °C using a more conventional couple technique and the Boltzmann-Matano method. (Good agreement is obtained between the two techniques and with equations given by Zanio and Massopust [17] and Tang and Stevenson [18].)

The method described here has a number of attractive features in the case of analysis, the material quality, and the ability to control the thermodynamic state of the diffusing system. The analysis itself does not require the determination of either the Boltzmann-Matano interface or any areas. Isothermal vapor phase growth is one of the simplest methods for producing this material. The epilayers produced are single crystal oriented (111), and of high surface quality when growth is performed on single crystal (111) CdTe substrates. By contrast, the traditional couple technique does not utilize oriented wafers and there is a discontinuity in crystal structure at the junction between the slabs of CdTe and HgTe which comprise the couple.

The state of the system (deviation from stoichiometry) is easily controlled during isothermal vapor phase epitaxy. The state of the diffusing host is important since it determines the concentration of point defects and diffusion proceeds via these defects. To ensure reproducibility and to meaningfully compare with other work, it is necessary to thermodynamically fix the materials' defect state before and during the interdif-

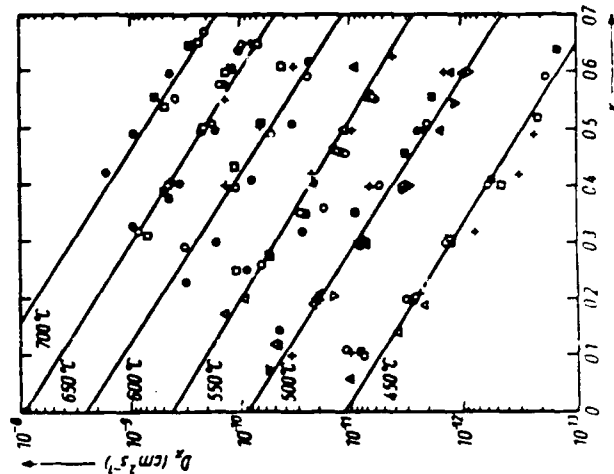


Fig. 5. Experimental results showing the change in interdiffusion coefficient with fraction CdTe in the Hg<sub>1-x</sub>Cd<sub>x</sub>Te for a series of temperatures. Different sets of symbols represent data from different growth runs. The present data from different growth runs are shown as + symbols at 500 °C and points taken from Leute et al. [13].

fusion experiment. In the binary II-VI's, the state of the system can be readily controlled using a two-zone system that fixes the temperature and the partial pressure of the higher vapor pressure species [14, 15]. The situation for  $\text{Hg}_{1-x}\text{Cd}_x\text{Te}$  is complicated by the fact that the system is a ternary with an additional degree of freedom, in accord with the Gibbs phase rule.

The problem of fixing the state of the diffusion system is illustrated using the system temperature-pressure diagrams which have been determined by Tung et al. [11, 12], with a relevant portion shown in Fig. 6. Suppose that we wish to investigate interdiffusion under Te-rich conditions using the conventional couple technique and attempt to do this by preannealing the slabs of  $\text{HgTe}$  and  $\text{CdTe}$  to their Te-rich condition and by establishing a Te-rich ambient during the interdiffusion experiment. This can be accomplished by adding a mixture of  $\text{HgTe}$  and  $\text{Te}$  to the ampoule in which the interdiffusion takes place. Leute and coworkers [13] have used this approach in their work. The three-phase mixture of solid ( $\text{HgTe}$ ), liquid (Te-rich), and vapor fixes the condition of the ambient on the portion of the mercury pressure-temperature diagram shown at point A of Fig. 6. However, within the diffusion couple, there is the whole range of composition from  $\text{CdTe}$  to  $\text{HgTe}$ , and only the  $\text{HgTe}$  exists in its most Te-rich condition. For example, the points B, C and D correspond to the most Te-rich condition of material with mole fractions of  $\text{CdTe}$  of 0.197, 0.416, and 0.7. Also, in order for the preanneal to be useful it must be done at or near the interdiffusion temperature, since the materials' defect nature changes with temperature [16].

During isothermal vapor phase growth, the state of the system is fixed by the source. In the present study, Te-rich  $\text{Hg}_{1-x}\text{Cd}_x\text{Te}$  sources were used. Since the pressure-temperature diagrams for the system have been determined, [11, 12], the ambient component partial pressures are known. Also, since the material is actually being grown during the diffusion experiment, a preanneal is not necessary. Using different source compositions, it is possible to fix a series of Te-rich ambients. However, to within experimental error, this has no effect on the interdiffusion coefficient, within the range of partial pressures obtainable. This agrees with the study made by Leute et al. [13], who reported that there was no significant difference in the interdiffusion coefficient for Te-rich or Hg-rich  $\text{HgTe}$  conditions.

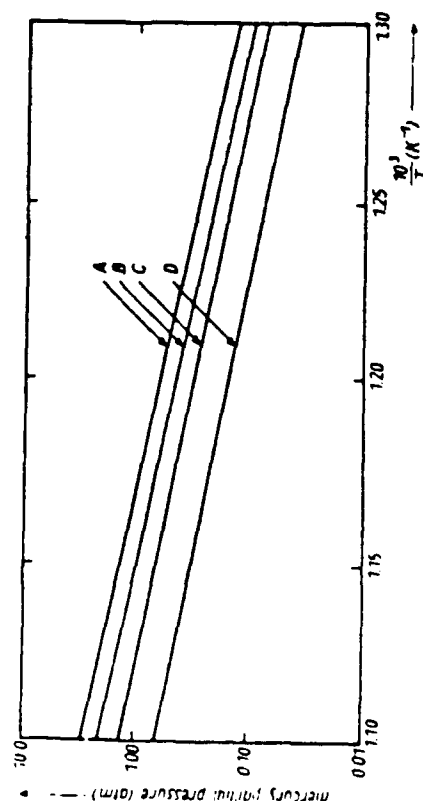


Fig. 6. The vapor pressure of Hg along a portion of the Te-rich blades of the  $\text{Hg}_{1-x}\text{Cd}_x\text{Te}$  pressure-temperature diagram determined by Tung et al. [12]. Notice that the minimum Hg pressure is different for material with different fractions of  $\text{CdTe}$ . (A)  $x = 0.197$ , (C)  $x = 0.416$ , (D)  $x = 0.7$ .

## 6. Summary

A method has been presented for the determination of interdiffusion coefficients in the  $\text{Hg}_{1-x}\text{Cd}_x\text{Te}$  system by an analysis of isothermal vapor phase growth profiles. The analysis utilizes the diffusion controlled growth kinetics and the experimentally obtained profile shape. The technique has been applied to Te-rich conditions in the composition range  $0.1 < x < 0.7$  (in  $\text{Hg}_{1-x}\text{Cd}_x\text{Te}$ ) and  $450^\circ\text{C} < T < 700^\circ\text{C}$ . This method has been used to determine Hg-rich interdiffusion coefficients from epilayers grown by an isothermal liquid phase epitaxial technique that has recently been reported [18].

## Acknowledgements

The authors thank Dr. M. Brown of Grumman Corporate Research Center for helpful discussions and for supplying the  $\text{CdTe}$  substrates used in this work and Dr. K. Zanio of Ford Aerospace, Prof. H. Schmalzried of the University of Hannover, and Dr. M. F. S. Tang of Stanford University for helpful discussions. This project was sponsored by DARPA through the Office of Naval Research, contract No. N00014-84K-0423. One of the authors (J.G.F.) gratefully acknowledges the support of an Office of Naval Research Fellowship.

## Appendix

Fig. 7 represents a portion of two profiles, one grown slightly longer than the other. The quantity  $\Delta x$  measures the disparity in the overlap of the profiles; the closer the overlap, the better is the assumption that the same amount of material interdiffuses through a range of compositions. We will initially assume that the same amount interdiffuses through each portion of the material and then use the result to assess its validity. Using this assumption we have

$$\Delta Y_1 x^0 = D_2 (dx/dy)_2 \Delta t, \quad (\text{A1})$$

where the symbols used have been defined earlier in the text and are illustrated in Fig. 4. From simple geometrical considerations

$$\Delta x = (dx/dy)_2 \Delta Y_2. \quad (\text{A2})$$

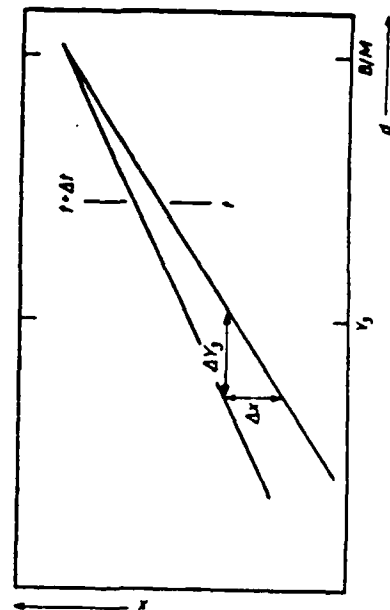


Fig. 7. A schematic of a portion of two profiles, one, the upper portion, grown slightly longer than the other. The quantity  $\Delta x$  is a measure of the closeness of the overlap between the two profiles. The closer the overlap the better is the approximation that the same amount of material interdiffuses throughout the growing layer.

Assuming a small  $\Delta t$ , we can, using the same methods given in the body of the text, express  $\Delta Y_3$  as

$$\Delta Y_3 = \Delta t Y_3 / 2t. \quad (\text{A3})$$

Solving for  $\Delta x$  using (A1), (A2), and (A3)

$$\Delta x = \Delta Y_3 x^2 Y_3 / 2t D_2. \quad (\text{A4})$$

Fig. 3 shows that the maximum value of  $\Delta x$  occurs at the most CdTe-rich portion of the profile and is on the order of  $(1 - x^*)/2$ . Thus:

$$\Delta x_{1,7} \sim Y_3(1 - x^*) D_1 / D_2 Y_1, \quad (\text{A5})$$

where  $D_1$  is the interdiffusion coefficient as the composition approaches CdTe and  $\Delta x_{1,7}$  is the  $\Delta x$  at some time  $t$  and position  $y$ . Information in the literature has established that the interdiffusion coefficient varies approximately three orders of magnitude in going from HgTe to CdTe [13, 17, 18]. Thus for the CdTe-rich region (where the value of  $\Delta x$  is a maximum)

$$\Delta x_{1,7} \sim (1 - x^*) / [10^3(1 - x^*)]. \quad (\text{A6})$$

This analysis establishes that the strong dependence of the interdiffusion coefficient on composition leads to a small value of  $\Delta x$ , provided the composition of the material does not approach that of pure CdTe. Since the composition in this region changes only slightly a quasi-steady state condition exists in this composition regime.

## References

- [1] A. F. W. WILLOUGHBY, *Mater. Letters* 1, 68 (1982).
- [2] O. N. TUTE and E. L. STELLER, *J. appl. Phys.* 40, 4559 (1969).
- [3] L. SVOB, Y. MARFAINO, R. TAIBOULET, F. BAILLEY, and G. COHEN-SOLAL, *J. appl. Phys.* 46, 4251 (1975).
- [4] F. BAILLEY, L. SVOB, G. COHEN-SOLAL, and R. TAIBOULET, *J. appl. Phys.* 46, 4244 (1975).
- [5] P. BECLA, J. LACOWSKI, H. C. GATOS, and H. RUDA, *J. Electrochem. Soc.* 128, 1171 (1981).
- [6] P. BECLA, J. LACOWSKI, H. C. GATOS, and L. JEDRAL, *J. Electrochem. Soc.* 129, 2853 (1982).
- [7] J. M. PAWLAKOWSKI, *Thin Solid Films* 44, 241 (1977).
- [8] T. NOUYEN-DUY, J. C. MORAND, and G. COHEN-SOLAL, 1980 Internat. Electron. Devices Meeting, Technical Digest, Washington (D.C.) (pp. 491 to 496).
- [9] P. BECLA, P. A. VOLZ, R. L. AGGARWAL, and Y. S. YUEN, *J. Vacuum Sci. Technol.* A3, 119 (1985).
- [10] J. G. FLEMING and D. A. STEVENSON, *J. Crystal Growth* 82, 621 (1987).
- [11] J. P. SCHWARTZ, T. TUNO, and R. F. BARBER, *J. Electrochem. Soc.* 128, 438 (1981).
- [12] T. TUNO, L. GOLOWKA, and R. F. BARBER, *J. Electrochem. Soc.* 128, 451 (1981).
- [13] V. LEUTE, H. M. SCHMIDTKE, W. STRATMANN, and W. WINKING, *phys. stat. sol. (a)* 67, 183 (1981).
- [14] H. H. WOODBURY and R. B. HALL, *Phys. Rev.* 157, 841 (1967).
- [15] P. M. BORSSENIEN and D. A. STEVENSON, *J. Phys. Chem. Solids* 29, 1277 (1968).
- [16] H. F. SCHAEKE, *J. electronic Mater.* 14, 513 (1985).
- [17] K. ZANTO and T. MASSOPUST, *J. electronic Mater.* 16, 103 (1986).
- [18] M. F. S. TANO and D. A. STEVENSON, *Appl. Phys. Letters* 50, 1272 (1987).
- [19] J. G. FLEMING and D. A. STEVENSON, *J. Electrochem. Soc.* 134, 1225 (1987).

(Received July 10, 1987)

# Isothermal Liquid Phase Epitaxial Growth of Mercury Cadmium Telluride

J. G. Fleming and D. A. Stevenson\*

Department of Materials Science and Engineering, Stanford University, Stanford, California 94305

## ABSTRACT

A method is presented for the isothermal growth of mercury cadmium telluride from a mercury or tellurium-rich melt. In accord with a proposed model, growth proceeds by HgTe deposition from the melt onto the substrate and interdiffusion between the Hg and Cd within the growing layer. Mercury-rich interdiffusion coefficients are determined from an analysis of experimental composition profiles.

Mercury cadmium telluride consists of a continuous series of solid solutions between mercury telluride and cadmium telluride. Currently it is of great interest for use in infrared detectors in the long wavelength regime, for use in optical communications systems, and in scientific spectroscopic applications. This interest is based on the continuous change of the direct bandgap as the composition varies from HgTe ( $-0.32$  eV) to CdTe ( $1.6$  eV) (1). However, there are substantial problems with growth and processing of this material, see for example Ref. (2). A large liquidus-solidus lens in the pseudobinary temperature-composition diagram makes it difficult to grow homogeneous bulk material. In addition, the material is mechanically weak, the mercury vapor pressure is high during processing and growth, and it is difficult to experimentally define the material thermodynamically since it is a ternary system. A great many growth techniques have been developed, both bulk and epitaxial. In this paper we present a new technique for growth from an isothermal melt and provide an analysis of the growth mechanism. In addition, mercury-rich interdiffusion coefficients are obtained from an analysis of the composition profiles.

## Experimental

The experimental geometry for growth from a mercury-rich melt is shown in Fig. 1. A CdTe (111) substrate is initially placed above a reservoir of mercury large enough to cover the substrate when the ampul is tilted  $180^\circ$ . Sufficient Te is added to the mercury to establish the equilibrium tellurium atomic fraction in the melt at the growth temperature for the composition of interest. We have been using a growth temperature of  $500^\circ\text{C}$  and a tellurium fraction of 8-10%; this produces material with  $X$  values ( $X$  in Hg<sub>1-X</sub>Cd<sub>X</sub>Te) in the range of 0.3-0.2. The ampul is then evacuated and sealed. Growth takes place within a tipping furnace equipped with a sodium heat pipe to ensure that the system is isothermal. The ampul is first annealed at the growth temperature to dissolve the Te into the liquid Hg. The furnace is then tipped  $180^\circ$ , thereby immersing the substrate in the melt which then saturates by dissolving some of the substrate. Growth is allowed to proceed for 60-70h. At the end of the growth cycle, the melt is tipped off the substrate. The furnace is then turned off and allowed to cool to below  $360^\circ\text{C}$  before removal of the ampul in order to avoid boiling the Hg melt which can spoil the layer surface quality. A schematic of this process is given in Fig. 2. Growth from a tellurium melt is similar except that the melt consists of the tellurium-rich liquid in equilibrium with the composition of interest. After growth is complete, the layers are examined optically, mounted, cross-sectioned, and the composition profiles determined by electron probe microanalysis.

In our initial experiments, the melt, tellurium, and substrate were all in contact as the system was heated. This produced layers with poor surface quality, probably due to Hg vapor bubble formation on the substrate as the mercury vapor pressure increased. When the melt is

heated separately from the substrate, the surface quality is improved. Also, while it is possible to use the substrate to saturate the Hg-Te melt, this results in poor surface quality since a relatively large amount of CdTe must be dissolved, on the order of  $80\text{ }\mu\text{m}$  for our geometry. This problem is easily avoided by adding some Cd or CdTe to the mercury melt, or by having a large area sintered "source" next to the substrate.

## Results

The surfaces of the grown layers exhibit a terraced structure like that found in LPE material (3, 4). Pinholes which penetrate through a good fraction of the layer thickness were occasionally present. There is little evidence of any gross melt retention on the substrate surface.

Figure 3 shows a typical growth profile. As we will see in the next section, growth is dependent on interdiffusion so that interdiffusion coefficients can be determined from these profiles using an analytical technique developed for the isothermal vapor phase epitaxial growth method (5). The results of the interdiffusion analysis are given in Fig. 4, along with points for mercury-rich conditions obtained by Leute and Stratmann (6). Due to the high mercury vapor pressures encountered, 8 atm at  $500^\circ\text{C}$  (7), growth was not attempted at higher temperatures to minimize the possibility of an explosion.

## Discussion

It is instructive to view this technique as a liquid phase analogue of the isothermal vapor phase epitaxial (ISOVPE) growth technique, for which we have recently proposed a mechanism (8). This vapor phase process is governed by the vapor transport of Te, from the source to the substrate and by interdiffusion between the Hg and Cd in the growing layer. As was already mentioned, interdiffusion coefficients can be determined by an analysis of the ISOVPE growth kinetics and the experimental growth profiles. These interdiffusion coefficients are of interest both theoretically and practically because they dictate the transition region in LPE material, the stability of superlattices of HgTe and CdTe, and the rate

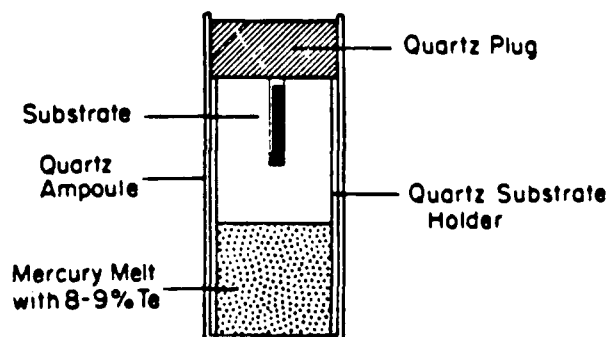


Fig. 1. The experimental geometry used in these experiments. In general, a source of Cd was added to the melt or placed next to the substrate.

\*Electrochemical Society Active Member.

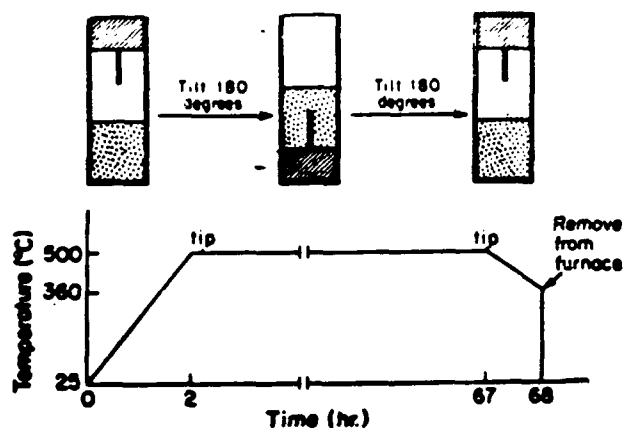


Fig. 2. A schematic of the heating and tipping schedule used for growth

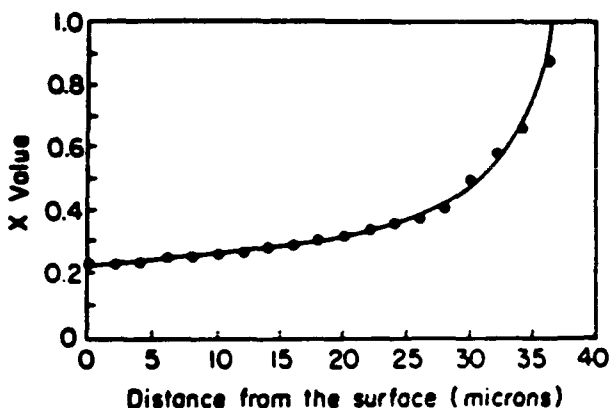


Fig. 3. A plot of composition vs. distance from the surface for a sample grown at 500°C for 63h in a melt containing 9% Te.

of homogenization of material. The vapor phase growth technique is practical only in Te-rich environments since the Te, partial pressures in Hg rich environments are extremely low. A motivation for developing the present isothermal LPE growth technique was to allow growth under Hg-rich conditions so that Hg-rich interdiffusion coefficients could be obtained.

The mechanism of growth can be seen with the aid of a schematic of the Hg-rich corner of the Hg-Cd-Te phase diagram, Fig. 5. The initial composition of the Hg-Te melt is determined by the amount of Te added to the Hg. When the melt comes into contact with the substrate, it dissolves enough CdTe to saturate the melt, 1. This melt is now in equilibrium with solid mercury cadmium telluride of a certain composition, via tie line 2. In order to ob-

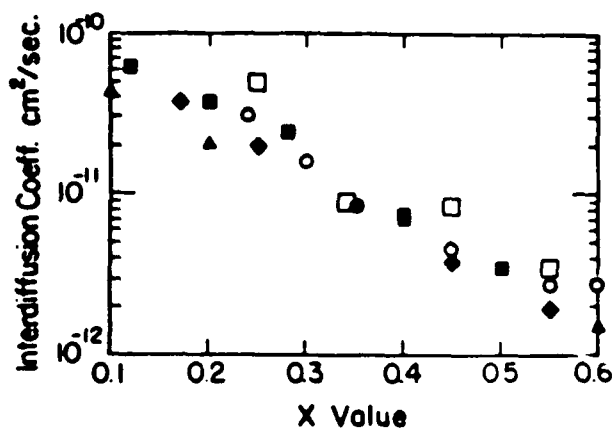


Fig. 4. A plot of mercury rich interdiffusion coefficients vs. composition. Different symbols represent different growth runs, the solid triangles are the data of Louie (6).

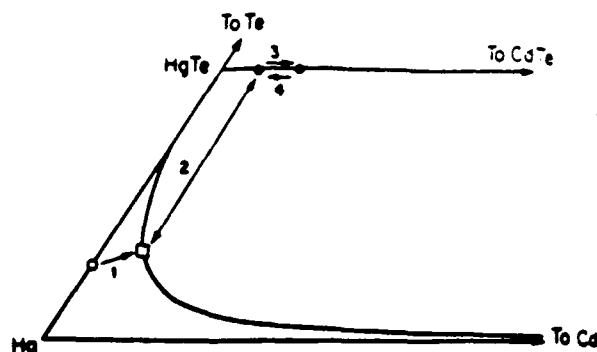


Fig. 5. A schematic of the Hg rich corner of the Hg-Cd-Te phase diagram indicating the growth mechanism. Initially, the melt is at the position denoted by the open circle on the Hg-Te binary. When the melt comes in contact with the substrate enough CdTe dissolves to saturate the melt, 1. This melt composition, denoted by the open square, is in equilibrium with solid  $\text{Hg}_{1-x}\text{Cd}_x\text{Te}$  via tie line 2. In order to approach equilibrium, some HgTe deposits from the melt onto the substrate where it interdiffuses with the CdTe, 3. This interdiffusion again forces the system out of equilibrium leading to further deposition bringing the substrate surface back towards equilibrium with the melt, 4, and so growth continues.

tain the equilibrium solid composition, some HgTe deposits from the melt onto the substrate surface. This HgTe then interdiffuses with the CdTe substrate. Due to this interdiffusion, the surface of the growing layer is again no longer in equilibrium with the melt, leading to further deposition of HgTe and so the cycle continues, 3, 4. Since the melt is very much larger than the amount of material deposited, the overall composition of the melt remains unchanged. However, as the layer thickens, the interdiffusion process slows so that the surface composition of the layer approaches equilibrium with the melt. Thus, fixing the Te to Hg ratio in the melt, which fixes the melt composition, allows us to control the surface composition of the layers. The Cd solubility in the melt is approximately two orders of magnitude lower than that of the Te (9) and does not play a major role in growth. In our experiments, we have used 8-10% Te in the Hg melt and have obtained layers with surface fractions of CdTe in the range of 0.3-0.2, as expected from the phase diagram work of Herning (9).

We have also observed the same growth process with layers grown on CdTe substrates from tellurium-rich melts, which is to be expected since growth is only dependent on the high interdiffusion coefficient and the thermodynamic driving force pushing the entire system, melt and substrate, towards equilibrium.

Despite the fact that the technique can only produce graded junctions, it may have some advantages as a growth technique. Mercury is the most easily purified of the three components and growth from the mercury corner should give material with fewer tellurium precipitates and mercury vacancies. Also there is the possibility for in situ mercury annealing by holding the sample at a lower temperature once growth has been completed. It has been noted in vapor grown samples that a problem exists due to impurities left on the surface of the substrate (10). This should not be a problem in the technique described here since the substrate surface can be melted back when it comes into contact with an undersaturated melt, thereby removing any surface impurities. A systematic effort is in progress to evaluate and optimize the electrical properties of the layers.

#### Summary

Mercury cadmium telluride epilayers have been grown by a mercury or tellurium-rich isothermal liquid phase growth technique. Growth is the result of HgTe deposition onto the substrate. The mercury and cadmium within the layer then interdiffuse to maintain the chemical potential gradient which leads to further HgTe deposition. From an analysis of the composition profiles, in-

terdiffusion coefficients were obtained which are in good agreement with those obtained using a conventional diffusion couple technique.

#### Acknowledgments

The authors gratefully acknowledge Dr. Margaret Brown of Rockwell International for supplying the CdTe substrates and for helpful discussions. One of the authors, J. G. F., gratefully acknowledges the support of an Office of Naval Research Fellowship. This work was sponsored by DARPA through the Office of Naval Research under Contract no. N00014-84K-0423.

Manuscript received July 7, 1986.

#### REFERENCES

1. J. L. Schmit, *J. Crystal Growth*, **65**, 249 (1983).

2. W. F. H. Micklewaite, in "Semiconductors and Semimetals," Vol. 18, R. K. Willardson, Editor, p. 47. Academic Press, Inc., New York (1981).
3. C. C. Wang, S. H. Shin, M. Chu, M. Lanir, and A. H. B. Vancorwyck, *This Journal*, **127**, 175 (1980).
4. D. D. Edwall, E. R. Gertner, and W. E. Tennant, *J. Appl. Phys.*, **55**, 1453 (1984).
5. J. G. Fleming and D. A. Stevenson, *J. Cryst. Growth*, In press.
6. V. Leute, H. M. Schmidtke, W. Stratmann, and W. Winking, *Phys. Status Solidi A*, **67**, 183 (1981).
7. T. Tung, L. Golonka, and R. F. Brebrick, *This Journal*, **128**, 451 (1981).
8. J. G. Fleming and D. A. Stevenson, Submitted for publication.
9. P. E. Herning, *J. Electron. Mater.*, **13**, 1 (1984).
10. P. Becla, P. A. Wolff, R. L. Aggarwal, and Y. S. Yuen, *J. Vac. Sci. Technol. A*, **3**(1), 119 (1985).



**VICKERS HARDNESS OF  $\text{Hg}_{1-x}\text{Cd}_x\text{Te}$  EPILAYERS GROWN BY ISOTHERMAL VAPOR PHASE EPITAXY**

J.G. FLEMING, L.J. FARTHING and D.A. STEVENSON

*Department of Materials Science and Engineering, Peterson Building, Stanford University, Stanford, California 94305, USA*

A novel method for preparing graded compositions of  $\text{Hg}_{1-x}\text{Cd}_x\text{Te}$  epilayers is presented. The epilayers are grown by an isothermal vapor phase epitaxial technique, which uses a CdTe substrate and either Te-rich HgTe or HgCdTe as the source. The substrate is positioned vertically to the source allowing a graded composition of HgCdTe epilayer to be deposited. Epilayer thicknesses of 100–200  $\mu\text{m}$  were deposited, with  $x$  values ranging from 0.1 to 0.7. Vickers hardness measurements were made over the composition range with hardness values ranging from 33 to 75  $\text{kg/mm}^2$ . These values are similar to hardness values in the literature which were measured on individual bulk specimens. Our method is particularly effective since a single oriented layer of varying composition is measured rather than separately prepared samples of different orientation.

**1. Introduction**

Mercury cadmium telluride,  $\text{Hg}_{1-x}\text{Cd}_x\text{Te}$ , is of interest since it is used in infrared detectors for a wide variety of applications, such as infrared focal plane arrays, spectroscopic detectors, and in optical communication systems [1,2]. The mechanical properties of HgCdTe are of interest since they relate to practical problems in processing the material. There is also interest in the theoretical basis of predicting mechanical properties of semiconductor alloy systems [3]. We present a novel method for preparing graded compositions of HgCdTe epilayers and determining Vickers hardness profiles of these epilayers.

The attractive feature of the HgTe–CdTe system is the ability to vary a direct band gap continuously from 0 to 1.6 eV [4]. The growth of HgCdTe by conventional solidification methods is difficult because the large separation between the liquidus and solidus in the pseudobinary causes interface breakdown due to constitutional supercooling. The solid state recrystallization technique is used to prepare bulk specimens [5], but there are several disadvantages: small grain size; lack of control over orientation; lack of reproducibility; and processing cost. Epitaxial growth of HgCdTe is usually accomplished by liquid phase epitaxial (LPE) techniques for both Te- and Hg-rich melts

[6–19]. The travelling heater method is favored as the next generation growth method for bulk growth, while LPE is favored for epitaxial growth. Isothermal vapor phase epitaxy (ISOVPE) is not utilized as extensively, but is has several advantages: (1) the surface quality is excellent; (2) many wafers can be processed simultaneously; (3) there are potentially lower impurity concentrations in the epilayers; (4) it is simple to implement. We present a modification of this method that produces a range of surface compositions on a single wafer.

The ISOVPE technique was first described in the mid-1960's by French researchers [20,21] and has been utilized fairly extensively since then [22–34]. Recent thermodynamic information provided a basis for elucidating the growth method, which has recently been described [35]. The method consists of a CdTe substrate wafer and a HgTe or HgTe-rich HgCdTe source in a closed evacuated ampule. During isothermal annealing, there is transport of Hg and Te from the source to the growing film of HgCdTe. Isothermal vapor phase growth is the result of two processes: transport of  $\text{Te}_2$  and Hg from the source to the substrate (the transport of  $\text{Te}_2$  is rate limiting); and interdiffusion between Hg and Cd within the growing layer. The driving force for the growth is a variation of the  $\text{Te}_2$  chemical potential with the CdTe fraction

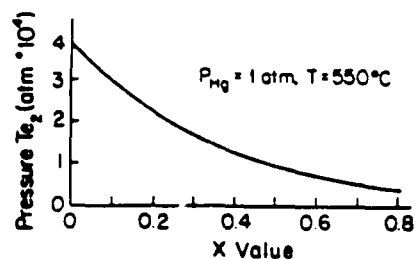


Fig. 1. The variation of  $\text{Te}_2$  partial pressure with composition for the conditions of ISOVPE growth, constant temperature and Hg partial pressure. A temperature of  $550^\circ\text{C}$  and Hg pressure of 1 atm are used as an example. The  $\text{Te}_2$  partial pressures were determined from a best straight line fit of the free energy of formation of  $\text{HgTe}$  determined from the data of Tullig et al. [37].

in the  $\text{HgCdTe}$ ; fig. 1 shows the variation of the  $\text{Te}_2$  partial pressure with composition for constant temperature and Hg pressure. The growth is limited by the transport of  $\text{Te}_2$  at short times, and is diffusion limited at longer times. Eventually, growth becomes entirely diffusion limited and the surface composition approaches that of the source. The time it takes for this to occur is greater for material with lower  $\text{CdTe}$  fractions, higher temperatures, higher Hg overpressures and greater source-to-substrate spacings. Fig. 2 shows the effect of source-to-substrate spacing on layer thickness and surface composition of the epilayer. Increasing the Hg overpressure decreases both the partial pressure and the mobility of  $\text{Te}_2$  vapor. Further details are given in ref. [35]. The novel

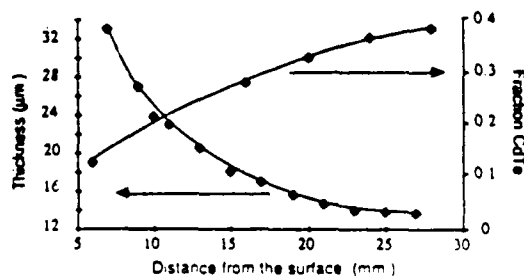


Fig. 2. The effect of source-to-substrate spacing (horizontal axis) on layer thickness (left-hand side vertical axis) and surface composition (right-hand side vertical axis). The source used was  $\text{Te}$ -rich  $\text{HgTe}$ , the temperature was  $500^\circ\text{C}$  and the growth time was 16h.

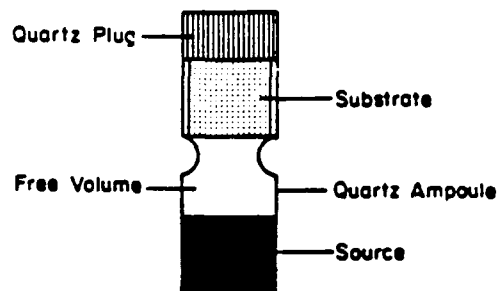


Fig. 3. The experimental arrangement used to investigate the effect of the source-to-substrate spacing. The substrate is oriented vertically with respect to the source so that different points on the substrate are different distances from the source.

approach we have used in the present study is to place the substrate vertically, not horizontally, with respect to the source (see fig. 3), which produces a  $\text{HgCdTe}$  epilayer of graded composition.

## 2. Experimental methods

Fig. 3 is a schematic diagram of the experimental arrangement used in the present study. The source, spacers, and substrate were placed in a quartz ampoule, which was evacuated to  $10^{-5}$  Torr and sealed. The ampoule was then annealed at  $550$  to  $638^\circ\text{C}$  for times from 69.5 to 162 h.

Substrates used were (111)  $\text{CdTe}$  wafers approximately  $4 \times 10 \text{ mm}^2$  and 0.75 mm thick and were etched in a 5% bromine-methanol solution for 30 s and then rinsed with methanol prior to use. The sources, either  $\text{HgTe}$  or  $\text{Hg}$ -rich  $\text{HgCdTe}$ , were prepared by annealing the elements at  $650^\circ\text{C}$  for 15 h in an evacuated and sealed quartz ampoule. The source was then removed and ground to powder. The powder was placed in a quartz ampoule, which was evacuated, sealed, and annealed at  $500^\circ\text{C}$  for 30 min to sinter the source.

Hardness measurements were made on the  $\text{HgCdTe}$  epilayers using a Vickers hardness tester. The indenter was kept in contact with the surface for 20 s. Weights ranged from 5 to 25 g. The diagonal lengths of the indentation were small at the lower weights and difficult to measure; there-

fore, most measurements were made with the 25 g weight.

Microprobe analyses were performed on the epilayers to determine the composition along the surface of the substrate. The samples were mounted in epoxy resin, polished using 600 grit SiC and  $0.3 \mu m$   $Al_2O_3$ , and then coated with sputtered carbon to produce a conducting layer for the microprobe. An accelerating voltage of 20 keV, a beam current of 15 nA, and a sampling time of 20 s were used. The computer program which calculates atomic fractions of Hg, Cd, and

Te was set for a standard deviation of 0.5%; the reproducibility of the microprobe analyses was 1% of the concentration in question.

### 3. Results and discussion

Fig. 4 shows the Vickers hardness as a function of  $x$  in  $Hg_{1-x}Cd_xTe$  epilayers with  $x$  values ranging from 0.1 to 0.7. The hardness values range from 33 to 75  $kg/mm^2$ , which are comparable to hardness values determined by Cole et al. [36],

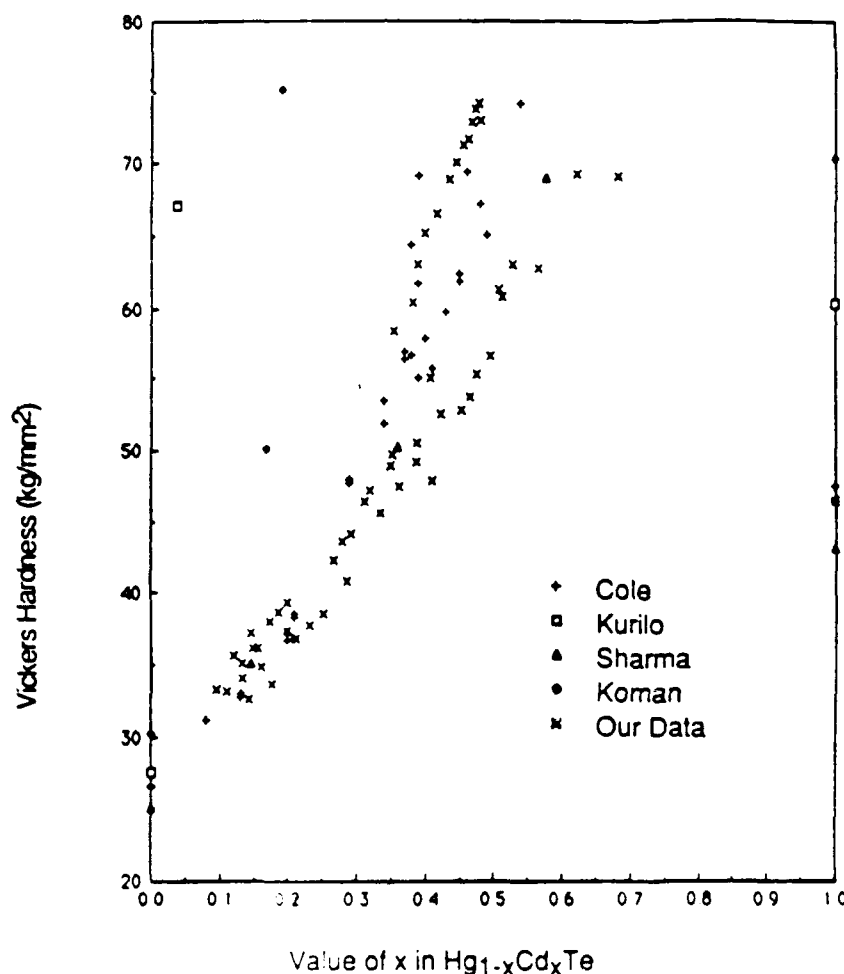


Fig. 4 Our data of Vickers hardness plotted as a function of composition in  $Hg_{1-x}Cd_xTe$  as compared with those of Cole et al., Kurilo et al., Sharma et al., and Koman and Pashovskii (as cited in ref. [36]).

who used individual bulk specimens grown by the Bridgman method. Fig. 4 presents a comparison of our data with those of Cole et al., Kurilo et al., Sharma et al., and Koman and Pashovskii (as cited in ref. [36]). There is a wide range in hardness values reported in the literature; for example, hardness values reported for CdTe range from 43 to 70 kg/mm<sup>2</sup>. Such large differences should be resolved or explained. Our data differ significantly from those reported by Kurilo et al. and by Koman and Pashovskii, but are in good agreement with the data reported by Cole et al. and by Sharma et al.

The advantage of our ISOVPE method in contrast to the traditional approach is that fewer samples are needed and that oriented samples are used. For example, Cole et al. [36] used many large-grained samples cut from a HgCdTe ingot grown by the Bridgman method and did not measure the crystallographic orientation of these samples. Using this new approach, we grew  $Hg_{1-x}Cd_xTe$  epilayers with  $x$  values ranging from 0.1 to 0.7 on just four (111) CdTe substrates.

As seen in fig. 4, there is a strong, nonlinear hardening effect seen in HgCdTe alloys. Cole et al. [36] describe possible mechanisms for solid solution hardening in HgCdTe. Solid solution hardening may arise from elastic and electrical interactions of solute atoms with dislocations. Fleisher (as cited in Cole et al. [36]) divides the elastic interaction into two misfit parameters: one parameter relates the local strain field arising from the size difference between the solute and matrix atoms; and another parameter represents a change in the local elastic modulus due to the presence of the solute atom. Cole et al. [36] propose that there may be a change in the local charge relative to the matrix by the addition of Cd or Hg atoms which causes electrical interactions with charged dislocations. Thus, if free carriers produce a screening effect, then, since the free carrier concentration decreases with increasing  $x$  from a maximum at  $x = 0.1$ , the elastic interaction would be the dominant factor contributing to hardening at low  $x$  values, while both elastic and electrical interactions contribute at high  $x$  values. The hardness values would therefore reach a maximum at high values of  $x$ , a trend which is clearly established by the data.

Sher et al. [3] have proposed a mechanism for solid solution hardening in ternary semiconductor alloys based on fundamental atomic properties. They state that the hardness of tetrahedrally bonded semiconductors are strong functions of the reciprocal of the bond length. Although pure CdTe and pure HgTe have nearly the same bond lengths (2.81 and 2.80 Å, respectively), their calculations show that during alloying the HgTe bond length gets smaller and the CdTe bond length gets larger. This then causes internal strains on an atomic scale and, thus, an increase in hardness. This behavior is unexpected from a comparison of the bond lengths of the two pure semiconductors.

#### 4. Summary

Graded compositions of  $Hg_{1-x}Cd_xTe$  epilayers are grown by an isothermal vapor phase epitaxial technique. Either Te-rich HgTe or HgCdTe are used as sources and a CdTe substrate is positioned vertically to the source allowing a graded composition of HgCdTe epilayer to be deposited. Epilayer thicknesses of 100–200 μm are deposited, with  $x$  values ranging from 0.1 to 0.7. Vickers hardness measurements are made over the composition range with hardness values ranging from 33 to 75 kg/mm<sup>2</sup>. These values are similar to hardness values in the literature which were measured on individual bulk specimens.

#### Acknowledgements

The authors gratefully acknowledge Dr. Margaret Brown of Grumman Corporation and Dr. A. Sher of SRI International for helpful discussions and to Dr. Brown for supplying some of the substrates used in this study. This work was sponsored by the Air Force Office of Scientific Research under contract AFOSR 86-0158 and by DARPA through the Office of Naval Research under contract No. N00014-84K-0423.

#### References

- [1] S.H. Shun, J.G. Pasko and D.T. Cheung, SPIE 272 (1981) 27.

- [2] T. Nguyen Duy, J. Meslage and G. Pichard, *J. Crystal Growth* 72 (1985) 490.
- [3] A. Sher, A.B. Chen and W.E. Spicer, *Appl. Phys. Letters* 46 (1985) 54.
- [4] J.L. Schmit, *J. Crystal Growth* 65 (1983) 249.
- [5] W.F.H. Mickelthwaite, in: *Semiconductors and Semimetals*, Vol. 18, Eds. R.K. Willardson and A.C. Beer (Academic Press, New York, 1981) p. 47.
- [6] E.R. Gertner, W.E. Tennant, J.D. Blackwell and J.P. Rode, *J. Crystal Growth* (1985) 462.
- [7] R.A. Reidell, E.R. Gertner, D.D. Edwell and W.E. Tennant, *Appl. Phys. Letters* 46 (1985) 64.
- [8] E. Janik, M. Ferah, R. Legros, R. Triboulet, T. Brossat and Y. Riant, *J. Crystal Growth* 72 (1985) 133.
- [9] J.A. Mroczkowski and H.R. Vidyantath, *J. Electrochem. Soc.* 128 (1981) 655.
- [10] C.F. Wan, D.F. Weirauch, R. Korenstein, E.G. Bylander and C.A. Castro, *J. Electron. Mater.* 15 (1986) 151.
- [11] J.L. Schmit, R.J. Hager and R.A. Wood, *J. Crystal Growth* 56 (1982) 485.
- [12] H. Ruda, R. Becla, J. Lagowski and H.C. Gatos, *J. Electrochem. Soc.* 13 (1983) 228.
- [13] T.C. Harman, *J. Electron. Mater.* 9 (1980) 945.
- [14] K. Nagahama, R. Ohkita, K. Nishitani and T. Murotani, *J. Electron. Mater.* 13 (1984) 67.
- [15] D.D. Edwell, E.R. Gertner and W.E. Tennant, *J. Appl. Phys.* 55 (1984) 1453.
- [16] Y. Nemirovsky, S. Margalit, E. Finkman, Y. Shacham-Diamand and I. Kidron, *J. Electron. Mater.* 11 (1982) 133.
- [17] T.C. Harman, *J. Electron. Mater.* 10 (1981) 1069.
- [18] P. Herning, *J. Electron. Mater.* 13 (1984) 1.
- [19] M.H. Kalisher, *J. Crystal Growth* 70 (1984) 365.
- [20] G. Cohen-Solal, Y. Marfaing, F. Bailly and M. Robot, *Compt. Rend. (Paris)* 261 (1965) 931.
- [21] Y. Marfaing, G. Cohen-Solal and F. Bailly in: *Crystal Growth*, Ed. H.S. Peiser (Pergamon, Oxford, 1967) p. 549.
- [22] G.S. Almasi and A.C. Smith, *J. Appl. Phys.* 39 (1968) 233.
- [23] O.N. Tufte and E.L. Stelzer, *J. Appl. Phys.* 40 (1969) 4559.
- [24] L.A. Bovina, V.P. Meshcheryskova, V.I. Stafcev and E.S. Banin, *Soviet Phys.-Semicond.* 7 (1973) 26.
- [25] J.M. Pawlikowski and P. Becla, *Phys. Status Solidi (a)* 32 (1975) 639.
- [26] J.M. Pawlikowski, *Thin Solid Films* 44 (1977) 241.
- [27] P. Becla, J. Lagowski, H.C. Gatos and H. Ruda, *J. Electrochem. Soc.* 128 (1981) 1171.
- [28] P. Becla, J. Logowski, H.C. Gatos and L. Jedral, *J. Electrochem. Soc.* 129 (1982) 2855.
- [29] P. Becla, J. Lagowski and H.C. Gatos, *J. Electrochem. Soc.* 129 (1982) 1103.
- [30] R.E. Kay, US Patent No. 4,447,470, May 8, 1984.
- [31] Y. Nemirovsky and A. Kepten, *J. Electron. Mater.* 13 (1984) 867.
- [32] P. Becla, P.A. Wolff, R.L. Aggarawal and Y.S. Yuen, *J. Vacuum Sci. Technol.* A3 (1985) 119.
- [33] F. Bailly, L. Svob, G. Cohen-Solal and R. Triboulet, *J. Appl. Phys.* 46 (1975) 4244.
- [34] L. Svob, Y. Marfaing, R. Triboulet, F. Bailly and G. Cohen-Solal, *J. Appl. Phys.* 46 (1975) 4251.
- [35] J.G. Fleming and D.A. Stevenson, *J. Crystal Growth* 82 (1987) 621.
- [36] S. Cole, M. Brown and A.F.W. Willoughby, *J. Mater. Sci.* 17 (1982) 2061.
- [37] T. Tung, L. Golonka and R.F. Brebnick, *J. Electrochem. Soc.* 128 (1981) 451.

# HARDNESS AND ELASTIC MODULUS MEASUREMENTS IN CdTe AND ZnTe THIN FILM AND BULK SAMPLES AND ZnTe-CdTe SUPERLATTICES

L. J. Farthing\*, T. P. Weihs\*, D. W. Kisker\*\*, J. J. Krajewski\*\*, M. F. Tang\*, and D. A. Stevenson\*

\* Department of Materials Science, Stanford University, Stanford, California 94305

\*\* AT&T Bell Laboratories, Holmdel, New Jersey 07733

## ABSTRACT

Hardness and modulus values of bulk and epilayer ZnTe and CdTe samples and of ZnTe-CdTe superlattices are reported. Both hardness and Young's modulus values increase with increasing ZnTe content in the ZnCdTe samples. Alloying effects and strains in the superlattice structure are proposed to explain the strengthening.

## INTRODUCTION

Compound semiconductor superlattices are of interest to the materials community because bandgaps can be finely tuned by the proper choice of the semiconductor materials and layer thicknesses. Mechanical properties relate to the changes in electronic and optical properties that may accompany the processing of semiconductor materials into devices, particularly the introduction of dislocations upon thermal processing and the application of films. Furthermore, the mechanical properties are of concern in the integrity of devices during service. In this paper, we report hardness and elastic modulus values for ZnTe and CdTe epilayer and bulk samples and ZnTe-CdTe strained layer superlattices. The ZnTe-CdTe system is of interest because of its promising optical properties [1].

## EXPERIMENTAL

The samples consist of two sets of ZnTe-CdTe strained layer superlattices grown by atmospheric pressure organometallic vapor phase epitaxy (OMVPE) [1], and epilayer and bulk samples of ZnTe and CdTe. The first set of the superlattices consists of 200 cycles of 25 Å ZnTe and 50 Å CdTe with a 25 Å CdTe cap and a 1.0 μm ZnTe buffer layer on a (100) GaAs substrate. The other set of superlattice samples consists of 200 cycles of 25 Å CdTe and 50 Å ZnTe with a 25 Å CdTe cap and a 1.0 μm ZnTe buffer layer on a (100) GaAs substrate. The ZnTe and CdTe have a lattice mismatch of 6%, so these are strained layer superlattices. The (100) ZnTe epilayer and (100) CdTe epilayer are grown on (100) GaAs substrates by OMVPE for thicknesses of 2.0 μm. The bulk samples are a single crystal (100) CdTe sample and a coarse grained ZnTe sample.

X-ray diffraction measurements were made using a Picker diffractometer with a Cu K $\alpha$  source. Hardnesses were measured by a Vickers hardness tester and a Nanoindenter, which can measure the hardness of very thin films. Important parameters of the Nanoindenter are a displacement resolution of 2 Å and a force resolution of 0.5 mN [2]. The data from the Nanoindenter give hardness values as a function of plastic

depth, while Young's modulus values can be calculated from the unloading portion of the load versus depth indentation curves. Most samples were tested for depths between 20 and 1500 nm; however, for the purpose of analysis, only the indentations with depths between 40 and 400 nm were considered.

## RESULTS AND DISCUSSION

Figure 1 shows the hardness of the ZnTe and CdTe epilayer and bulk samples as a function of plastic indentation depth. The hardness values for the ZnTe epilayer and bulk samples are very similar and show the same pattern of decreasing hardness with increasing plastic depth. The large increase in hardness at very small plastic depths is thought to be due to a surface oxide on these samples, which is evidenced by a discontinuity in the indentation curves at small values of plastic depth. Although the hardness values of the CdTe bulk sample are lower than those of the epilayer, the CdTe samples do show a similar pattern in hardness. There is no large increase in hardness at very small depths; indentation curves for the CdTe samples show no evidence of a surface oxide being broken. Both epilayer samples show increases in measured hardness at depths  $> 400$  nm as the much harder GaAs substrates begin to influence the data.

Figure 2 shows the hardness of the CdTe-rich and ZnTe-rich superlattices as a function of depth. As is expected (since ZnTe is harder than CdTe), the unannealed and annealed ZnTe-rich superlattices are harder than the corresponding unannealed and annealed CdTe-rich superlattices, respectively. Both unannealed superlattices are harder than the corresponding annealed superlattices, which is due to layering effects. Strengthening from multilayers arises from the strain in the layers (compressive in the CdTe layers and tensile in the ZnTe layers) and from different moduli in the layers [3]. Since ZnTe is stiffer than CdTe, dislocations in the CdTe layers are repelled by the ZnTe layers, thus requiring larger applied stresses to move dislocations. Both unannealed superlattices show similar patterns in hardness: decreasing hardness with increasing depths  $< 400$  nm. This pattern is thought to arise from annealing that occurs as the superlattices are being grown. Interdiffusion between the ZnTe and CdTe layers occurs to a greater degree in the layers grown first than in the layers grown later. This interdiffusion of the two components decreases the strengthening effects of layers; thus, the hardness values decrease as the indenter reaches the lower layers (i.e., those closer to the buffer layer and substrate).

The annealed superlattices are softer than the corresponding unannealed superlattices, since the layers have interdiffused to form ternary alloys. X-ray diffraction scans of the two annealed samples show no superlattice satellite peaks, indicating that the superlattice structure has been completely destroyed. There appears to be a difference in the patterns of hardness of the two annealed superlattices, since the hardness of the ZnTe-rich sample is fairly linear with depth while the hardness of the CdTe-rich sample decreases with increasing depth. At closer inspection, however, this apparent difference may be due to a difference in testing: hardness values of the CdTe-rich superlattice range from depths of 18 to 1182 nm, while those of the ZnTe-rich superlattice range from depths of 70 to 1234 nm. Also, the indentation curves at very small depths for the annealed CdTe-rich sample indicate the breaking of a surface oxide. Since we have no data for the annealed ZnTe-rich sample at depths  $< 70$  nm, we do not know if this difference in patterns is real.

Figure 3 shows hardness as a function of ZnTe fraction in the epilayer and bulk ZnTe and CdTe samples, in ZnCdTe samples, and in the ZnTe-CdTe superlattices. Hardness values measured by the Vickers tester and by the Nanoindenter are shown. The lower curve in figure 3 shows Vickers hardness values of the ZnCdTe alloys ranging from 0.5 GPa at 2% ZnTe content to a maximum of 1.0 GPa at 30% ZnTe

content. These hardness values show a bowing due to solid solution hardening [4]. This bowing is seen in several ternary semiconductor systems (e.g., HgCdTe [5], GaInSb [4], InAsP [4], etc.). The hardness values of the binary compounds of CdTe and ZnTe are seen at the endpoints of the curves in figure 3. The hardness values of the epilayers of CdTe and ZnTe, 1.1 GPa and 1.5 GPa, compare favorably to values of the bulk CdTe and ZnTe, 0.8 GPa and 1.4 GPa. These values, however, are higher than Vickers hardness values of bulk CdTe and ZnTe, 0.46 GPa and 0.8 GPa. This difference can be explained by the fact that measured hardness typically increases as the applied load decreases [6]. The Vickers measurements were made using a weight of 25 g (245 mN), while the largest load applied by the Nanoindenter at depths of 400 nm was approximately 12 mN. The middle curve in figure 3 shows the hardness of the annealed superlattices. The hardness values of both the CdTe-rich and ZnTe-rich superlattices are 1.7 GPa. If these two values are joined to the hardness values of the binary epilayers, the resulting curve shows a bowing due to solid solution hardening. The upper curve in figure 3 shows the hardness of the unannealed superlattices. The hardness of the CdTe-rich superlattice is 2.2 GPa, while that of the ZnTe-rich superlattice is 2.4 GPa. If these values are joined to the hardness values of the binary epilayers, the resulting curve shows an even more pronounced bowing due to the strengthening by the multilayer structure.

Figure 4 shows Young's modulus values as a function of ZnTe content in the epilayer and bulk ZnTe and CdTe samples and in the superlattices. This figure shows modulus values from the literature [7] and values from the Nanoindenter indentation curves. The lower curve in figure 4 shows calculated modulus values for an isostress model for uniaxial deformation of a (100) multilayer [8]. These moduli for the model are significantly lower than the measured values and the literature aggregate values. This suggests that the modulus extracted from the Nanoindenter data is an aggregate value, not a modulus for the crystallographic orientation of the measured sample. The moduli of the binary compounds are seen at the endpoints of the curves in figure 4. Measured modulus values for the bulk and epilayer CdTe (41.3 GPa and 41.6 GPa, respectively) are very close; however, these values are a little higher than the literature aggregate value (38.1 GPa). Moduli for ZnTe from the literature aggregate value (61.0 GPa) and from the measured bulk (61.3 GPa) and epilayer (61.8 GPa) values are extremely close. The middle curve in figure 4 shows modulus values of the annealed superlattices. The modulus of the CdTe-rich superlattice is 49.8 GPa, while that of the ZnTe-rich superlattice is 52.5 GPa. If these values are joined to the moduli of the binary epilayers, the resulting curve shows a linear increase with increasing ZnTe fraction due to alloying. The upper curve in figure 4 shows moduli of the unannealed superlattices. The modulus of the CdTe-rich superlattice is 51.0 GPa, while that of the ZnTe-rich superlattice is 61.2 GPa. If these values are joined to the moduli of the binary epilayers, the resulting curve shows a slight bowing due to the strain in the multilayers.

## CONCLUSIONS

Hardness and modulus values of bulk and epilayer ZnTe and CdTe samples and of unannealed and annealed ZnTe-CdTe superlattices of two compositions (one third ZnTe content and two thirds ZnTe content) were measured. Increases in hardness in both ZnCdTe samples and annealed superlattices due to solid solution hardening were found. Increases in hardness with increasing ZnTe content in the unannealed superlattices, as compared to the corresponding annealed superlattices, due to the layering effects, were found. Hardness values of bulk ZnTe and CdTe show reasonable agreement with hardness values of epilayer ZnTe and CdTe. A linear increase in modulus values with increasing ZnTe content of annealed superlattices is



due to alloying and a slight increase (beyond the linear increase) in moduli of unannealed superlattices is due to the superlattice structure. Modulus values of bulk and epilayer samples of ZnTe and CdTe agree with each other and with the literature aggregate moduli for ZnTe and CdTe. The modulus value measured by the Nanoindenter appears to be an aggregate modulus.

## ACKNOWLEDGEMENTS

This work is supported by the Air Force Office of Scientific Research (contract AFOSR 85-0158, Project Task 2306/B1).

## REFERENCES

1. D. W. Kisker, P. H. Fuoss, J. J. Krajewski, R. M. Amirtharaj, S. Nakahara, and J. Menendez, *J. Crystal Growth* **86**, 210 (1988).
2. M. F. Doerner and W. D. Nix, *J. Mater. Res.* **1**, 601, (1986).
3. M. F. Doerner, Ph.D. thesis, Stanford University, 1987.
4. N. A. Goryunova, A. S. Borshchevskii, and P. N. Tretiakov, in Semiconductors and Semimetals, volume 4, edited by R. K. Willardson and A. C. Beer (1968) pp. 3-34.
5. J. G. Fleming, L. J. Farthing, and D. A. Stevenson, *J. Crystal Growth* **36**, 506 (1988).
6. D. Tabor, in Microindentation Techniques in Materials Science and Engineering ASTM STP 889, edited by P. J. Blau and B. R. Lawn (1986) pp. 125-159.
7. G. Simmons and H. Wang, Single Crystal Elastic Constants and Calculated Aggregate Properties: A Handbook, 2nd ed. (The M.I.T. Press, Cambridge, Massachusetts and London, England, 1971).
8. W. D. Nix (private communication).

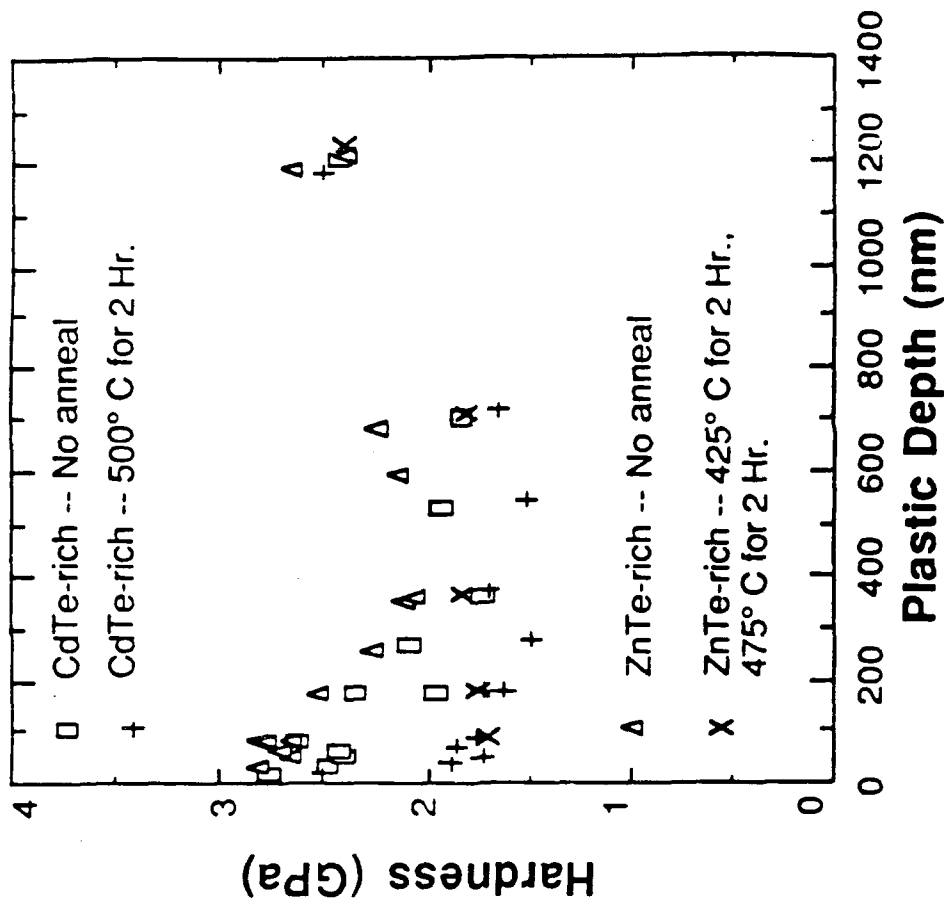


Figure 2. Hardness of ZnTe-CdTe superlattices as a function of plastic depth

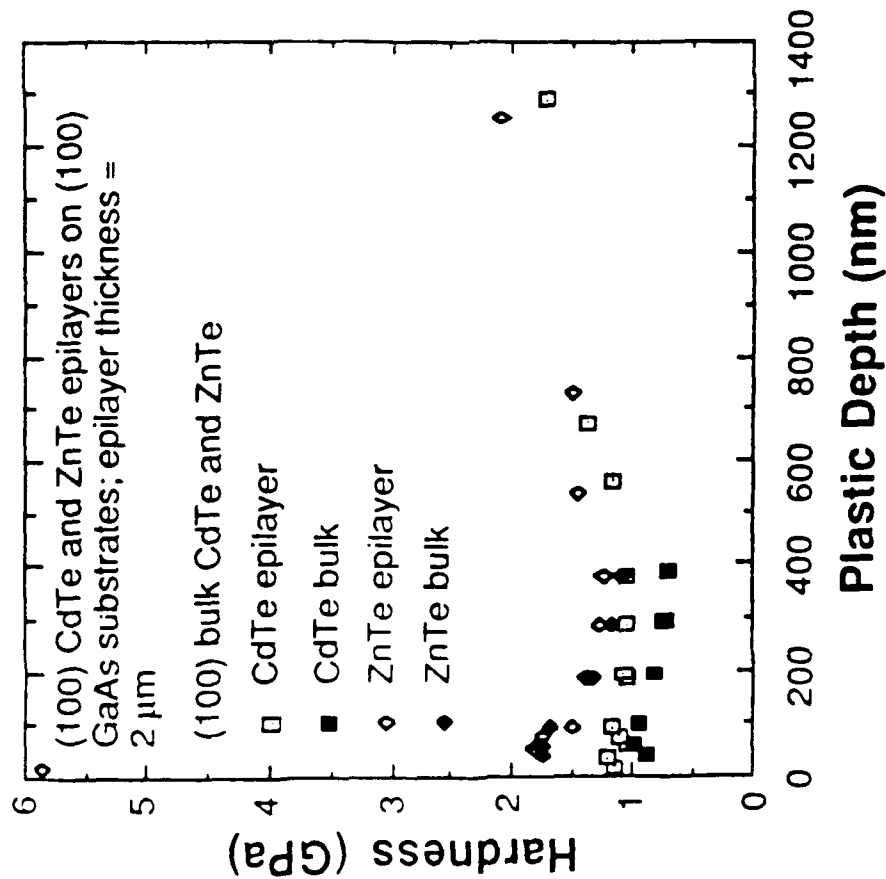


Figure 1. Hardness of epilayer and bulk ZnTe and CdTe as a function of plastic depth

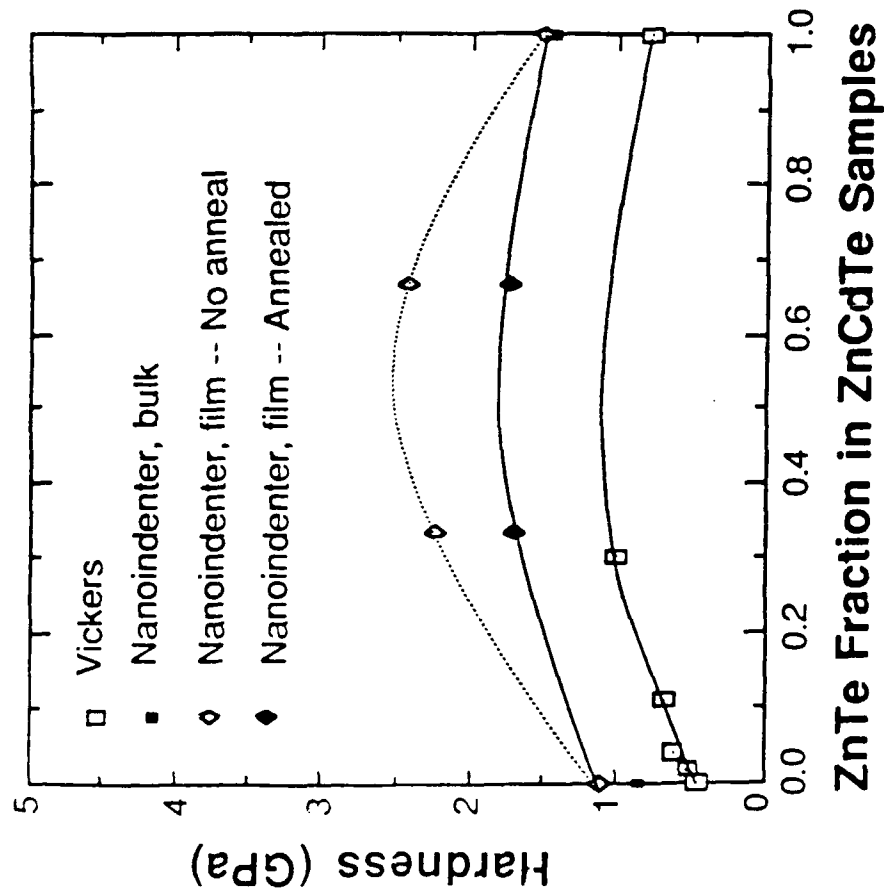


Figure 3. Hardness as a function of ZnTe fraction in epilayer and bulk ZnTe and CdTe and in ZnTe-CdTe superlattices

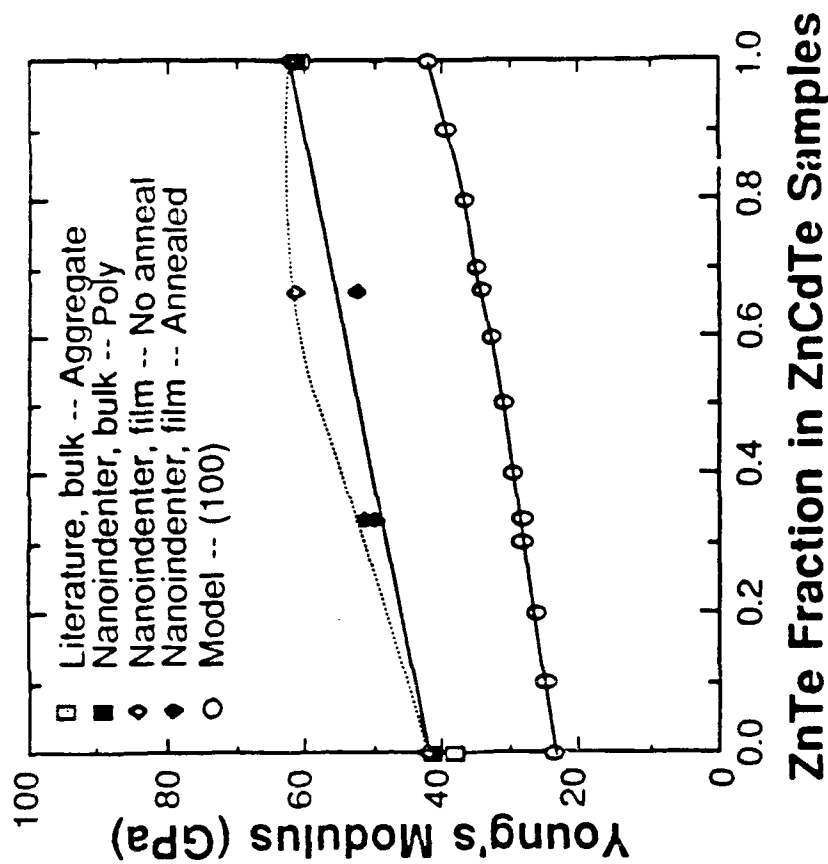


Figure 4. Young's moduli as a function of ZnTe fraction in epilayer and bulk ZnTe and CdTe and in ZnTe-CdTe superlattices

## Appendix H:

### The Determination of the Free Energy of Formation of Binary Tellurides Using Lithium Coulometric Titration Techniques.

J.G.Fleming and D.A.Stevenson.

*Department of Materials Science and Engineering  
Stanford University, Stanford ,CA 94305.*

**Abstract:** A low temperature electrochemical coulometric titration technique using Li was developed and used to determine the Gibbs free energies of formation of binary telluride compounds. The approach is based on the metal/ lithium/ tellurium phase diagram and relies upon the rapid diffusion of Li in these systems. The Gibbs free energy of formation of  $\text{Li}_2\text{Te}$  was determined by electrochemically titrating Li into pure Te until a 2 phase  $\text{Li}_2\text{Te}/\text{Te}$  mixture was formed. A value of  $-82.1 \pm 0.3$  kcal was calculated. With this information, the Gibbs free energies of formation of HgTe, CdTe and ZnTe were determined from the measured Li electrochemical potential found in appropriate metal/telluride/ $\text{Li}_2\text{Te}$  Gibbs tie triangle regions. ZnTe and CdTe were investigated by depositing a large amount of Li on the sample in question and observing a constant potential region after long annealing times. HgTe and  $\text{Hg}_{0.8}\text{Cd}_{0.2}\text{Te}$  were investigated by depositing a small amount of Li on the sample and observing the short time transient, with no plateau observed, but a characteristic "kink potential". Suitable analysis of the potential-time response characteristics for these cases leads to values for the free energies of formation of CdTe and ZnTe and HgTe of  $-23.2 \pm 0.6$  and  $-26.4 \pm 0.9$  kcal. and  $-6.8 \pm 1.1$  kcal., respectively, in good agreement with the information in the literature.

## Introduction

There is currently interest in the use of tellurides for infrared detection in the long wavelength regime and for possible use in optical communications. In order to understand and model the

growth mechanisms and the relevant phase equilibria, it is necessary to have reliable information on the thermodynamic properties of the binary compounds which make up the ternary solid solutions. Thermodynamic data on CdTe, ZnTe and HgTe has been obtained by a variety of techniques such as solution calorimetry, dissociation pressures and galvanic cell measurements. The results of these studies are analyzed and tabulated by K.C.Mills (1) and, in turn, incorporated in the tabulation of Barin and Knake (2). Currently most uncertainty exists in the data for HgTe, which is the binary of most interest.

Galvanic cell measurements are a direct and accurate method for determining thermodynamic information. In this approach, a galvanic cell is used to electrochemically titrate one of the components into, or out of, the sample. Thermodynamic data are then determined from the measured potentials in ternary tie triangle regions where, under constant temperature conditions, the component chemical potentials are constant. A study of this sort has recently been completed by Zabdyr on the ZnTe-CdTe system for temperatures between 503 and 692°C using a molten salt electrolyte (3). The high Hg partial pressures over HgTe at these temperatures, however, make similar experiments on HgTe impractical. This problem could be obviated if the required measurements could be made at room temperature. The kinetics of the relevant solid state reactions, however, are then impractically slow using standard techniques. For example, even at the higher temperatures investigated by Zabdyr (3), times of at least 12 hours were required before equilibrium was achieved.

The requirements of low temperatures and reasonable growth kinetics have led us to develop a technique using lithium as an electrochemical probe. Lithium is used because of its high mobility at low temperatures and because it forms an extremely stable  $\text{Li}_2\text{Te}$  compound. Furthermore, due to interest in Li for use in batteries, electrochemical techniques for dealing with Li are well developed.

### Basic Approach.

Fig. 1 shows the applicable portion of the room temperature Li/Cd/Te phase diagram determined using the thermodynamic data of Barin and Knake(2) and Huggins and coworkers (4). This diagram is dominated by the extremely stable  $\text{Li}_2\text{Te}$  compound. There are no reported ternary compounds in these systems and we found no evidence of any in the present work. The phase  $\text{LiTe}_3$  has been reported in the literature (5). However, it has been shown that  $\text{LiTe}_3$  decomposes to Te and  $\text{Li}_2\text{Te}$  at temperatures below  $250^\circ\text{C}$  (6,7). This conclusion was reached on the basis of annealing and X-ray studies and as a result of the extrapolation of thermodynamic data obtained by vapor pressure studies (7).

Application of the Gibbs phase rule to a ternary system indicates that the chemical potentials of the elements are fixed in three phase regions at constant temperature. For example, the component chemical potentials in triangles 1 and 2 are determined by the reactions:



and



The free energy of formation of  $\text{Li}_2\text{Te}$  can be determined from the potential measured in triangle 1 relative to pure Li using the equation:

$$\Delta G_r = -z F E_{\text{Li}} \quad [3]$$

where  $\Delta G_r$  is the free energy of the reaction,  $F$  is the Faraday,  $z$  is the stoichiometric coefficient, and  $E_{\text{Li}}$  is the potential measured with respect to pure Li. Similarly, the free energy of reaction [2] is given by equation [3] using the Li potential measured with respect to pure Li in triangle 2. Since the free energy of formation of  $\text{Li}_2\text{Te}$  is known from triangle 1 and the only other two participants in reaction [2] are elements, the free energy of formation of  $\text{CdTe}$  can be determined from the potential measured in triangle 2.

### Experimental.

The cells used were of the type:

$\text{Mo} \mid \text{Li} \mid 1\text{M LiF}_6\text{As in propylene carbonate} \mid \text{sample} \mid \text{Mo}$

All experiments were undertaken at  $25^\circ\text{C}$  under high purity He in a controlled atmosphere glove box.

The  $\text{HgTe}$  investigated was either supplied by Cominco or made by reacting stoichiometric amounts of Hg (5n8, Cominco) and Te (6n, Cominco) in an evacuated and sealed quartz ampoule.  $\text{CdTe}$  was supplied by Dr. M. Brown of Grumman Aircraft, and the  $\text{ZnTe}$  used was grown from the vapor. A variety of cell geometries were utilized, for long time experiments on  $\text{CdTe}$  and  $\text{ZnTe}$  the experimental geometry shown in Fig. 2 was employed. The powdered  $\text{CdTe}$  or  $\text{ZnTe}$

was mixed with a roughly equal volume of powdered W and pressed into a stainless steel container along with a Mo ribbon contact. Each container held ~0.04 grams of sample. The powdered W was added to the cell to provide electrical contact to the CdTe and ZnTe, which are highly resistive in their pure form at room temperature, and to reduce flaking off of the  $\text{Li}_2\text{Te}$  product phase. The potentiostat used was a PAR 173 equipped with a coulometer. The potential was measured with a Fluke multimeter and recorded by a chart recorder. In order to avoid current leakage through the voltmeter or chart recorder, a buffer amplifier was employed.

Before use, the electrolyte (1M  $\text{LiF}_6\text{As}$  in propylene carbonate) was conditioned by depositing Li onto a steel wool cathode from a ~5  $\text{cm}^2$  Li anode at 1 milliamp current for 70 hours. Pure Li was scraped clean in glove box and was used as both the working and reference electrodes. Enough Li was titrated into the samples to give ~20 to 30 atomic percent Li. Care was taken not to allow the potential to drop below 1.0 volts versus Li in order to avoid the formation of any  $\text{Cd}(\text{Zn},\text{Hg})/\text{Li}$  compounds. In all the experiments performed, it was noted that the  $\text{Li}_2\text{Te}/\text{Cd}(\text{Zn},\text{Hg})$  phases which form are brittle and tend to flake off so that the actual amount of Li within the sample can be much less than expected. It was necessary to wait ~4 to 6 weeks before a voltage plateau was approached. During this time the potential was monitored once every two days. Periodically a small amount of Li was titrated onto the sample in order to break down surface films which may have formed on the sample. Due to the long times involved and flaking and reversibility problems (discussed below), no attempt was made to titrate completely across the whole



of the three phase region of interest. Cells employing HgTe and  $\text{Hg}_{0.8}\text{Cd}_{0.2}\text{Te}$  failed before equilibrium had been obtained.

Transient experiments were undertaken on HgTe and  $\text{Hg}_{0.8}\text{Cd}_{0.2}\text{Te}$ . These cells were made by either attaching a sample onto a Mo ribbon using indium to bond the two together, or by using small Mo spring clamps. Experiments were then performed by titrating small amounts of Li onto the sample and monitoring the potential as the system recovers. The actual amount deposited depended on the sample surface area, in general  $\sim 0.05$  coulombs/cm<sup>2</sup> was used. Again, the potential with respect to the Li electrode was kept above 1.0 V in order to avoid the formation of any Li(Hg, Zn, Cd) compounds. Once the Li had been plated onto the sample, the cell was open circuited and the recovery of the potential with respect to Li electrode noted using a strip chart recorder. These experiments take hours to perform compared to the many weeks required for the long time experiments.

The same geometry was used to determine the free energy of formation of  $\text{Li}_2\text{Te}$ . The two phase Te/ $\text{Li}_2\text{Te}$  regime was accessed by plating Li onto the surface of pieces of Te using a current density of  $\sim 0.05$  microamps per cm<sup>2</sup> for  $\sim 10$  days. The low current density was used in order to minimize the amount of  $\text{Li}_2\text{Te}$  that flakes off the surface. After the Li was plated onto the sample, the potential with respect to pure Li was monitored daily.

Bulk samples of Li/Te/Hg were formed by annealing the desired amounts of pure HgTe,  $\text{Li}_2\text{Te}$  and Hg. Since quartz is not stable with respect to Li, all annealing was done in graphite crucibles, which, in turn, were enclosed in evacuated and sealed quartz

ampoules.

### Results and Discussion.

The results of experiments to determine the free energy of formation of  $\text{Li}_2\text{Te}$  are given in Fig. 3 which shows the potential versus Li plotted against time. The presence of a plateau centered about 1.779 volts indicates the presence of a two phase region at the surface of the samples. The increase in potential with time after the plateau potential had been reached in one of the samples shows that, in this sample, enough Li is present to move the surface into the one phase Te regime. Another possibility is that there was a sudden flaking off of the Li rich surface, which seems unlikely since the cell had been stable for more than 10 days prior to the increase in potential.

On the basis of these results, a value of  $1779 \pm 3 \text{ mV}$  is assigned to the potential with respect to Li of the 2 phase  $\text{Te}/\text{Li}_2\text{Te}$  regime corresponding to a value of  $-82.1 \pm 0.3 \text{ kcal.}$  for the free energy of formation of  $\text{Li}_2\text{Te}$  at  $25^\circ\text{C}$ , in excellent agreement with the value given by Mills,  $-82.8 \pm 5 \text{ kcal (1).}$

Fig. 4 shows a plot of potential versus time in days for two  $\text{CdTe}/\text{W}$  pressed powder cells. After rising sharply, the potential becomes approximately constant as the surface of the sample moves into the  $\text{CdTe}-\text{Cd}-\text{Li}_2\text{Te}$  three phase region (triangle 2 of Fig. 1). However, after approaching a constant value, the potential again begins to rise. This is unexpected since the amount of Li added to the samples, 20 and 30%, was thought to be well outside the limit of solubility of Li in the  $\text{CdTe}$ . Several explanations are possible for this

behavior. Li-rich material which flakes off during plating (observed experimentally) is lost so that the actual amount of Li within the sample may be significantly less than that generated coulometrically. It was noted that when Li was plated onto samples consisting only of pressed W powder the potential also increased with time, probably due to some side reaction occurring between the Li and the W or some contamination on the large surface area of the pressed W powders, or a side reaction involving the electrolyte. However, a similar effect was observed in experiments performed with ZnTe, except that the plateau potential was different in this case, indicating that these potentials are related to the sample and not the W powder which serves as a electrical contact.

Similar long time experiments were attempted for HgTe and  $\text{Hg}_{0.8}\text{Cd}_{0.2}\text{Te}$  but these cells either failed or no plateau was observed. The reason for this cell behavior is currently unknown. Because of this, the Gibbs free energy of HgTe was determined using shorter time transient measurements. The results of an experiment of this sort are given in Fig. 5. The kink in the plot of the recovery potential versus time is thought to be related to the movement of the surface of the sample towards the three phase regime, as is discussed below. The "kink potential" was, within experimental error, the same for HgTe and  $\text{Hg}_{0.8}\text{Cd}_{0.2}\text{Te}$ .

Fig. 6 shows the appropriate portion of the Li/Hg/Te ternary system with the tie lines between compounds and elements greatly exaggerated. In our transient recovery experiments, the Li is introduced at a fixed potential,  $\sim 1.0$  V for HgTe and 1.4 V for  $\text{Hg}_{0.8}\text{Cd}_{0.2}\text{Te}$ ; these potentials are selected to fix the surface in the

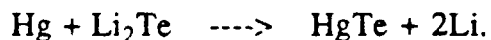
two phase Hg-Li<sub>2</sub>Te region (point A in Fig 6) so that no Li/Hg/Cd compounds form on the surface of the sample. After the desired period of time, the cell circuit is opened and the potential with respect to pure Li monitored with a voltmeter and a strip chart recorder.

The reason for the kink in the potential during recovery is shown with the aid of Figs. 6 and 7. The situation during plating is indicated in Fig. 7 which schematically shows the fraction of Li in the sample as a function of distance from the surface at several times. Since the potential at the surface is maintained constant by the potentiostat during charging (point A in Fig. 6), the concentration of Li at the sample surface is also constant as a function of time in accord with the Nernst equation. Because the activity of all the components is constant within a three phase regime and since there is Li diffusing into the sample, there must exist a three phase front which moves through the sample. The velocity of this front depends on both the rate of Li diffusion through the one and two phase regions and the rate of the solid state reaction which takes place at the three phase front:



The compositions of the high and low Li concentrations of the front are given by compositions A and B of Fig. 7, respectively. When the circuit is opened, Li continues to diffuse into the interior of the sample and the surface of the sample begins to approach point B on the border of the Hg/Li<sub>2</sub>Te/HgTe three phase region by diffusion of Li out of the Hg and Li<sub>2</sub>Te. Since the Li diffusion coefficients are high, the system should be reversible during this phase of the experiment,

in the sense that one could cycle between points A and B in Fig 6. Also, while there is a large change in potential in going from point A to point B (on the order of 600 mV), the change in composition required is small. If the system were completely reversible, the 3 phase zone (indicated by the vertical line in Fig. 7) would eventually move back towards the surface as Li continues to diffuse into the semi-infinite sink of the HgTe sample. (The amount of Li added is not expected to be outside the solubility limit of Li in HgTe.) However, movement of the 3 phase line requires the solid state reaction:



[5]

It is known that  $\text{Li}_2\text{Te}$  can decompose at room temperature, as shown by the increase in potential of one of the samples seen in Fig. 3. However, the formation of HgTe from Hg and Te may not occur in a reasonable time at room temperature. Exactly what happens after the surface has reached point B on the surface is not known. After this point the potential appears to approach that of the  $\text{Te}/\text{Li}_2\text{Te}$  triangle. That is, the system seems to behave as if the Hg is no longer present in the system. Regardless of what happens after composition B has been reached, it is evidenced by a change in the rate of change of potential. This forms the kink on the potential-time curve and allows us to determine the potential at point B. Since the potential at point B is, in turn, the same as that in the three phase region, it is possible to obtain the free energy of formation of HgTe. Whether or not the system remains reversible past point B is immaterial, so long as this

point is identified by a variation in the rate of change of the potential with time.

The "kink potential" was found to be independent of the rate of recovery, except when the potential changes rapidly (for small amounts of Li charging) Fig.8. Only data from experiments in which the rate of approach was slow enough,  $>0.1$  V/hr., to be rate independent was used to determine the potential at the kink position. Taking the mean value of  $1635 \pm 8$  mV with respect to pure Li gives the free energy of formation of HgTe as  $-6.8 \pm 1.1$  kcal., in excellent agreement with that given by Mills,  $-6.7 \pm 1.5$  kcal. (1).

The motivation behind investigating both HgTe and  $\text{Hg}_{0.8}\text{Cd}_{0.2}\text{Te}$  was to determine experimentally if there is any change in the HgTe chemical potential when alloying with CdTe; as has been suggested experimentally, see for example (8). However, as was already mentioned, little difference was found between HgTe and  $\text{Hg}_{0.8}\text{Cd}_{0.2}\text{Te}$ . Perhaps a longer systematic study could address this question more accurately. However, such a study would also have to satisfactorily deal with the problem introduced by Cd, which adds another degree of thermodynamic freedom to the system.

It is possible that non-equilibrium effects also occur in the longer time CdTe and ZnTe experiments and are responsible for the increase in potential beyond the  $\tau'$  region. In this case, the plateau potential observed should be that of the three phase region, in accord with our interpretation. The experimentally observed plateau potentials are  $1278 \pm 3$  mV for CdTe and  $1207 \pm 6$  mV for ZnTe. Using these values and the free energy of formation obtained for  $\text{Li}_2\text{Te}$  determined earlier leads to values for the free energies of

formation of CdTe and ZnTe of  $-23.2 \pm 0.6$  kcal. and  $-26.4 \pm 0.9$  kcal. respectively. As can be seen from Table 1, these results are in good (CdTe) or reasonable (ZnTe) agreement with those found in the Mills Handbook (1).

### Summary and Conclusions.

In summary, new data is presented on the room temperature free energies of formation of HgTe, CdTe, ZnTe and  $\text{Li}_2\text{Te}$ . The new technique developed uses Li as an electrochemical probe and offers kinetic advantages which make room temperature experiments possible in reasonable times. Problems arising from irreversibility can be overcome through an understanding of what is happening during the recovery process. This approach has the potential to be used on a whole range of binary chalcogenide materials to relatively quickly determine accurate thermodynamic data on this increasingly important class of materials.

### References.

1. K. C. Mills, "Thermodynamical Data for Inorganic Sulphides, Selenides and Tellurides," Butterworths, London (1974).
2. I. Barin and O. Knake, "Thermochemical properties of inorganic substances," Springer-Verlag, Berlin (1973). I. Barin, O. Knake and O. Kubaschewski, "Thermochemical properties of inorganic substances, supplement." Springer-Verlag, Berlin (1977).
3. L. A. Zabdyr, *This Journal*, **131**, 2157 (1984).
4. R. Huggins et al. personal communication.

5. P. T. Cunningham, S. A. Johnson and E. J. Cairns, *This Journal*, **120**, 328 (1973).
6. D. Y. Valentine, O. B. Cavin and H. C. Yakel, *Acta Cryst. B***33**, 1389 (1977).
7. M. S. Foster and C. C. Lin, *J. Physical Chem.* **70**, 950 (1966).
8. A.Sher, A.-B.Chen, W.E.Spicer, and C.-K.Shih, *J. Vac. Sci. Technol.* **A3**, 105 (1985)



Table 1. A summary of the results obtained in this study and those given elsewhere.

Fig. 1. The Li/Cd/Te ternary phase diagram with the Cd/Li compounds not shown for clarity. No evidence was found in this work of ternary phases in triangles 1 and 2. In accord with the Gibbs phase rule the chemical potentials of the elements are constant in these ternary tie triangles, and the potential of Li with respect to pure Li can be measured by an electrochemical cell.

Fig. 2. The electrochemical cell geometry used in long time experiments investigating CdTe and ZnTe. The sample was pressed into the stainless steel container together with powdered W in order to provide electrical contact to the highly resistive samples and to prevent excess flaking of Li rich material during Li deposition.

Fig. 3. The results of 4 experiments in which Li was plated onto Te and the potential with respect to pure Li then monitored as a function of time. The "0" of time represents the beginning of monitoring, which started several days after the Li was plated.

Fig. 4. The results of two experiments in which the Li potential with respect to pure Li was monitored with time after 20 and 30% Li had been plated onto the CdTe/W electrode. The "0" in time represents the beginning of monitoring which commenced about 10 days after plating.

Fig. 5. The shape of a typical potential versus time curve in the region of the kink potential. In all short time experiments using HgTe or  $\text{Hg}_{0.8}\text{Cd}_{0.2}\text{Te}$  a similar kink was observed.

Fig. 6. This figure shows the portion of the Hg/Li/Te phase diagram relevant to short time experiments. The width of the tie lines to different phases has been exaggerated for the purpose of illustration. Point A gives the composition at the surface of the sample during plating of Li. Under these conditions only Hg and  $\text{Li}_2\text{Te}$  are stable at the surface. When the cell is open-circuited, Li continues to diffuse in and the overall composition at the surface moves to point B on the border of the Hg/HgTe/ $\text{Li}_2\text{Te}$  ternary tie triangle. The potential measured at point B is the same as that within the tie triangle. Point C represents the Li poor limit of the Hg/HgTe/ $\text{Li}_2\text{Te}$  ternary tie triangle along a line joining HgTe and Li. If the system is completely reversible then the composition at the surface of the sample will move back and forth along this line as Li is plated onto, and removed from the surface.

Fig. 7. A schematic of the situation during plating of Li at different times. The composition at the surface is fixed since the potential with respect to pure Li is maintained constant by the potentiostat. The compositions A, B and C are those given in Fig. 6. The potential must remain constant within three phase regions giving rise to a three phase front (B-C) which moves into the sample as Li indiffuses. The rate of movement of the front is a function of the rates of Li diffusion in the two (A-B) and one phase regions and the rate of the solid state reaction:

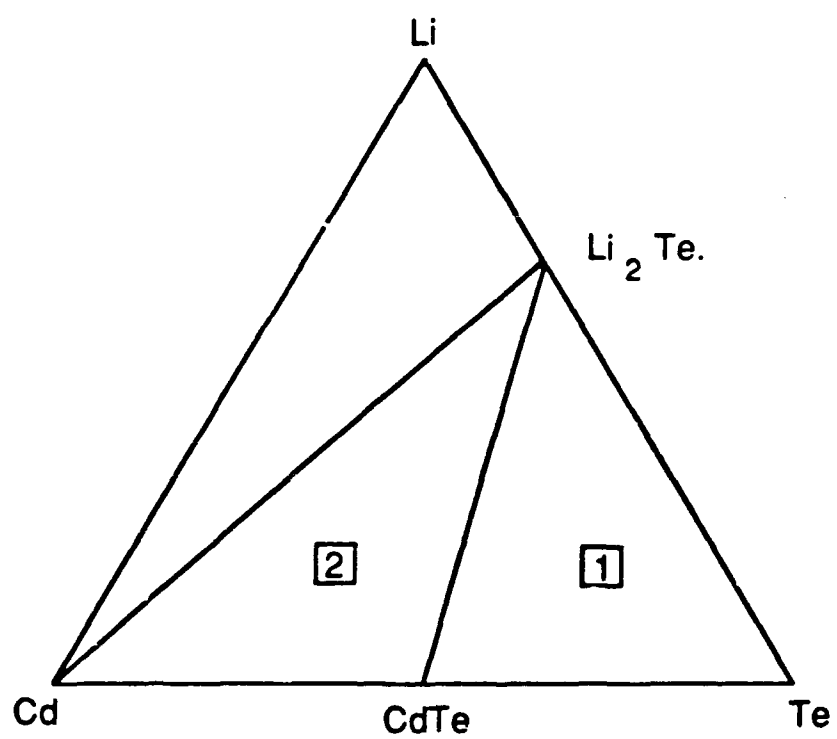


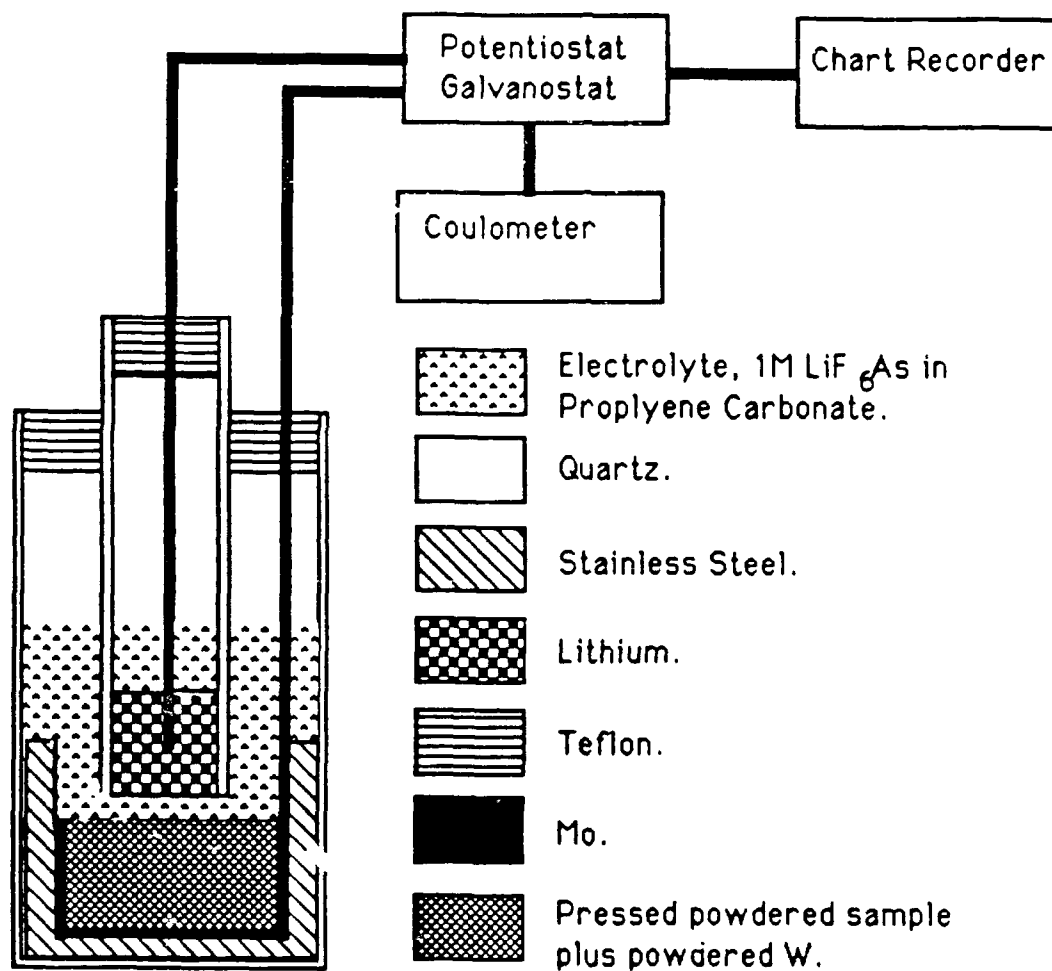
Fig. 8. The dependence of the value of the kink potential on the rate of change of potential, the samples in this case being  $\text{Hg}_{0.8}\text{Cd}_{0.2}\text{Te}$ . For higher rates there is a strong dependence of the potential observed, however, for low rates the kink potential is independent of the rate of change. The reason for the strong effect at higher rates is unknown, only data from experiments in the rate independent regime was used to determine free energies of reaction.

Table 1

Material	Free energy of Formation (kcal.)		
	This Study	Barin	Zabdyr
Li <sub>2</sub> Te	-82.1±0.3	-82.9±5	-
HgTe	-6.8 ±1.1	-6.7 ±1.5	-
CdTe	-23.2±0.6	-23.7±0.3	-23.7±0.1
ZnTe	-26.4±0.9	-27.5±0.2	-27.5±0.2

Table 1. A summary of the results obtained in this study and those given elsewhere.





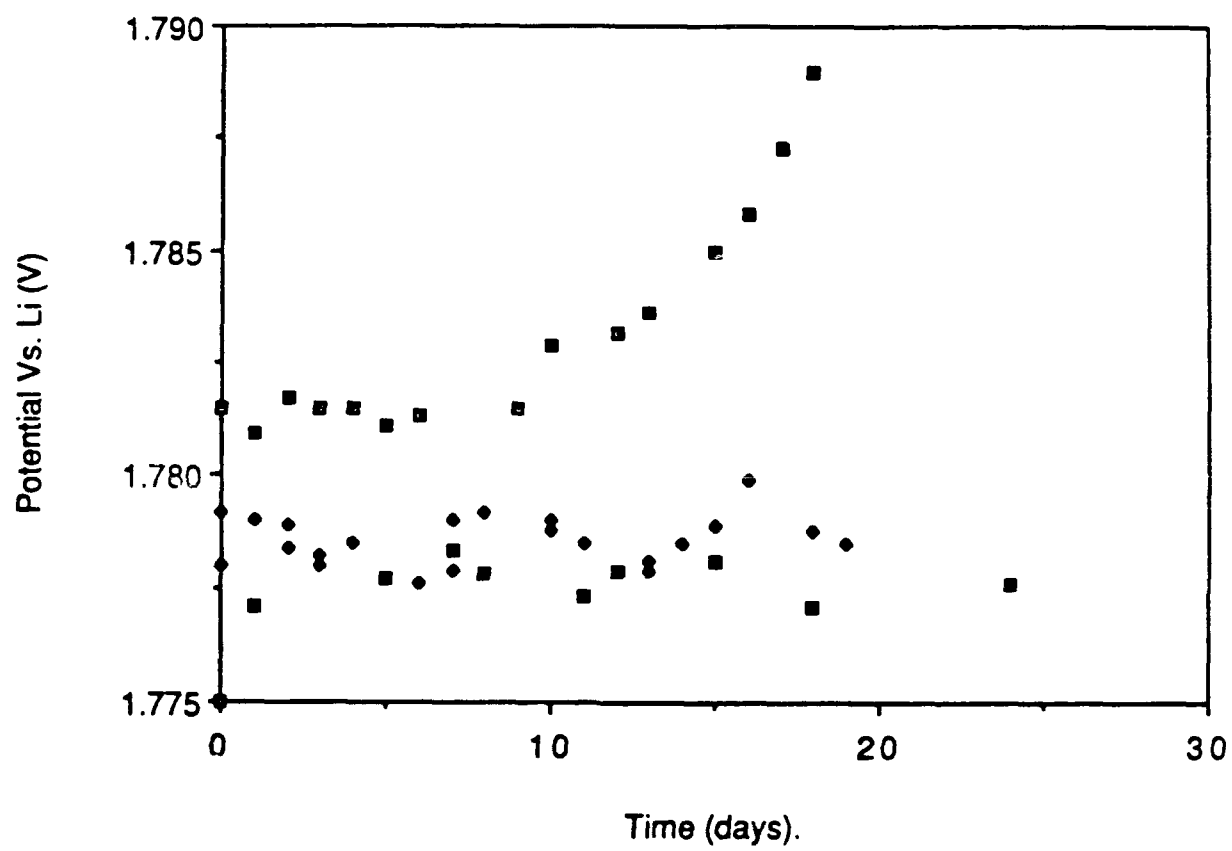


Fig. 3

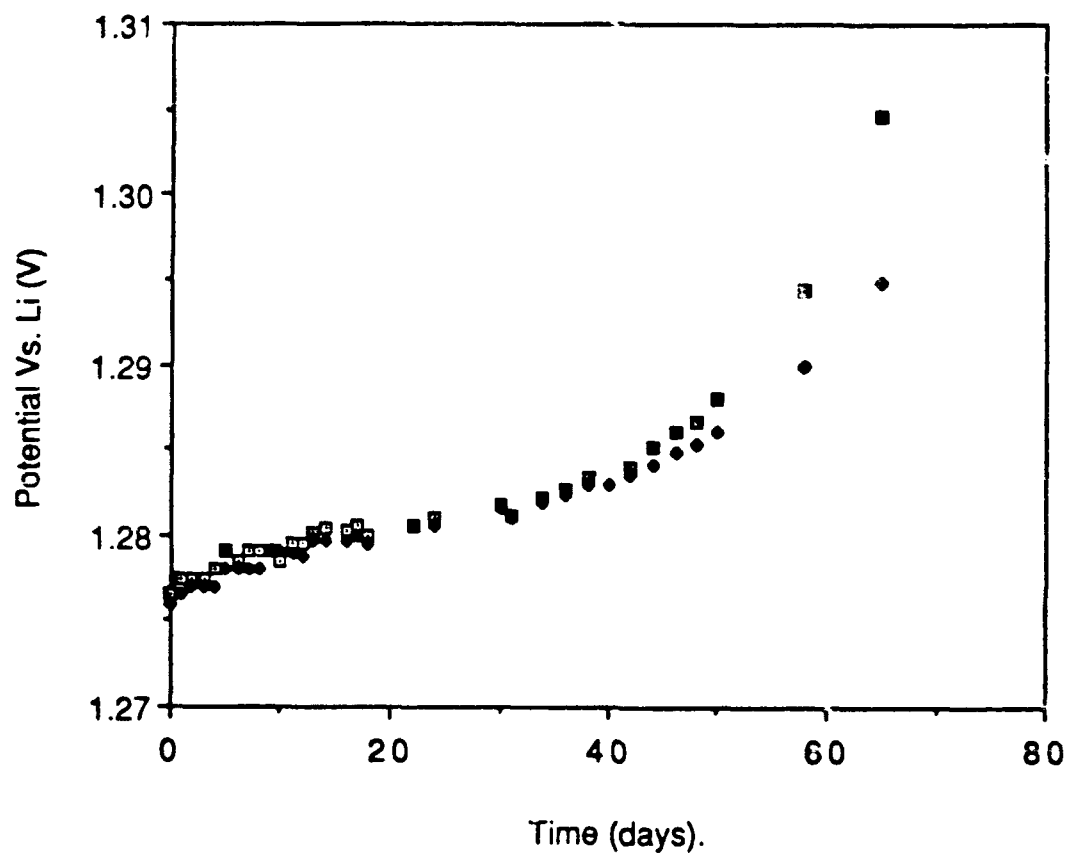


Fig 4



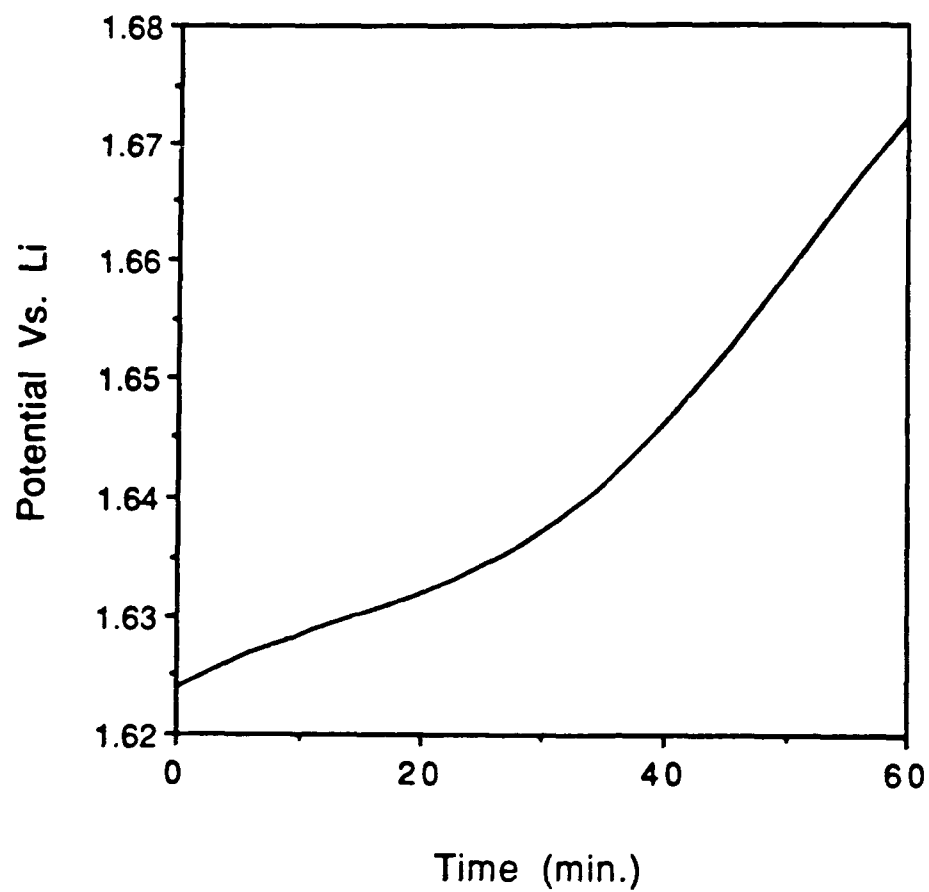
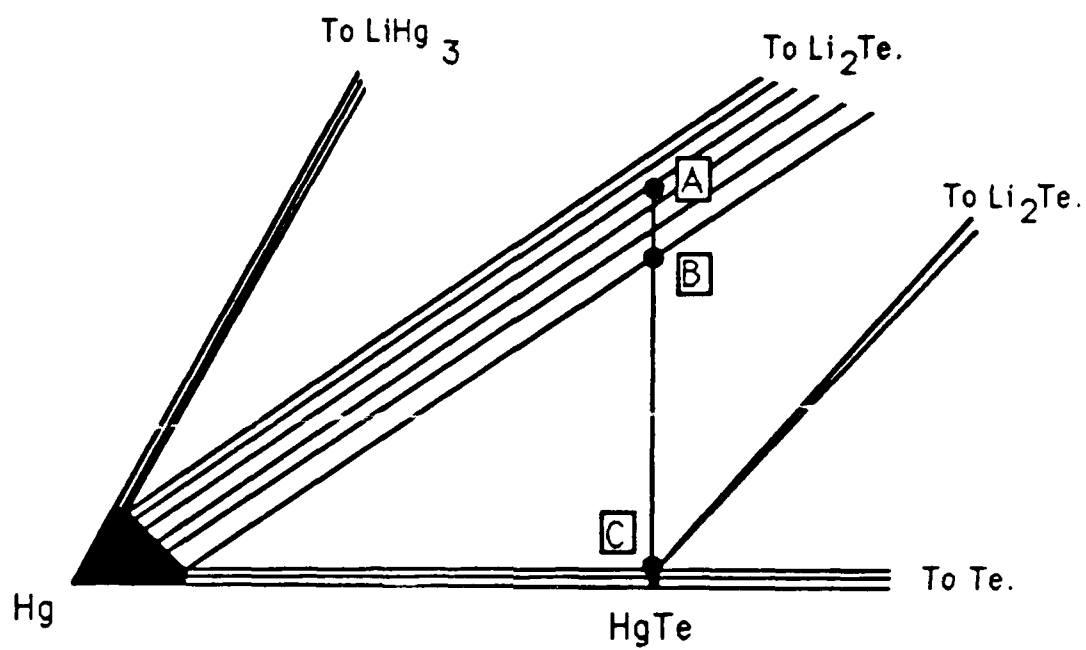


Fig 5



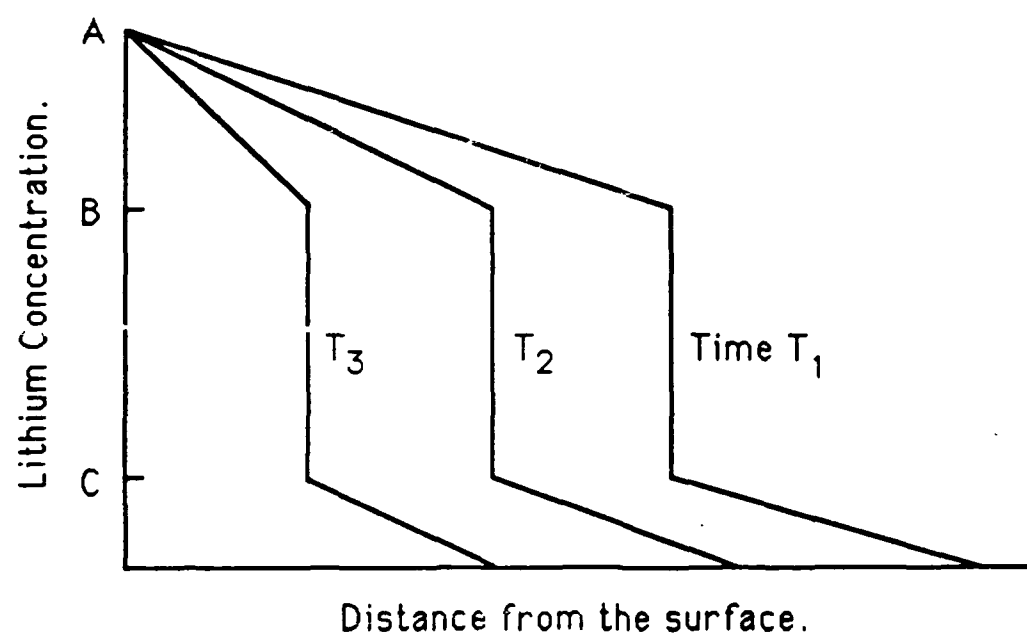


Fig 7

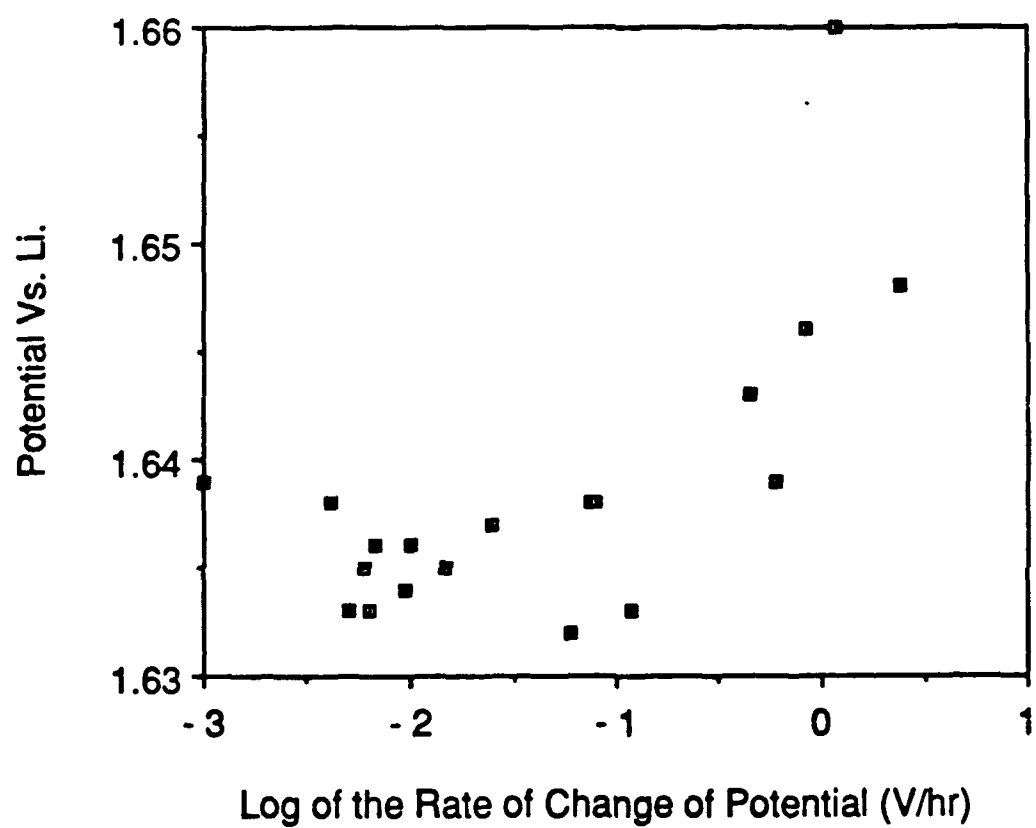


Fig 8

## Interdiffusion behavior of HgTe-CdTe junctions

Mei-Fan S. Tang and David A. Stevenson

Department of Materials Science and Engineering, Stanford University, Stanford, California 94305

(Received 12 December 1986; accepted for publication 3 March 1987)

Interdiffusion coefficients ( $\bar{D}$ ) were measured from 600 to 300 °C for HgTe-CdTe diffusion couples. The influence of the binary composition, temperature, and Hg overpressure on  $\bar{D}$  has been established. Significant differences have been found in the behavior of  $\bar{D}$  in two temperature regions. A dual mechanism is proposed for diffusion at higher temperatures ( $T > 450$  °C), with a vacancy mechanism and an interstitial mechanism dominating at low and high  $x$  value regions, respectively, and an interstitial mechanism predominating at lower temperatures. The proposed model is confirmed by electrical property, tracer diffusion, and theoretical studies, and provides a basis for predicting the interdiffusion behavior at even lower temperatures.

The  $\text{Hg}_{1-x}\text{Cd}_x\text{Te}$  (MCT) quasi-binary alloy is an attractive long wavelength material, since its band gap can be tuned by varying the alloy composition. Interdiffusion in MCT is of interest because of its relevance to the sharpness of junctions in epitaxial films and to the stability in HgTe-CdTe superlattices.<sup>1</sup> The currently available information on interdiffusion in this system is limited for the lower temperatures<sup>1-4</sup> where epitaxial layers and superlattices are grown.<sup>5</sup> An x-ray method has been used to obtain  $\bar{D}$  at lower temperatures by analyzing the decay of the intensities of satellite peaks while the molecular beam epitaxial (MBE) grown superlattices were annealed.<sup>6</sup> The calculations in this method assume that  $\bar{D}$  is independent of  $x$ , whereas the present experimental information shows a strong  $x$  dependence. The currently available low-temperature self-diffusion data are difficult to apply for interdiffusion, because the mechanism associated with each of the multiple branches in the tracer concentration profiles is not resolved.<sup>7,8</sup> In the present paper, we describe a study of the interdiffusion behavior as a function of temperature, composition, and ambient Hg overpressure, with particular emphasis on the lower temperature region.

A conventional junction was made by clamping HgTe-CdTe single crystals together with a quartz spring. To provide a well defined vapor environment and to establish an adequate junction for interdiffusion, either Hg-saturated or Te-saturated HgTe powder was placed around the diffusion couple in a quartz ampoule. The ampoule was then evacuated and sealed. The annealing temperatures ranged from 300 to 600 °C. After an appropriate annealing time (long enough to establish an interdiffused region of at least 20  $\mu\text{m}$ ), the diffusion couple was removed from the ampoule, mounted, and angle lapped. The interdiffusion coefficients ( $\bar{D}$ ) were obtained by a Boltzmann-Matano analysis of the composition profiles, which were determined by electron microprobe analysis using a JEOL 733 Superprobe. Before each profile was determined, the electron beam was stabilized and the system calibrated using HgS, Cd, and Te standards. The software program was set for a standard deviation of 0.5%, and with this procedure, the reproducibility was 1% of the concentration in question. This was confirmed by analyzing single crystals of CdTe. The electron beam was 20 keV, with

a stability greater than 0.2%; at this beam energy, the penetration depth (>90% of the emitted x ray) was 5000 Å, so that the penetration depth does not seriously perturb the profiles obtained with the angle lapping method. A 0.1- $\mu\text{m}$  concentration resolution can be achieved by using a 1.75° angle lapping and 3  $\mu\text{m}$  stepping.

A plot of the  $\log \bar{D}$  vs  $x$  is shown in Fig. 1 for both Hg-rich and Te-rich conditions. The activation energy ( $\Delta E_a$ ) for each  $x$  value is obtained from the slope of  $\ln \bar{D}$  vs  $1/kT$ , with  $\Delta E_a$  values given in Table I for each  $x$  and Hg overpressure condition. The dependence of activation energy on  $x$  was determined by evaluating  $(\partial \ln \bar{D} / \partial x)kT$ , and the results are listed in Table II.

These results show a strong dependence of  $\bar{D}$  on  $x$  and  $T$ , but not on  $P_{\text{Hg}}$ , at  $T > 450$  °C; for  $x < 0.5$ ,  $\bar{D}$  is expressed as  $\bar{D}(x, T) = 1.0 \exp - (1.53 + 0.51x/kT)$ , with the activa-

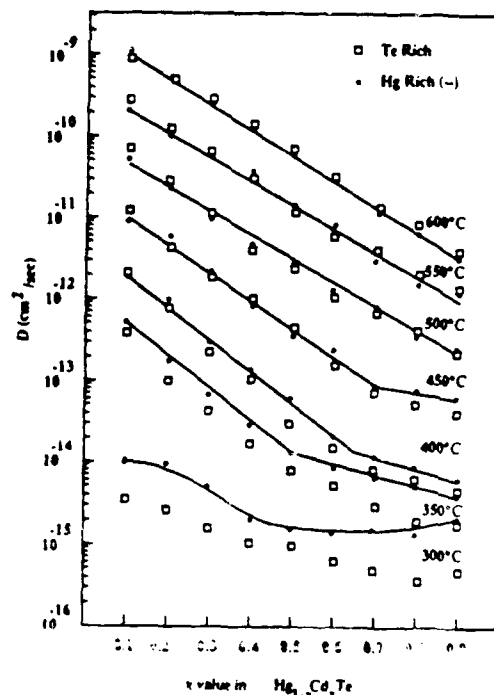


FIG. 1.  $\bar{D}$  vs  $x$  for different temperatures and Hg overpressure.

TABLE I Activation energy (eV) for different  $x$  values and Hg overpressure in two temperature regions.

Temperature region	$x$	Te-rich	Hg-rich
$T > 450^\circ\text{C}$	0.1	1.53	1.75
	0.2	1.63	1.74
	0.3	1.70	1.80
	0.4	1.77	1.84
	0.5	1.82	1.83
	0.6	1.73	1.81
	0.7	1.70	1.63
	0.8	1.68	1.54
	0.9	1.60	1.47
300–400 $^\circ\text{C}$	0.7	0.92	0.74
	0.8	0.94	0.67
	0.9	0.81	0.56

tion energy increasing linearly with increasing  $x$ . For  $x > 0.5$ ,  $\Delta E_a$  decreases slightly and there are differences in  $\Delta E_a$  for Hg-saturated and Te-saturated conditions (Table I). The behavior of  $\bar{D}$  for  $T < 400^\circ\text{C}$  shows the following trends with decreasing temperature: (i) the activation energy decreases, (ii) the composition dependence of  $\bar{D}$  decreases, and (iii)  $\bar{D}$  depends on the ambient Hg overpressure. These changes are more pronounced in the higher  $x$  value region, and extend to the lower  $x$  value region as temperature decreases. Since the  $x$  dependence of  $\bar{D}$  changes continuously as the temperature decreases, there is no simple expression for  $\bar{D}$  for temperatures below  $450^\circ\text{C}$ .

For the quasi-binary  $\text{Hg}_{1-x}\text{Cd}_x\text{Te}$  system, the interdiffusion coefficient ( $\bar{D}$ ) is related to the cation intrinsic chemical diffusion coefficients ( $D_i$ ), namely,  $D_{\text{Hg}}$  and  $D_{\text{Cd}}$ , by the Darken equation<sup>9</sup>:  $\bar{D} = D_{\text{Hg}}x + D_{\text{Cd}}(1-x)$ , where  $D_i$  is a defect density-defect diffusivity product. The exponential dependence of  $\bar{D}$  on  $x$  at higher temperatures ( $T > 450^\circ\text{C}$ ) requires two conditions:  $\bar{D} = D_{\text{Hg}} = D_{\text{Cd}}$ <sup>8,9</sup>; and the defect concentration is an exponential function of  $x$ . The latter condition arises from the enthalpy of formation of cation defects being a linear function of  $x$ , which arises mainly from the linear dependence of  $E_g$  on  $x$ . If a simple vacancy mechanism for interdiffusion is assumed and information on the  $x$  dependence of defect concentration is obtained from existing

TABLE II.  $x$  dependence of  $\Delta E_a$  for different temperatures, Hg overpressure and  $x$  value regions.

Temperature region	Range of $x$	Te-rich	Hg-rich
600 $^\circ\text{C}$	0.1–>0.7	0.51	0.52
	0.1–>0.7	0.51	0.49
	0.1–>0.7	0.50	0.49
	0.1–>0.7	0.51	0.47
	0.7–>0.9	0.15	0.13
400 $^\circ\text{C}$	0.1–>0.6	0.58(0.1–>0.5)	0.50
	0.7–>0.9	0.25(0.6–>0.9)	0.15
350 $^\circ\text{C}$	0.1–>0.5	0.45(0.2–>0.4)	0.49
	0.6–>0.9	0.26(0.6–>0.8)	0.12
300 $^\circ\text{C}$	0.2–>0.8	0.16	0.39
	0.6–>0.8	0.13	0.00

theoretical calculations<sup>10</sup> and experimental Hall measurements<sup>11–13</sup> (Fig. 2), the predicted  $x$  dependence ( $\sim 0.78$ ) is higher than is observed ( $\sim 0.5$ ) (Table II). The vacancy mechanism would also imply a strong dependence of  $\bar{D}$  on Hg overpressure, in contrast to the observed behavior. The insensitivity of  $\bar{D}$  to  $P_{\text{Hg}}$  is consistent with a dual vacancy-interstitial mechanism for interdiffusion. The  $x$  dependence of  $\bar{D}$  implies that the concentration of interstitial species is less  $x$  dependent than vacancy species.

The observed trends in  $\bar{D}$  and the corresponding  $\Delta E_a$  values with  $x$ ,  $T$ , and stoichiometry (metal-rich versus Te-rich) can be explained by the following model: (i) both interstitial and vacancy metal species may participate in the metal diffusion process, and one or the other may dominate in different temperature and  $x$  value regions, depending on the concentration-mobility product; (ii) vacancy species have a lower formation enthalpy in the lower  $x$  value region and a lower mobility than interstitial species in general; (iii) at higher temperatures, the mobility is not a dominant factor determining the diffusion, and the concentration of vacancy species is higher than interstitial species for lower  $x$  values; (iv) interstitial species have a lower activation energy for motion, thus, at lower temperatures, when their concentration is sufficiently high, interstitial species will dominate; and (v) the metal vacancy concentration decreases more rapidly than the metal interstitial concentration with increasing  $x$  value, leading to a dominance of interstitials at higher  $x$  values.

This model is supported by electrical measurements (Fig. 2) which show that vacancies are dominant defects at  $T > 450^\circ\text{C}$  for both Hg-rich and Te-rich conditions for lower  $x$  values<sup>11–13</sup> ( $x < 0.5$ ), and by the theoretical calculations of Morgan-Pond and Raghavan,<sup>10</sup> which indicate that Cd in-

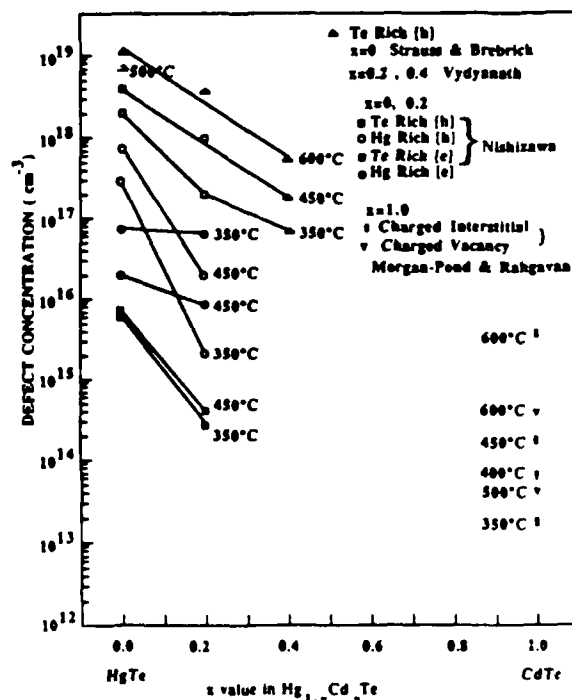


FIG. 2. Defect concentration vs  $x$  for different temperatures and Hg overpressure.

terstitials are a dominant metal defect in CdTe even for Te-saturated conditions. Furthermore, tracer diffusion studies of  $x = 0.2$  MCT indicate that Hg diffuses by both vacancy and interstitial mechanisms,<sup>8</sup> and most tracer diffusion studies for CdTe suggest that Cd moves by a vacancy-interstitial complex, consistent with the observed independence on Cd overpressure.<sup>14,15</sup>

For  $T > 450^\circ\text{C}$ , from  $x = 0.1$  to  $0.5$ , diffusion proceeds dominantly via a vacancy mechanism with  $\Delta E_a$  increasing with  $x$  in accord with the increasing vacancy formation energy. As  $x$  increases further from  $0.6$  to  $0.9$ ,  $\Delta E_a$  decreases (Table I) in accord with an increased contribution of an interstitial mechanism. This explains the trend that  $\Delta E_a$  is higher for Hg-saturated conditions than for Te-saturated conditions in the lower  $x$  value region, whereas  $\Delta E_a$  is lower for Hg-saturated conditions than for Te-saturated conditions in the higher  $x$  value region.

Both electrical measurements<sup>16</sup> and theoretical calculations<sup>10</sup> show an increase in metal interstitial concentration with decreasing temperature below  $450^\circ\text{C}$ , and interstitials may be higher than metal vacancies at larger  $x$  values. In addition, the observed  $\Delta E_a$  value for  $x = 0.9$  for Hg-saturated conditions is  $0.56\text{ eV}$  (Table I), which is close to  $\Delta E_a$  for Hg interstitials in  $x = 0.2$  MCT obtained from self-diffusion studies.<sup>8</sup> The interstitial mechanism is relatively more important in the higher  $x$  value regions, and extends to the lower  $x$  value regions as the temperature decreases. The increased importance of the interstitial mechanism explains the observed changes in  $\bar{D}$  below  $450^\circ\text{C}$ , since the interstitial mechanism has a lower activation energy and is less  $x$  dependent than is the vacancy mechanism. Meanwhile, as expected,  $\bar{D}$  for Hg-saturated conditions is higher than  $\bar{D}$  for Te-saturated conditions, and the difference of  $\bar{D}$  between two Hg overpressure conditions is larger for lower temperatures and larger  $x$  values.

The dominant interstitial mechanism for higher  $x$  values provides a basis for extrapolating  $\bar{D}$  values to temperatures below  $300^\circ\text{C}$ , whereas for low  $x$  values, one needs information on defect concentrations for that region. Recently,  $\bar{D}$  values have been obtained for HgTe-CdTe superlattices using x-ray methods, assuming  $\bar{D}$  is independent of  $x$ .<sup>6</sup> Since our results indicate that the dependence of  $\bar{D}$  on  $x$  decreases as temperature decreases below  $450^\circ\text{C}$ , assuming  $\bar{D}$  to be constant at  $185^\circ\text{C}$  may be reasonable. The first Fourier component diffusion coefficient  $\bar{D}(\pm 1)$  for the sample annealed under He ambient at  $185^\circ\text{C}$  is close to our  $\bar{D}(x = 0.9)$  for Te-rich conditions, and the activation energies of  $\bar{D}(\pm m)$  for  $1 < m < 3$  are close to our  $\Delta E_a$  for higher  $x$  values. This indicates an interstitial mechanism becomes dominant for all the  $x$  values at temperatures below  $300^\circ\text{C}$ .

In summary, the interdiffusion coefficients for

HgTe-CdTe couples have been measured from  $300$  to  $600^\circ\text{C}$  for both Hg-rich and Te-rich conditions using an angle lapping method. There is a significant difference in diffusion behavior above and below  $450^\circ\text{C}$ ; at lower temperatures, there is a lower activation energy, less dependence on  $x$ , and a dependence on stoichiometry. Extrapolation of high-temperature diffusion data ( $>450^\circ\text{C}$ ) to lower temperatures would predict  $\bar{D}$  values that are too low. Referring to our results and information on the dominant defects in the MCT described in the literature leads to several conclusions: (i) the exponential dependence of  $\bar{D}$  on  $x$  in the higher temperature region arises from identical intrinsic diffusion coefficients for both cations along with an enthalpy of defect formation which depends linearly on  $x$ ; (ii) interdiffusion proceeds by a dual mechanism at  $T > 450^\circ\text{C}$  with a vacancy and an interstitial dominant in regions of lower  $x$  and higher  $x$  values, respectively, resulting in  $\bar{D}$  being relatively insensitive to the Hg overpressures; and (iii) as temperature decreases below  $450^\circ\text{C}$ , the interstitial mechanism increases in importance, with an increase in  $\bar{D}$ , a corresponding decrease in the  $x$  dependence, and an increase in Hg overpressure dependence, especially at higher  $x$  values. The defect model provides a basis for understanding the trends in  $\bar{D}$  at the lower temperatures. With appropriate assumptions, extrapolation of our data to lower temperatures gives good agreement with  $\bar{D}$  obtained by x-ray studies of HgTe-CdTe superlattices grown by MBE.

We thank Professor H. Schmalzried, Dr. M. Brown, and C. R. Zercher for helpful discussions and to Dr. M. Brown for providing some of the CdTe substrates used in this work. This work is sponsored by Defense Advanced Research Projects Agency through Office of Naval Research, contract N000-(84K-0423).

<sup>1</sup>J. N. Schulman and Y. C. Chang, Appl. Phys. Lett. **46**, 571 (1985).

<sup>2</sup>V. Leute, H. M. Schmidtke, W. Stratmann, and W. Winking, Phys. Status Solidi A **67**, 183 (1981).

<sup>3</sup>L. Svob and Y. Marfaing, J. Appl. Phys. **46**, 4251 (1975).

<sup>4</sup>K. Zanio and T. Massopust, J. Electron. Mater. **15**, 103 (1986).

<sup>5</sup>J. P. Faure, A. Million, and J. Piagnet, Appl. Phys. Lett. **41**, 713 (1982).

<sup>6</sup>J. L. Staudenmann, R. D. Horning, R. D. Knox, J. Reno, I. K. Sou, J. P. Faure, and D. K. Arch, Trans. Met. Soc. AIME (to be published).

<sup>7</sup>M. Brown and A. F. W. Willoughby, J. Cryst. Growth **59**, 27 (1982).

<sup>8</sup>M. F. S. Tang and D. A. Stevenson (unpublished).

<sup>9</sup>M. F. S. Tang and D. A. Stevenson (unpublished).

<sup>10</sup>C. G. Morgan-Pond and R. Raghavan, Phys. Rev. B **31**, 6616 (1985).

<sup>11</sup>J. Strauss and R. F. Brebrick, J. Phys. Chem. Solids **31**, 2283 (1970).

<sup>12</sup>H. R. Vydyanath, J. Electrochem. Soc. **128**, 260 (1981).

<sup>13</sup>H. R. Vydyanath, J. C. Donovan, and D. A. Nelson, J. Electrochem. Soc. **128**, 2685 (1981).

<sup>14</sup>P. M. Borsenberger and D. A. Stevenson, J. Phys. Chem. Solids **29**, 1277 (1968).

<sup>15</sup>S. S. Chern and F. A. Kroger, J. Solid State Chem. **14**, 299 (1975).

<sup>16</sup>J. Nishizawa and K. Suto, J. Phys. Chem. Solids **37**, 33 (1976).

# Interdiffusion and related defect mechanisms in the HgTe–CdTe system

M. F. S. Tang and D. A. Stevenson

Department of Materials Science and Engineering, Stanford University, Stanford, California 94305

(Received 17 November 1986; accepted 12 May 1987)

Interdiffusion coefficients ( $D$ ) were measured from 300 to 600 °C using an angle lapping technique and electron microprobe analysis. The influence of the binary composition, temperature, and Hg overpressure was studied. There is a significant difference in the behavior of  $D$  in the higher and lower temperature regions. At higher temperatures ( $T > 450$  °C),  $D$  is a strong function of composition and temperature and is insensitive to the Hg overpressure. At lower temperatures ( $T < 450$  °C), we observe the following trends with decreasing temperature: (i) the activation energy decreases, (ii)  $D$  is less dependent on  $X$  ( $X$  is the CdTe mole fraction), and (iii)  $D$  depends on Hg overpressure. Based on an analysis of our interdiffusion data, we propose a dual mechanism for higher temperatures with a vacancy and an interstitial mechanism dominating at low and high  $X$  values, respectively, and an interstitial mechanism at lower temperatures.

## I. INTRODUCTION

The  $\text{Hg}_{1-x}\text{Cd}_x\text{Te}$  (MCT) quasibinary alloy is an attractive long-wavelength material since the band gap of MCT can be tuned by varying the alloy composition. Adjusting the layer thicknesses in HgTe–CdTe superlattices accomplishes the same goal and may be easier to control than varying the alloy composition.<sup>1</sup> Interdiffusion in the HgTe–CdTe pseudobinary system is of interest because it is relevant to the sharpness of junctions in both epitaxial films and HgTe–CdTe superlattices, and to the effectiveness of CdTe capping layers. The currently available experimental information on interdiffusion in this system is for higher temperatures ( $> 450$  °C),<sup>2–6</sup> and there is only limited information at lower temperatures where epitaxial layers and superlattices are grown.<sup>7</sup>

HgTe–CdTe superlattices were first made with the molecular-beam epitaxy (MBE) technique by Faurie *et al.*<sup>8</sup> The measured band gap appeared to be larger than predicted by theory,<sup>9</sup> which may arise from the interdiffusion between HgTe and CdTe during the growth at  $\sim 200$  °C. Calculation using  $D$  values extrapolated from higher temperatures underestimated the apparent intermixing.<sup>10</sup> The interdiffusion in superlattices has been evaluated with x-ray methods at low temperature,<sup>11</sup> but it was necessary to assume that  $D$  is independent of composition, although the present literature indicates a strong dependence on composition.<sup>2–6</sup> Junction profiles of epilayers grown by other low-temperature techniques (e.g., metal–organic chemical vapor deposition) are also influenced by interdiffusion behavior in the lower-temperature region. To estimate  $D$  from currently available low-temperature self-diffusion data is difficult because there are multiple branches in self-diffusion profiles<sup>12–15</sup> and it is not clear which branch is appropriate for  $D$ . In the present paper, we present results of studies of the interdiffusion of HgTe/CdTe junctions to determine the influence of temperature, composition, and ambient Hg pressure. These methods are effective to determine  $D$  values as low as  $10^{-16}$   $\text{cm}^2/\text{s}$  at 300 °C. We have analyzed the diffusion results and express  $D$  in an Arrhenius form:  $[D = D_0 \exp(-\Delta E_a/kT)]$  with an activation energy ( $\Delta E_a$ ) dependent on  $X$ , ( $\Delta E_a = a + bX$ ). We have observed a significant difference

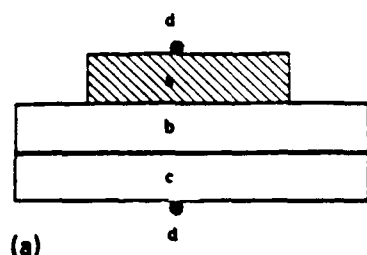
in the behavior of  $D$  in the different temperature regions. It is therefore inappropriate to extrapolate diffusion data above 450 °C to lower temperatures. Based on our results and information in the literature on defects in MCT,<sup>16–21</sup> we propose a dual mechanism for interdiffusion at  $T > 450$  °C: there are contributions from both vacancies and interstitials, with vacancies more important in the lower  $X$  value region, and interstitials, with a lower activation energy and a lower  $X$  dependence, in the higher  $X$  value regions. The interstitial mechanism becomes increasingly important with decreasing temperature. Our proposed model provides a basis for estimating interdiffusion behavior at temperatures below 300 °C.

## II. EXPERIMENTAL METHODS

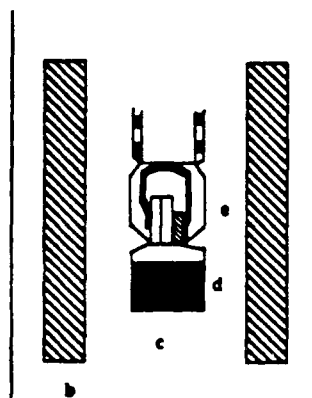
A conventional diffusion junction was made by clamping HgTe–CdTe single crystals with a quartz spring [Fig. 1(a)]. A defined vapor ambient was provided by adding either Hg-saturated or Te-saturated HgTe powder around the diffusion couple in a quartz ampoule, which was evacuated and sealed [Fig. 1(b)]. After annealing at the selected temperatures (300–600 °C), the diffusion couple was removed from the ampoule, mounted, and angle lapped. The interdiffusion coefficients ( $D$ ) were obtained by an improved Boltzmann–Matano analysis<sup>22</sup> of the composition profiles which were determined by electron microprobe analysis.

The microprobe used was a JEOL 733 Superprobe. Before each profile was determined, the electron beam was stabilized and the system calibrated using HgS, Cd, and Te standards. The software program was set for a standard deviation of 0.5% and, with this procedure, the reproducibility was 1% of the concentration in question. This was confirmed by analyzing single crystals of CdTe. The electron beam was 20 keV, with a stability greater than 0.2%. At this beam energy, the penetration depth ( $> 90\%$  of the emitted x rays) was  $< 5000$  Å, therefore, the penetration depth does not seriously perturb the profiles obtained with the angle lapping method. The lapping angles varied for each sample.





(a)



(b)

FIG. 1. Experimental arrangement for interdiffusion. (a) a: CdTe single crystal, b, c: HgTe single crystals, d: quartz spring. (b) a: 1 zone furnace, b: thermal mass, c: quartz ampoule, d: HgTe powder, e: diffusion couple.

and several stepping distances in the microprobe analysis were used to obtain the most reliable resolution. For example, a  $3^\circ$  angle lap with a  $5\text{-}\mu\text{m}$  step in the probe analysis gives a  $0.26\text{-}\mu\text{m}$  concentration resolution, which is accurate enough for the  $\sim 20\text{-}\mu\text{m}$  interdiffusion region established after long anneals at the lower temperatures.

### III. RESULTS

A plot of the logarithm of the interdiffusion coefficient ( $D$ ) versus composition ( $X$ ) for both Hg-rich and Te-rich conditions is shown in Fig. 2. Our data for higher temperature regions are consistent with those of Leute *et al.* ( $500 < T < 600^\circ\text{C}$ ).<sup>6</sup> The data from Bailly *et al.*<sup>3</sup> ( $400 < T < 600^\circ\text{C}$ ) were converted to the same units and are shown in Fig. 2. Their  $D$  values were generally lower than ours in the higher-temperature regions, whereas at  $400^\circ\text{C}$ , their results agree with ours at lower  $X$  values but are higher than ours at higher  $X$  values. This may be caused by a decrease in the resolution at the higher  $X$  values where the concentration gradient is larger. Their paper did not give details of the microprobe analysis nor of methods to control the component vapor pressure. Since  $D$  is an exponential function of  $X$ , we express  $D$  as  $D = D_0 \exp(-\Delta E_a/kT)$ , with an  $X$ -dependent  $\Delta E_a$  ( $\Delta E_a = a + bX$ ). The activation energy ( $\Delta E_a$ ) for each  $X$  value was obtained from the slope of  $\ln D$  vs  $1/kT$  and values are listed in Table I for each  $X$  and Hg overpressure condition, with an estimated accuracy of 5%. The composition ( $X$ )-dependent term in the activation energy ( $b$ ) for each temperature is obtained from calculating  $(\partial \ln D / \partial X)kT$ , and the results are listed in Table II.

There is a strong dependence of  $D$  on  $X$  and  $T$  but not on

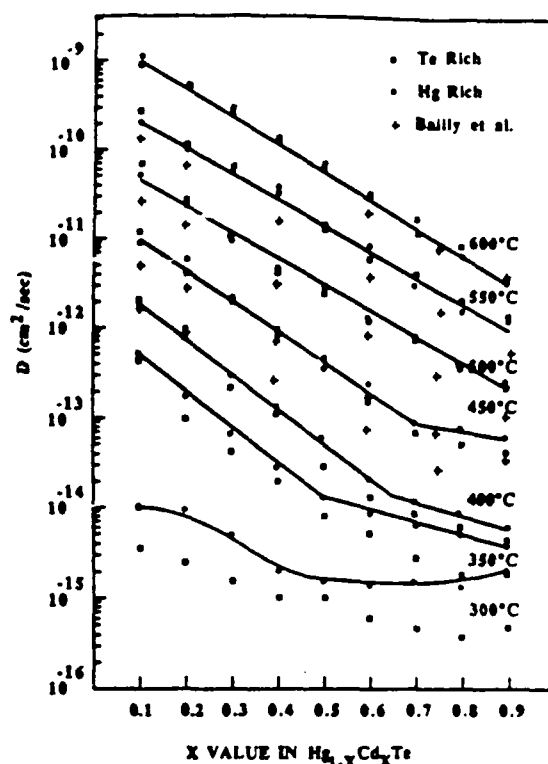


FIG. 2.  $D$  vs  $X$  for different temperatures and Hg overpressure. Solid lines are through the Hg-rich points.

the ambient vapor pressure for  $T > 450^\circ\text{C}$ , and  $D$  can be expressed as  $D(X, T) = 1.0 \exp[-(1.53 + 0.51X)/kT]$  for  $X < 0.5$ . For  $X > 0.5$ ,  $\Delta E_a$  decreases slightly for both Hg-rich and Te-rich conditions and there are differences in  $\Delta E_a$  for Hg-rich and Te-rich conditions.

For  $T < 400^\circ\text{C}$ , the following trends are observed with decreasing temperature: (i) the activation energy decreases, (ii) the composition dependence of  $D$  decreases, and (iii)  $D$  depends on the ambient Hg vapor pressure. These changes are more pronounced for higher  $X$  values, and extend to the lower  $X$  values as the temperature decreases. There is no

TABLE I. Activation energy (eV) for different  $X$  values and Hg overpressure in two temperature regions.

Temperature region	$X$	Te-rich	Hg-rich
$T > 450^\circ\text{C}$	0.1	1.53	1.75
	0.2	1.63	1.74
	0.3	1.70	1.80
	0.4	1.77	1.84
	0.5	1.82	1.83
	0.6	1.73	1.81
	0.7	1.70	1.63
	0.8	1.68	1.54
	0.9	1.60	1.47
300–400 $^\circ\text{C}$	0.7	0.92	0.74
	0.8	0.94	0.67
	0.9	0.81	0.56

TABLE II.  $X$  dependence of  $\Delta E_f$  for different temperatures, Hg overpressure, and  $X$  value regions

Temperature region (°C)	Range of $X$	Te-rich	Hg-rich
600	0.1-0.7	0.51	0.52
550	0.1-0.7	0.51	0.49
500	0.1-0.7	0.50	0.49
450	0.1-0.7	0.51	0.47
	0.7-0.9	0.15	0.13
400	0.1-0.6	0.58(0.1-0.5)	0.50
	0.7-0.9	0.25(0.6-0.9)	0.15
350	0.1-0.5	0.45(0.2-0.4)	0.49
	0.6-0.9	0.26(0.6-0.8)	0.12
300	0.2-0.4	0.16	0.39
	0.6-0.8	0.13	0.00

simple analytical expression for  $D$  for the low-temperature region.

#### IV. DISCUSSION

In Sec. IV A, we describe a mechanism to explain the insensitivity of  $D$  to the  $P_{H_2}$  and the exponential dependence of  $D$  on  $X$  at  $T > 450^\circ\text{C}$ , and then explain the changes of  $D$  below  $450^\circ\text{C}$  by a change in mechanism. In Sec. IV B, we extrapolate our results to temperatures below  $300^\circ\text{C}$  and compare with the  $D$  values measured by x-ray methods.<sup>11</sup>

##### A. Defect mechanism

A study of the dependence of diffusion coefficients on the component vapor pressure provides information on the defect mechanism for diffusion. In a pseudobinary system, it is necessary to define two-component vapor pressures in order to provide a reproducible diffusion ambient. Controlling solely the Hg overpressure, which has the highest vapor pressure in the system,<sup>23</sup> is sufficiently accurate for tracer diffusion studies<sup>12</sup> and makes the study through the whole stoichiometry region possible. It was found by experience that some Te in the vapor is needed to establish an adequate junction for diffusion, otherwise a Hg liquid film remains at the junction and prevents a proper diffusion bond. Therefore, we use either a Te-saturated or Hg-saturated HgTe powder to establish the ambient vapor pressure for interdiffusion studies. Although we measure  $D$  under these two conditions, the Te-saturated or Hg-saturated condition for HgTe ( $X = 0.0$ ) does not correspond to the Te-saturated condition or Hg-saturated condition for all the  $X$  values which appear during interdiffusion. Since these saturation pressures depend on  $X$ , it is not possible to establish local saturation conditions for the whole range of stoichiometry; however, it is possible to relate  $D$  to  $D^*$ , the tracer diffusion coefficients.<sup>24</sup> Further information and insight on the  $X$  dependence of  $D$  and the independence of  $D$  on  $P_{H_2}$  for  $T > 450^\circ\text{C}$  is presented by deriving  $D$  for pseudobinary systems using the fundamental relations between respective diffusion coefficients.

The Darken equation  $D(X) = [D_A X + D_B (1 - X)]$ ,

which relates the interdiffusion coefficient ( $D$ ) to the component intrinsic chemical diffusion coefficients  $D_i$  ( $D_A, D_B$ ), is the same for a binary and a pseudobinary system  $A_{1-x}B_xC$ .<sup>24</sup> However, in relating  $D$  to the  $D^*$  values, there are additional constraints that arise from the preservation of stoichiometry and the Gibbs-Duhem equation and the resulting equations differ from the Darken equation for a binary system. The derivation shows that  $D = D_A = D_B$  if the nonmetal ( $C$ ) moves more slowly than the metal components ( $A, B$ ), and  $D$  will be very close to the self-diffusion coefficient ( $D^*$ ) of the slower metal component.<sup>24</sup>

Referring to tracer diffusion studies for  $X = 0.2$  MCT,<sup>12</sup> it was observed that  $D \approx D_{Cd}^*$ . The assumption that Te moves relatively slowly is consistent with tracer diffusion studies<sup>12</sup> and with marker experiments.<sup>25</sup> Our interdiffusion experiments are performed for Hg-saturated or Te-saturated conditions, and the insensitivity of  $D$  to  $P_{H_2}$  in those two conditions may result from interstitials in Hg-saturated conditions diffusing as fast as vacancies diffusing in Te-saturated conditions. However, the tracer diffusion coefficient of Cd is independent of  $P_{H_2}$  through the whole stoichiometry range,<sup>12</sup> and since  $D \approx D_{Cd}^*$ ,  $D$  is independent of  $P_{H_2}$  over the whole stoichiometry range. This behavior is consistent with a vacancy-interstitial complex as the dominant mobile species.

Further insight into the defect mechanism can be obtained by exploring the relationship of  $D$  to the intrinsic chemical and tracer diffusion coefficients. As mentioned in the previous paragraph, for the present system, with  $D_{Te}^* < D_{H_2}^*$ , one can show that<sup>12,24</sup>  $D = D_{H_2} = D_{Cd} \approx D_{Cd}^*$ , with  $D_{H_2}^* > D_{Cd}^*$ . One can relate the tracer diffusion coefficient to a product of defect diffusivity  $D_d$  and defect concentration  $[d]$ . The available information on the Hg tracer diffusion studies for both  $X = 0.0$ ,<sup>12,26</sup> and  $0.2$ ,<sup>12,15</sup> and the defect concentrations (mainly vacancy),<sup>17,18</sup> implies that the  $D_d$  dependence on composition is negligible. Since  $[d]$  depends on the formation energy ( $\Delta E_f$ ) according to the expression  $[d] = d_0 \exp(-\Delta E_f/kT)$ , a linear dependence of  $\Delta E_f$  on composition  $X$  produces a linear dependence of  $\Delta E_f$  on  $X$ , and  $D$  will depend exponentially on  $X$ .

The following provides insight into the  $X$  dependence of  $\Delta E_f$ . To analyze the defect formation energy, we assume that the ionized defects are dominant for an ionic semiconductor MCT. The formation energy of doubly charged cation vacancies is<sup>16</sup>

$$\Delta E_f(V_{V''}^{\cdot\cdot}) = \Delta H_{V_{V''}^{\cdot\cdot}} - (2E_f - E_{V_{V''}^{\cdot\cdot}} - E_{V_{V''}^{\cdot\cdot}}),$$

where  $\Delta H_{V_{V''}^{\cdot\cdot}}$  is the neutral cation vacancy formation enthalpy,  $E_f$  is the self-consistent Fermi energy,  $E_{V_{V''}^{\cdot\cdot}}$  is the first ionization energy level of cation vacancies, and  $E_{V_{V''}^{\cdot\cdot}}$  is the second ionization energy level of cation vacancies. ( $E_f, E_{V_{V''}^{\cdot\cdot}}$ , and  $E_{V_{V''}^{\cdot\cdot}}$  are referenced to valence-band edge.) Taking values of  $\Delta H_{V_{V''}^{\cdot\cdot}}$  for CdTe and for  $X = 0.2$ ,<sup>16</sup> and using  $E_f$  values from theory<sup>16</sup> and the  $E_{V_{V''}^{\cdot\cdot}}$  and  $E_{V_{V''}^{\cdot\cdot}}$  values at 300 K from the literature,<sup>27,28</sup> we obtain  $\Delta E_f(V_{V''}^{\cdot\cdot}) = 0.44 + 0.88X$  (eV). The  $X$  dependence of  $\Delta E_f$  is larger than our  $X$  dependence of  $\Delta E_f$  in the higher temperature region (Table II).

Using the currently available electrical data for hole concentrations ( $p$ ) for  $X = 0.0$ ,<sup>17</sup>  $X = 0.2$ ,<sup>18</sup> and  $X = 0.4$ <sup>19</sup> and a theoretical calculation<sup>16</sup> for  $X = 1.0$ , and assuming that  $p = 2[V_{\text{Te}}^{\bullet}]$ , the slope of  $\ln[V_{\text{Te}}^{\bullet}]$  vs  $X$  (Fig. 3) is  $\sim 0.78$  in the high-temperature region. Thus, a pure vacancy mechanism predicts a higher  $X$  dependence of  $D$  than is observed. Either a pure vacancy mechanism or a pure interstitial mechanism would also imply a strong dependence of  $D$  on  $P_{\text{Hg}}$ , which is contrary to our results, thus, a dual vacancy-interstitial mechanism is appropriate.

Tracer diffusion studies for  $X = 0.2$  MCT indicate that Hg diffuses by both a vacancy and an interstitial mechanism,<sup>12</sup> and most tracer diffusion studies for Cd in CdTe indicate that Cd moves by a vacancy-interstitial complex and is independent of Cd overpressure.<sup>29,30</sup> Therefore, it is reasonable that HgTe and CdTe interdiffuse by a dual mechanism involving both vacancies and interstitials with the interstitial concentration less dependent on  $X$  than the vacancy concentration.

The dominant native electrically active defects influencing the electrical properties are metal vacancies in both Hg-rich and Te-rich conditions for the low  $X$  value region ( $X < 0.5$ ) at  $T > 450^\circ\text{C}$  (Fig. 3). According to calculations of Morgan-Pond and Raghavan,<sup>16</sup> metal interstitials are the dominant defects on the metal sublattice in CdTe, even in a Te-saturated condition. The observed increase in  $\Delta E_a$  as  $X$  increases from 0.1 to 0.5, and decrease as  $X$  increases from 0.6 to 0.9 (Table I) for both ambient conditions may arise from the increased importance of vacancies in the low  $X$  value regions and interstitials, with a lower activation energy

in the high  $X$  value regions. This explains the trends in  $\Delta E_a$  with  $P_{\text{Hg}}$ : at low  $X$  values,  $\Delta E_a$  is higher for Hg-rich conditions than for Te-rich conditions, but for  $X > 0.5$ ,  $\Delta E_a$  is lower for Hg-rich conditions than for Te-rich conditions.

There is evidence that the interstitial mechanism becomes more important for temperatures below  $450^\circ\text{C}$ , especially for higher  $X$  values. Nishizawa and Suto reported Hall measurements for  $X = 0.0$  and  $X = 0.2$  from  $350$  to  $450^\circ\text{C}$  with different magnetic fields and resolved the  $n$  and  $p$  values under different Hg overpressure conditions.<sup>20</sup> Their results show that at lower temperatures ( $350^\circ\text{C}$ ),  $n$  increases to be comparable to  $p$ , and  $n$  is higher than  $p$  for  $X = 0.2$  in Hg-rich conditions (Fig. 3). From Nishizawa and Suto's data at  $350^\circ\text{C}$ , we calculate the slope of  $\ln(n)$  vs  $\ln(P_{\text{Hg}})$  to be 1, which is consistent with a charged cation interstitial donor defect. In addition, for  $X = 1.0$ , the ionized cadmium interstitial concentration is higher than the ionized vacancy concentration, with the difference increasing as the temperature decreases<sup>16</sup> (Fig. 3). For Hg-saturated conditions at lower temperatures,  $\Delta E_a$  is  $0.56\text{ eV}$  for  $X = 0.9$ , which is close to the  $\Delta E_a$  value for Hg interstitials in  $X = 0.2$  MCT obtained from tracer diffusion studies.<sup>12,15</sup> Thus, electrical measurements, theoretical calculations, and tracer studies all indicate an increased importance of interstitial defects with decreasing temperature.

An increased importance of metal interstitial species also explains the observed trends for  $D$  with temperatures decreasing below  $450^\circ\text{C}$ . The decrease in the activation energy is consistent with the lower activation energy of an interstitial mechanism. Furthermore, a decrease in the dependence of  $D$  on  $X$  is consistent with a less  $X$ -dependent defect species. Although, there is currently no information for the dependence of interstitial concentrations on  $X$ , the behavior of  $D$  at higher temperatures ( $T > 450^\circ\text{C}$ ) implies that interstitial species depend less on  $X$  than vacancy species, as mentioned previously. The increase in the  $X$  dependence of the vacancy concentration with decreasing temperature (Fig. 3) and the observed decrease in the  $X$  dependence of  $D$  is consistent with an increased importance of metal interstitial species. Finally,  $D$  values are higher for Hg-rich conditions than for Te-rich conditions, and the difference of  $D$  between the two ambient conditions is larger for lower temperatures and larger  $X$  values; this is expected for lower temperatures where cation interstitial defects are more important. Since the  $X$  dependence of  $D$  changes continuously at different  $X$  values as temperature decreases,  $D$  cannot be expressed in a simple form for temperatures below  $450^\circ\text{C}$ .

## B. Extrapolation to lower temperatures

Extrapolation of our current results to lower temperatures requires a knowledge of defect concentrations for the lower  $X$  value region. For the higher  $X$  value region, we can reliably extrapolate based on the dominance of the interstitial mechanism at higher  $X$  values and lower temperatures. Most electrical measurements<sup>31-33</sup> for bulk material indicate that  $\text{Hg}_{1-x}\text{Cd}_x\text{Te}$  with  $0.12 < X < 0.22$  is  $n$  type below  $260^\circ\text{C}$  in Te-saturated conditions for the lower  $X$  value region. This implies that metal interstitials are dominant, but it does not rule out a possible role for vacancies

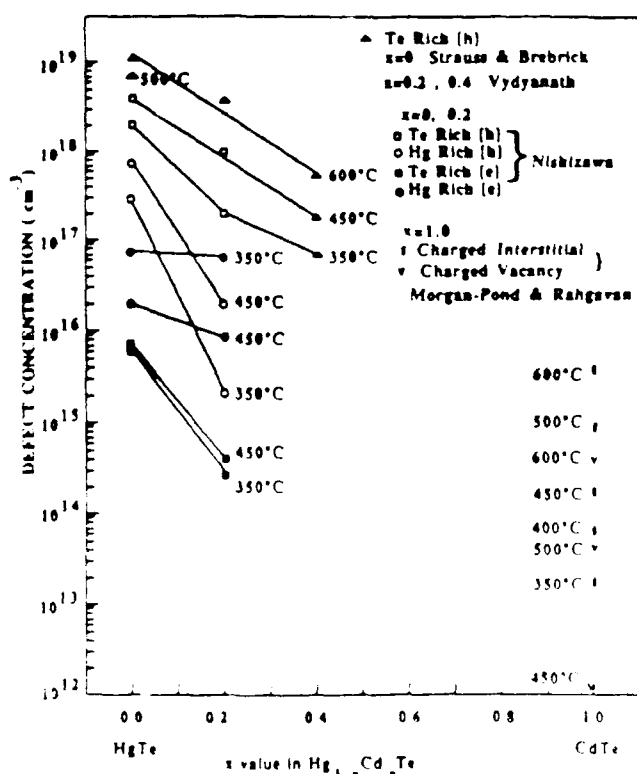


FIG. 3. Defect concentration vs  $x$  for different temperatures and Hg overpressure.

If we assume that interdiffusion proceeds by a dual mechanism at lower temperatures for the lower  $X$  value region and an interstitial mechanism for the higher  $X$  value region and extrapolate our data to 185 °C, we obtain  $D(X=0.2) = 2 \times 10^{-19}$  cm<sup>2</sup>/s and  $D(X=0.9) = 6 \times 10^{-18}$  cm<sup>2</sup>/s for Te-rich conditions. Staudenmann *et al.* obtained  $D$  values by analyzing the intensities of satellite peaks obtained from x-ray diffraction of the superlattices.<sup>11</sup> The decay of the  $m$ th satellite peak (1st, 2nd, 3rd, etc.) was associated with a  $m$ th Fourier component of the diffusion coefficient,  $D(\pm m)$ , assuming that  $D$  is independent of composition.<sup>11</sup> Since our results indicate that the dependence of  $D$  on  $X$  decreases with decreasing temperature below 450 °C, it may be reasonable to assume a constant  $D$  at 185 °C. Their results do show different  $D$  values for different orders ( $m$ ) of diffraction, indicating some dependence of  $D$  on concentration. Their results show that the  $D(\pm 1)$  value for HgTe-CdTe superlattices annealed under He ambient and at 185 °C ( $3.1 \times 10^{-18}$  cm<sup>2</sup>/s) is close to our  $D(X=0.9)$  for Te-rich conditions, and is between our values of  $D$  at  $X=0.2$  and 0.9, and the activation energies of  $D(\pm m)$  for  $m=1, 2, 3$  (0.9, 0.72, and 0.51 eV, respectively) are close to our  $\Delta E_s$  for high  $X$  value region. This agrees with our prediction of an increased importance for interstitial species at lower temperatures.

## V. CONCLUSION

Conventional HgTe-CdTe diffusion couples with angle lapping techniques were used to measure  $D$  for temperatures from 300 to 500 °C. The temperature, composition, and Hg overpressure dependence of  $D$  was determined for different temperature and composition regions, and the results were analyzed using proposed defect models. Referring to information in the literature on defect concentrations, we conclude that (i) the exponential dependence of  $D$  on  $X$  in the higher-temperature region is due to a combination of identical values for the intrinsic diffusion coefficients for both cations and a linear dependence of defect formation energy on  $X$ ; (ii) at temperatures higher than 450 °C, HgTe and CdTe interdiffuse by a dual mechanism, with vacancy and interstitial diffusion more dominant at low and high  $X$  value regions, respectively, and with  $D$  relatively insensitive to the Hg overpressure; and (iii) as temperature decreases below 450 °C, the interstitial mechanism increases in importance, as evidenced by lower activation energy, decreased dependence of  $D$  on  $X$ , and increased dependence of  $D$  on the Hg overpressure, especially in the higher  $X$  value regions. Our model provides a basis for understanding the trends in  $D$  at the lower temperatures. With appropriate assumptions, our data are extrapolated to the MBE growth temperatures and

give good agreement with  $D$  values obtained by x-ray methods.

## ACKNOWLEDGMENTS

We thank Professor H. Schmalzried, Dr. M. Brown, Dr. K. Zanio, and C. R. Zercher for helpful discussions and to Dr. M. Brown for providing some of the CdTe substrates used in this work. This work is sponsored by Defense Advanced Research Projects Agency through Office of Naval Research, Contract No. N000-(84K-0423).

- <sup>1</sup>J. N. Schulman, *Appl. Phys. Lett.* **43**, 180 (1983).
- <sup>2</sup>H. Rodot and J. Hencot, *C.R. Acad. Sci.* **256**, 1954 (1963).
- <sup>3</sup>F. Bailly, G. Cohen-Solal, and Y. Marfaing, *C.R. Acad. Sci.* **277**, 103 (1963).
- <sup>4</sup>F. Bailly, *C. R. Acad. Sci.* **262**, 635 (1966).
- <sup>5</sup>L. Svob and Y. Marfaing, *J. Appl. Phys.* **46**, 4251 (1975).
- <sup>6</sup>V. Leute, H. M. Schmidtke, W. Stratmann, and W. Winking, *Phys. Status Solidi A* **67**, 183 (1981).
- <sup>7</sup>J. N. Schulman and Y. C. Chang, *Appl. Phys. Lett.* **46**, 571 (1985).
- <sup>8</sup>J. P. Faurie, A. Million, and J. Piagnet, *Appl. Phys. Lett.* **41**, 713 (1982).
- <sup>9</sup>J. P. Faurie, in *Proceedings of the First International Conference on Superlattices, Microstructures and Microdevices* (Champaign Academic, London, 1985).
- <sup>10</sup>K. Zanio and T. Massopust, *J. Electron. Mater.* **15**, 103 (1986).
- <sup>11</sup>J. L. Staudenmann, R. D. Horning, R. D. Knox, J. Reno, I. K. Sou, J. P. Faurie, and D. K. Arch, *Trans. Metall. Soc. AIME* (to be published).
- <sup>12</sup>M. F. S. Tang and D. A. Stevenson (to be published).
- <sup>13</sup>M. Brown and A. F. W. Willoughby, *J. Cryst. Growth* **59**, 27 (1982).
- <sup>14</sup>F. A. Zaitov, A. V. Gorshkov, and G. M. Shalyapina, *Sov. Phys. Solid State* **21**, 112 (1979).
- <sup>15</sup>J. S. Chen, F. A. Kroger, and W. L. Ahlgren, *Extended Abstracts of U.S. Workshop on the Physics and Chemistry of Mercury Cadmium Telluride*, 1984, p. 109.
- <sup>16</sup>C. G. Morgan-Pond and R. Raghavan, *Phys. Rev. B* **31**, 6616 (1985).
- <sup>17</sup>J. Strauss and R. F. Brebrick, *J. Phys. Chem. Solids* **31**, 2283 (1970).
- <sup>18</sup>H. R. Vydyanath, *J. Electrochem. Soc.* **128**, 260 (1981).
- <sup>19</sup>H. R. Vydyanath, J. C. Donovan, and D. A. Nelson, *J. Electrochem. Soc.* **128**, 2685 (1981).
- <sup>20</sup>J. Nishizawa and K. Suto, *J. Phys. Chem. Solids* **37**, 33 (1976).
- <sup>21</sup>H. F. Schaake, *J. Electron. Mater.* **14**, 513 (1985).
- <sup>22</sup>F. J. A. der Broeder, *Scr. Metall.* **3**, 321 (1969).
- <sup>23</sup>T. Tung, L. Golonka, and R. F. Brebrick, *J. Electrochem. Soc.* **128**, 451 (1981).
- <sup>24</sup>M. F. S. Tang and D. A. Stevenson (to be published).
- <sup>25</sup>M. F. S. Tang and D. A. Stevenson (to be published).
- <sup>26</sup>F. A. Zaitov, A. V. Gorshkov, and G. M. Shalyapina, *Sov. Phys. Solid State* **20**, 927 (1978).
- <sup>27</sup>W. A. Harrison, *Electronics Structure* (Freeman, San Francisco, 1980).
- <sup>28</sup>S. S. Chen, H. R. Vydyanath, and F. A. Kroger, *J. Solid State Chem.* **14**, 33 (1975).
- <sup>29</sup>P. M. Borsenberger and D. A. Stevenson, *J. Phys. Chem. Solids* **29**, 1277 (1968).
- <sup>30</sup>S. S. Chen and F. A. Kroger, *J. Solid State Chem.* **14**, 299 (1975).
- <sup>31</sup>C. L. Jones, M. J. T. Quelch, P. Capper, and J. J. Gosney, *J. Appl. Phys.* **53**, 9080 (1982).
- <sup>32</sup>J. L. Schmit and C. J. Speerschnieder, *Infrared Phys.* **8**, 247 (1968).
- <sup>33</sup>R. A. Farar, C. J. Gillham, B. Bartlett, and M. Quelch, *J. Mater. Sci.* **12**, 836 (1977).

## Mechanisms of component diffusion in mercury cadmium telluride

Mei-Fan Sung Tang and David A. Stevenson  
Stanford University, Stanford, California 94305

(Received 11 October 1988; accepted 8 November 1988)

The component diffusion coefficients for the  $\text{Hg}_{0.8}\text{Cd}_{0.2}\text{Te}$  (MCT) system are measured using radioactive tracers. Multiple branches are observed in the tracer diffusion profiles which are related to fast and slow-diffusing components. Diffusion models for each component are proposed based on the defect chemistry of MCT, a calculation of the thermodynamic factor, and the relationship between component diffusion coefficients and the interdiffusion coefficients for pseudobinary systems. The model provides insight into the thermodynamic properties of the system, the mechanisms for diffusion, and the practical application of tracer diffusion data to interdiffusion and  $p$ -to- $n$  conversion by Hg annealing.

### 1. INTRODUCTION

Different types of diffusion coefficients have different practical and theoretical interest: the dependence of the self-diffusion coefficients ( $D_i^*$ ) on stoichiometry and temperature is important for determining diffusion mechanisms; the intrinsic (chemical) diffusion coefficient ( $D_i$ ) is important in estimating and controlling the stoichiometry of the crystal; and the interdiffusion behavior is important for determining profiles of junctions between epilayers and the substrate, and in predicting the stability of superlattices.

The information on the component diffusion coefficient for  $\text{Hg}_{1-x}\text{Cd}_x\text{Te}$  in the literature<sup>1-10</sup> is not consistent (in particular, for  $x = 0.2$ ). Much of the inconsistency arises from imprecise definitions of diffusion coefficients and incomplete control and definition of the diffusion source and ambient. Using the defect chemistry models described by Kroger,<sup>11</sup> diffusion-pressure isotherms ( $\log D_i^*$  vs  $\log P_{\text{Hg}}$ ) can be used to establish the defect mechanism responsible for diffusion. Radiotracer diffusion techniques provide the self-diffusion coefficients under isoconcentration conditions, and there are convenient tracers for all three components. However, the information is complicated by the complex profiles that are observed in the tracer diffusion results.

There are three studies of Hg tracer diffusion in MCT ( $x = 0.2$ ): Zaitov *et al.*,<sup>1</sup> Chen,<sup>2</sup> and Brown and Willoughby.<sup>3</sup> In all of these studies, there are two or three branches reported for the Hg tracer diffusion profiles, but the results differ by at least one order of magnitude, and the diffusion-pressure isotherms also are different. The results for the lower temperature study (300 °C) of Zaitov *et al.* are even contradictory to their earlier work,<sup>4</sup> and they do not explain the coexistence of the two diffusion mechanisms for tracer-diffusion studies. One mechanism proposed by Chen involved the exchange of the Hg isotope with Hg in the diffusion host; however, a detailed presentation is not given.<sup>2</sup> Brown and Willoughby<sup>3</sup> report three branches in their 225 °C Hg tracer diffusion studies, with all the branches preannealed.

There are two studies of Hg diffusion using  $p$ - $n$  junction measurements<sup>5,6</sup>; however, the resulting diffusion coefficients differ by more than an order of magnitude. In both studies, there is uncertainty in the assumptions used to calculate the diffusion coefficients (e.g., surface concentration

and diffusion profiles). Schaake *et al.*<sup>7</sup> has used a diffusion model to calculate the Hg diffusion rate associated with the annihilation of Te precipitates at low temperatures ( $T < 350$  °C), and obtained a value very close to the slowest component of Brown and Willoughby.

There is limited information on Cd diffusion in MCT ( $x = 0.2$ ).<sup>2,8,9</sup> Zaitov *et al.*<sup>8</sup> report results of an electrodiffusion experiment, from which they obtain a diffusion coefficient for Cd, but they do not specify the ambient for diffusion studies. Chen<sup>2</sup> reports two components for Cd diffusion, which are independent of Hg overpressure. Chen attributes the behavior to the exchange of Cd tracer with Hg and Cd, respectively, but a detailed explanation is not given. Shaw<sup>9</sup> reports a single component for the Cd tracer diffusion. In the Hg-rich region, the diffusion isotherm changes from 0 to  $-1$  as the temperature decreases below 400 °C, which Shaw attributes to a possible change in the electroneutrality condition.

There is even less information on the Te diffusion in MCT ( $x = 0.2$ ).<sup>2,10</sup> Gorshkov<sup>10</sup> reports one measurement of the Te tracer diffusion coefficient at 450 °C. The results show a change of slope for the diffusion-pressure isotherm as the stoichiometry changes from the Te-rich conditions to the Hg-rich condition, corresponding to a change from an interstitial to a vacancy mechanism. Chen<sup>2</sup> proposes that Te diffuses by a neutral interstitial species based on doping effects and a constant diffusion isotherm over the whole stoichiometric region. There is a difference between Chen and Gorshkov's diffusion values of three orders of magnitude.

In our studies of tracer diffusion in MCT,<sup>12</sup> we have observed complex profiles for metal tracer diffusion results which are fit with multiple-component profiles. Possible reasons for these profiles are diffusion short circuits, nonequilibrium, or a complex diffusion mechanism. In the present paper, we describe the component tracer diffusion studies in detail and provide evidence that the observed multiple components represent lattice diffusion. A model was previously<sup>12</sup> proposed for this lattice diffusion that assumes two independent networks develop as a result of clustering, and a relationship between the experimental values of  $D_i^*$  and  $D$  was derived assuming that the thermodynamic factor of this pseudobinary system is equal to 1. In the present paper, we discuss the shortcomings of that model and present an improvement that uses a calculated thermodynamic factor.

This model provides insight into the thermodynamic properties of the system, the mechanisms of the component diffusion, and the use of tracer diffusion data to describe the kinetics of  $p$ -to- $n$  conversion by Hg annealing.

## II. EXPERIMENTS

### A. Thermodynamic consideration for tracer diffusion studies in MCT

Meaningful and reproducible diffusion measurements must be performed under well-defined conditions. According to the Gibbs phase rule, for a ternary system with a single condensed phase in equilibrium with its vapor, two intensive variables must be fixed at a constant diffusion temperature in order to define the system. For binary II-VI compound semiconductors and their alloys, the component partial pressures are customarily controlled using a separate reservoir containing the element in question at a fixed temperature. Tracer diffusion or annealing experiments in the  $\text{Hg}_{1-x}\text{Cd}_x\text{Te}$  ternary system are usually performed under controlled Hg overpressure using pure liquid Hg as the reservoir material. With the temperature and the mercury ambient pressures fixed, there is one remaining degree of freedom for the diffusion system. Brebrick<sup>13</sup> has developed a statistical thermodynamic analysis showing that for pseudobinary systems such as MCT, there are "stoichiometry invariants" for the sums or differences of pairs of chemical potentials for small ratios of defect concentrations to lattice sites. That is, the chemical potentials of HgTe and CdTe are independent of the stoichiometry and are only functions of temperature and the  $x$  value. The partial pressure of Cd or Hg for any composition  $x$  in MCT is related to the vapor pressure of Te by the chemical potential of the corresponding binary.<sup>14</sup> Therefore, fixing Hg for a given composition ( $x$ ) fixes all the other component vapor pressures at the annealing temperature.

### B. Experimental procedures

The native defect equilibria may be related to the dependence of the component tracer diffusion as a function of temperature (from 350 to 500 °C) and the ambient Hg partial pressure under conditions of uniform stoichiometry and defect concentration in the diffusion host. This is achieved by preannealing wafers in evacuated quartz ampoules with a fixed mercury pressure ambient, under conditions identical to the diffusion anneal. This is accomplished using a two-zone furnace with a pure liquid-mercury reservoir at the lower temperature. The diffusion hosts are polished single-crystal wafers cut from coarse grained MCT (from Cominco Company).

A liquid-mercury source containing  $\text{Hg}^{203}$  provides a constant surface activity of  $\text{Hg}^{203}$ , with the relevant solution to Fick's second law given by

$$C(x,t) = C_0 \operatorname{erfc}(x/2\sqrt{Dt}), \quad (1)$$

where  $C_0$  is the surface concentration and  $\operatorname{erfc}$  is the error function complement. The tracer source for Cd and Te were  $\text{Cd}^{109}$  and  $\text{Te}^{124m}$  applied as a thin layer ( $\approx 0.1 \mu\text{m}$ ) on the surface by electrodeposition. The relevant solution is

$$C(x,t) = (M^*/\sqrt{\pi Dt}) \exp(-x^2/4Dt), \quad (2)$$

where  $M^*$  represents the total amount of the radiotracer deposited on the crystal surface.

Thin parallel slices of the sample ( $\approx 5$ – $15 \mu\text{m}$ ) are removed by a special grinding apparatus described by Goldstein.<sup>15</sup> The layer thickness is determined by weight loss, assuming a constant cross-section area. The gamma ray tracer activity in each section was determined with a thallium doped sodium iodide crystal scintillation counter.

## III. EXPERIMENTAL RESULTS

The values of  $D_i^*$  for the three components (Hg, Cd, Te) are determined by analyzing the tracer profiles developed for specific boundary conditions. In this section, we present the results of the tracer diffusion for three components.

### A. Hg tracer diffusion coefficient

There are typically two branches in the  $\log C$  vs  $x$  plots of the Hg tracer diffusion profiles, and each branch may be fitted with one erfc function. The diffusion coefficients obtained from these two branches are not affected by the preannealing, indicating that the equilibrium defect structure has been established within the diffusion period.

The results of the Hg tracer diffusion coefficients versus  $P_{\text{Hg}}$  for the fast and slow component at various temperatures are plotted in Fig. 1. (The designation  $f$  and  $s$  are used in subscript for the fast and slow component, respectively.) Our results are more consistent with those of Chen.<sup>2</sup> The slope on the plot of the diffusion-pressure isotherm  $n$  changes from  $-1$  to  $+1$  for the fast component as the stoichiometry changes from the Te-rich to the Hg-rich conditions. The  $D_{\text{Hg}}^*$  values for the slow component are essentially independent of  $P_{\text{Hg}}$ .

According to the analysis of defect chemistry developed for  $x = 0.2$  MCT<sup>16</sup> and the observed  $P_{\text{Hg}}$  dependence of  $D_{\text{Hg},f}^*$ , the dominant atomic disorder responsible for the fast diffusing Hg component is a vacancy or an interstitial for Te-rich or Hg-rich conditions, respectively. Since  $x = 0.2$  MCT is intrinsic at the diffusion temperatures, the analysis does not specify the charge state of the diffusion species for pure MCT. However, according to the literature, the metal defect ionization energy is very small, and most defects are doubly ionized.<sup>17-19</sup> It is reasonable, therefore, to assume that the diffusion species are doubly charged vacancies and interstitials for the fast component of Hg. The independence of  $P_{\text{Hg}}$  for the slow component of Hg can arise from a vacancy-interstitial complex mechanism similar to that for Cd diffusion in CdTe.<sup>20</sup> Exceptionally long annealing times (three months at 300 °C) are required to detect the slow component for temperatures lower than 350 °C; therefore, we do not perform experiments at temperatures lower than 350 °C. In the studies by Brown and Willoughby,<sup>3</sup> the slowest component of  $D_{\text{Hg}}^*$  for Hg-rich conditions corresponds to our interstitial mechanism (the fast component). It is possible that they do not detect the slow component with 14-day diffusion anneals at 225 °C. The temperature and mercury overpressure dependence of the diffusion coefficients for two components (fast and slow) can be expressed as

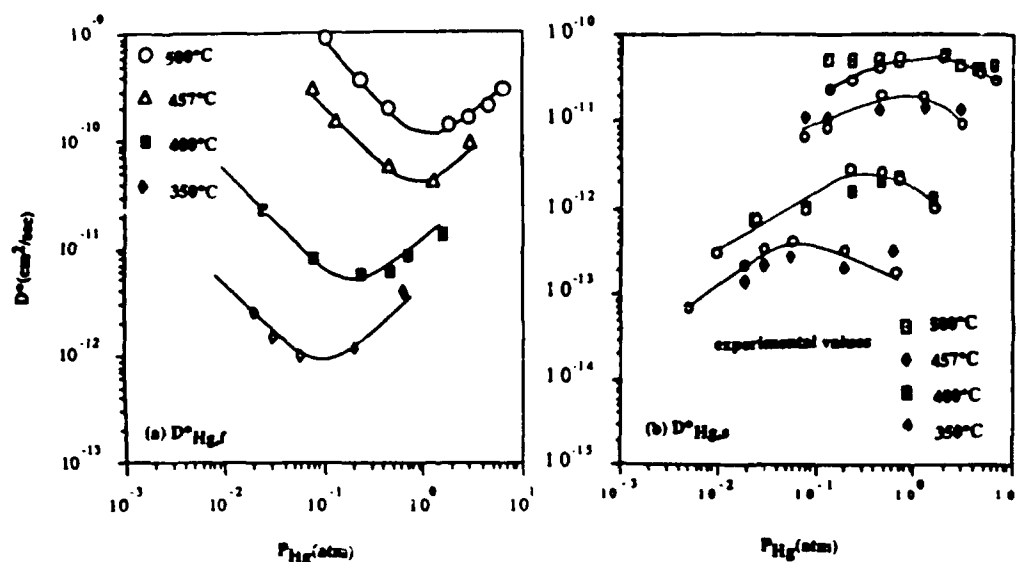


FIG. 1.  $D^*_{\text{Hg}}$  ( $\text{cm}^2/\text{s}$ ) vs  $P_{\text{Hg}}$  for (a)  $D^*_{\text{Hg},f}$  and (b)  $D^*_{\text{Hg},s}$  of both experimental values and the calculated values ( $\cdots\circ\cdots$ ) assuming a V-I in series mechanism.

$$D^*_{\text{Hg},f} = 4.87 \times 10^4 \exp(-2.10 \text{ eV}/kT) P_{\text{Hg}}^{-1};$$

at  $P_{\text{Hg}} = 0.1$  atm,

$$D^*_{\text{Hg},f} = 5.5 \times 10^{-7} \exp(-0.61 \text{ eV}/kT) P_{\text{Hg}};$$

at  $P_{\text{Hg}} = 1$  atm,

and

$$D^*_{\text{Hg},s} = 6.07 \exp(-1.70 \text{ eV}/kT);$$

independent of  $P_{\text{Hg}}$ .

### B. Cd tracer diffusion coefficient

The plots of  $\log C$  vs  $x^2$  always show two branches for preannealed samples indicating two isoconcentration diffusion mechanisms. Figure 2 displays the Cd tracer diffusion coefficients versus  $P_{\text{Hg}}$  for the fast and slow components at various temperatures. Both components are almost independent of Hg overpressure, with the slow component increasing slightly in the Hg-rich region. Our results are similar to those of Chen<sup>2</sup>; however, we do observe a slight increase in

$D^*_{\text{Cd},s}$  at the lower temperatures and in the Hg-rich region.

This increase is not as pronounced as described by Shaw<sup>9</sup> who reports observing only a single diffusion component. When we overlay his 350 °C data with ours, we find that the higher values of  $D^*_{\text{Cd}}$  in the Hg-rich region in Shaw's results correspond to our  $D^*_{\text{Cd},f}$ . The two diffusion coefficients of Cd can be expressed in an Arrhenius form as

$$D^*_{\text{Cd},f} = 38.4 \exp(-1.70 \pm 0.08 \text{ eV}/kT),$$

$$D^*_{\text{Cd},s} = 1.48 \exp(-1.65 \pm 0.05 \text{ eV}/kT).$$

### C. Te tracer diffusion coefficient

For samples that are not preannealed, the Te tracer diffusion profiles show two branches; however, for preannealed samples only the slower branch is detected. Therefore, the fast component is assumed to be related to chemical diffusion and does not represent true isoconcentration self-diffusion. The plot of  $\log D^*_{\text{Te}}$  vs  $\log P_{\text{Hg}}$  for the slow diffusion component shows a slope of  $-1$ , indicating an interstitial

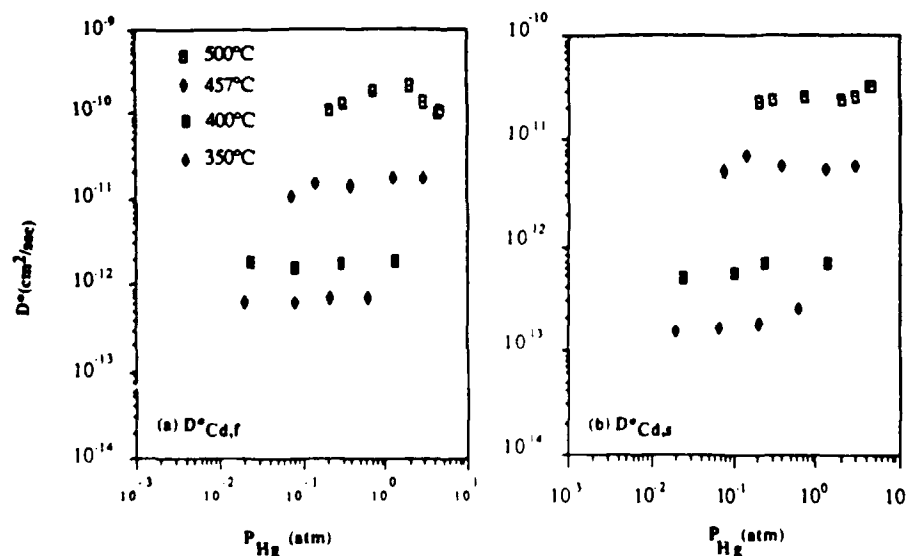


FIG. 2.  $D^*_{\text{Cd}}$  ( $\text{cm}^2/\text{s}$ ) vs  $P_{\text{Hg}}$  for (a)  $D^*_{\text{Cd},f}$  and (b)  $D^*_{\text{Cd},s}$ .

mechanism. Our results agree with those of Chen.<sup>2</sup> Since we do not perform experiment with doped crystals, the charge state of Te interstitials cannot be identified. The expression for the Te diffusion coefficient is

$$D_{Te}^* = 88.6 \exp(-2.15 \pm 0.1 / kT) P_{Hg}^{-1/2}$$

at  $P_{Hg} = 1$  atm.

#### IV. DISCUSSION

In this section, we first discuss possible reasons for the multiple branches in the tracer diffusion profiles. Previously,<sup>12</sup> it was proposed that diffusion proceeds in two independent networks for the two metal species. The shortcomings of the model are discussed, and a new model is proposed. The previously derived relationship between component diffusion coefficients ( $D_i^*$  and  $D_i$ ) and the interdiffusion coefficient ( $D$ ) for pseudobinary systems is used to confirm the proposed models. The thermodynamic properties of this system and the practical application of tracer diffusion results are discussed.

The observation that the diffusion-pressure isotherms of the two branches of the metal diffusion are well behaved and that the results are the same for different samples is evidence that neither branch is associated with diffusion short circuits, because the defect densities responsible for the short circuits (i.e., dislocations or subgrain boundaries) should vary from sample to sample. Therefore, the two branches are associated with lattice diffusion. Furthermore, the diffusion coefficients calculated from the two branches are independent of preannealing schedules, indicating that the stoichiometry of the sample is established rapidly compared to the development of self-diffusion profiles.

A single self-diffusion coefficient is expected for a homogeneous diffusion matrix which has equilibrium defect concentrations. Based on evidence of clustering effect in the MCT system,<sup>21,22</sup> we previously proposed that there may be two self-diffusion coefficients in two independent diffusion networks for each metal species. Two mechanisms were proposed for Hg based on the diffusion-pressure isotherm and the relationship between the two branches, namely, a vacancy (V)-interstitial (I) proceeding either in parallel or in series for the fast and the slow diffusion components, respectively. (Figure 3 displays these two diffusion paths.) When diffusion proceeds by a V-I in parallel path, the fast diffusion species dominates and is detected as a vacancy mechanism in the Te-rich condition and as an interstitial mechanism in the Hg-rich condition. For the V-I in series path, the opposite dependence of the V and I on  $P_{Hg}$  leads to the independence of  $D_{Hg,i}^*$  on  $P_{Hg}$ , and  $D_{Hg,i}^*$  is related to  $D_{Hg,f}^*$  by the relationship:

$$1/D_{Hg,i}^* = \frac{1}{2} (1/D_{Hg,f}^* + 1/D_{Hg,i}^*),$$

[the calculated values of  $D_{Hg,i}^*$  are plotted with the experimental values in Fig. 2(b)], which is consistent with the in-series mechanism.<sup>23,24</sup> The relationship between the magnitude of  $D_{Hg,i}^*$  and  $D_{Cd,i}^*$  and  $D_{Cd,f}^*$ , which have a similar dependence on  $P_{Hg}$ , are explained by the correlation factor.<sup>16</sup>

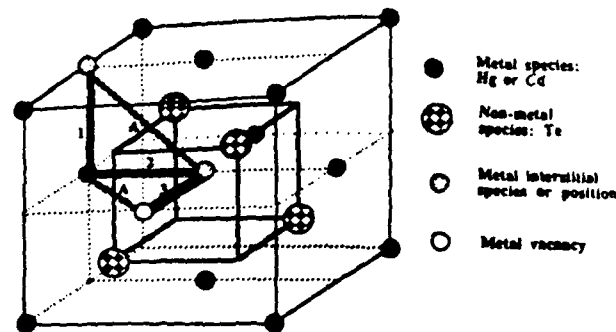


FIG. 3. Display of the metal diffusion paths: (■) indicates the path for the vacancy-interstitial in parallel process and (■) indicates the path for the vacancy-interstitial in series process following the sequence of 1-2-3. "A" indicates the distance of the closest approach to the Te atom; there the distance between the diffusing metal and Te atom is  $\sim \frac{1}{2}$  of the lattice parameter of the zinc-blende structure.

The relationship between  $D$  and the component diffusion coefficients for pseudobinary systems<sup>12,25</sup> establishes a simple Darken equation

$$D = [D_{Hg}(1-x) + D_{Cd}x]$$

relating the metal intrinsic diffusion coefficients ( $D_i$ ) and  $D$ , whereas the component self-diffusion coefficients are related to  $D$  by a complicated formula involving three  $D^*$  values. There are two important limiting forms of this formula: when  $D_{Te}^* \gg D_{Hg}^*$  or  $D_{Cd}^*$ , the limiting formula is a Darken-type equation

$$D = [D_{Hg}^*(1-x) + D_{Cd}^*x][T.F.],$$

where [T.F.] is the thermodynamic factor, and when  $D_{Te}^* \ll D_{Hg}^*$  or  $D_{Cd}^*$ , the limiting formula is a Nernst-Planck type of equation

$$D = [D_{Hg}^* D_{Cd}^*][T.F.]/[D_{Hg}^*x + D_{Cd}^*(1-x)].$$

From our tracer results,  $D_{Te}^* \ll D_{Hg}^*$  under all stoichiometric conditions. In our previous model,  $D_{Hg,f}^*$  and  $D_{Cd,f}^*$  are related to  $D$  by the Nernst-Planck type of equation and  $D_{Hg,i}^*$  and  $D_{Cd,i}^*$  can satisfy either type of equation, assuming a thermodynamic factor of 1, which assumes that the MCT system is an ideal solution of HgTe and CdTe. However, one cannot interrelate  $D_{Hg,f}^*$ ,  $D_{Cd,f}^*$ , and  $D$  by either equation. In addition, the relating formula for  $D_{Hg,f}^*$  and  $D_{Hg,i}^*$  suggests that the defect density in the two diffusion matrices is the same, but this seems unlikely if there are clustering effects in the system.

We propose a different model that is based on a calculation of the thermodynamic factor. One can calculate the thermodynamic factor of the HgTe-CdTe pseudobinary system from the thermodynamic data (chemical potential of HgTe and CdTe in the alloy) provided by Tung *et al.*<sup>14</sup> Chemical potentials can be related to activities in the customary way:  $\mu_i = \mu_i^0 + RT \ln a_i$ , where  $a_i$  is the activity of component  $i$ . Thus:

$$\mu_i = \mu_i^0 + RT \ln \gamma_i x_i; \quad (3)$$

$\gamma_i$  is the activity coefficient of component  $i$  with  $\mu_i$  expressed in terms of  $x_i$  and one can obtain  $\partial \ln \gamma_i / \partial \ln x_i$  and the



thermodynamic factor:  $1 + \partial \ln \gamma_i / \partial \ln x_i$ . From the analytical fit<sup>26</sup> of Brebrick's data,  $\mu_{\text{CdTe}}(x) = -(70\,855 - 45T - 2540x)$  cal, we obtain  $\partial \ln \gamma_i / \partial \ln x_i = -0.67$ , and  $[T.F.] = 0.33$  for MCT  $x = 0.2$  at  $500^\circ\text{C}$ .

Treating MCT as a quasiregular solution, the chemical potential of the components  $i$ , ( $i = \text{HgTe}$  or  $\text{CdTe}$ ), can be written as

$$\mu_i = \Omega(1 - x_i)^2 + RT \ln x_i + \mu_i^*, \quad (4)$$

where  $\Omega$  is the interaction energy  $\{\Omega = [H_{\text{AB}} - (H_{\text{AA}} + H_{\text{BB}})/2]$  for alloy AB} of HgTe and CdTe for the current system. Equating Eqs. (3) and (4):

$$RT \ln \gamma_i = \Omega(1 - x_i)^2,$$

and

$$\partial \ln \gamma_i / \ln x_i = 2\Omega(x_i - 1)x_i / RT. \quad (5)$$

Since  $(x_i - 1)x_i$  is always negative, if  $\partial \ln \gamma_i / \partial \ln x_i < 0$  ( $[T.F.] < 1$ ), then  $\Omega > 0$ , and the mixing enthalpy of the binary system is positive. The same conclusion was obtained by Tung *et al.*<sup>14</sup> from the slope of the plot  $\Omega(1 - x_i)^2$  vs  $x_i$ , whereas the theoretical models indicate a near zero and a slight negative value for the mixing enthalpy.<sup>22,27</sup>

The following are the major assumptions of the new model: there is only one self-diffusion coefficient for each metal species; there is only one diffusion matrix; the fast components of Hg and Cd are true self-diffusion coefficients; and the slow components of the two metal "tracer" diffusion coefficients arise from the interdiffusion between the tracer  $\text{Hg}^*$  and Cd in the diffusion host for Hg and vice versa for tracer  $\text{Cd}^*$ . There is the following evidence that the two fast components are true self-diffusion coefficients: Te moves much more slowly than either of the cations;  $D_{\text{Cd},f}^* < D_{\text{Hg},f}^*$  for  $x = 0.2$ ;  $D \approx D_{\text{Cd},f}^* [T.F.]$  and  $D_{\text{Cd},f}^*$  and  $D_{\text{Hg},f}^*$  can be related to  $D$  by a Nernst-Planck type of equation. The two slow diffusion coefficients,  $D_{\text{Hg},s}^*$  and  $D_{\text{Cd},s}^*$  are intrinsic diffusion coefficients and can be related to  $D$  by the Darken equation; however, that is different from the chemical diffusion coefficient that is responsible for homogenizing the stoichiometry. The fact that the intrinsic diffusion coefficient for each metal species is smaller than the self-diffusion coefficient arises from the positive mixing enthalpy of the mixing the HgTe and CdTe, as indicated by the calculated  $[T.F.]$ .

In this model, the diffusion mechanism for each component is the same as in our previous model, but the role of each component is different. The slow component of Hg is related to the fast component of Hg by the same relationship as in the previous model, but it is assumed in the new model that these two components diffuse in a single diffusion matrix with same defect density. When Hg interdiffuses with Cd, because of the relatively slow diffusion rate of Te, Hg is slowed to maintain stoichiometry, and the intrinsic diffusion coefficient of Hg ( $D_{\text{Hg},s}^*$ ) behaves differently from the self-diffusion coefficient ( $D_{\text{Hg},f}^*$ ), since the former involves the slower diffusing Cd species which proceeds only by the V-I in series mechanism. Figure 3 illustrates that when a metal species diffuses by a V or an I mechanism, it surmounts a higher energy barrier (because of a closer distance of approach to Te) than the V-I in series mechanism. Since the

Cd-Te bond is stronger than the Hg-Te bond, the V-I in series process is, therefore, a preferred one for Cd diffusion.

In the practical process of  $p$ -to- $n$  conversion by low-temperature annealing in a Hg-rich ambient, the Hg diffusion is initiated under certain stoichiometric conditions which are normally Te-rich, and the stoichiometry changes as the process proceeds. One may calculate diffusion profiles using the diffusion coefficient of the fast component of Hg under the  $P_{\text{Hg}}$  conditions of the annealing experiments. The analysis of Hg annealing at low temperature made by Schaake *et al.*<sup>7</sup> gives a diffusion coefficient close to the slow component of Hg reported by Brown and Willoughby,<sup>3</sup> and the latter is consistent with our  $D_{\text{Hg},f}^*$  extrapolated to the low temperature. Furthermore, the model of Schaake *et al.* indicates that both vacancies and interstitials are involved in Hg annealing which is consistent with our fast component of Hg which proceeds by V-I in parallel.

## V. CONCLUSIONS

The diffusion coefficients for the three components in the MCT ( $x = 0.2$ ) system are studied by tracer techniques. The thermodynamic considerations of the experiment are addressed. There are two branches in the tracer diffusion profiles for each component. We propose diffusion models based on the diffusion isotherm studies, the defect chemistry and thermodynamic properties of the system, and the relationship between different diffusion coefficients for pseudo-binary systems. The results are summarized as follows: Te diffuses much more slowly than either metal species, and the fast component of Te is related to chemical diffusion for attaining equilibrium stoichiometry and do not appear in preannealed samples. The two components for each metal both appear after preannealing and are related to the lattice diffusion. In contrast to our former model, we propose that there is only one diffusion matrix. The fast components for Cd and Hg are true self-diffusion coefficients, and they are related to the interdiffusion coefficient by a Nernst-Planck type of equation, with a thermodynamic factor calculated from available thermodynamic data. The slow components of the metal species in the tracer diffusion profile are the intrinsic diffusion coefficients and they are related to the interdiffusion coefficient by a Darken equation. The MCT system exhibits modest positive from ideality, with a thermodynamic factor less than one. This indicates a positive mixing enthalpy of HgTe and CdTe, and is consistent with the observed results that the intrinsic diffusion coefficient of the metal species is smaller than the self-diffusion coefficient. The following mechanisms are proposed for the diffusion of the three components: Te diffuses by interstitials; Hg diffuses by vacancies and interstitials proceeding in parallel, and Cd diffuses by vacancies and interstitials proceeding in series, because of the higher bonding energy of Cd-Te. When Hg interdiffuses with Cd, the diffusion is slowed to conserve lattice sites, and the mechanism is changed to be the same as that of Cd, the V-I in series. The Hg diffusion coefficient used to estimate the  $p$ - $n$  junction conversion by Hg annealing is the fast component of Hg, a sum of  $D_{\text{Hg},s}^*$  and  $D_{\text{Hg},f}^*$  under the experimental Hg pressure.

## ACKNOWLEDGMENTS

We thank Professor H. Schmalzried of the University of Hannover, Professor D. Shaw of Hull University, Dr. M. Brown of Grumman Corporate Research Center, and Dr. K. Zanio of Ford Aerospace and Communications Corporation for helpful discussions. This work is supported by DARPA through ONR, Contract No. N000-14-84K-0423.

- <sup>1</sup>F. A. Zaitov, A. V. Gorshkov, and G. M. Shalyapina, *Sov. Phys. Solid State* **21**(1), 112 (1979).
- <sup>2</sup>J. S. Chen, Ph. D. thesis, University of Southern California, 1985.
- <sup>3</sup>M. Brown and A. F. Willoughby, *J. Cyst. Growth* **59**, 27 (1982).
- <sup>4</sup>F. A. Zaitov, L. A. Bovina, and V. I. Stafeyev, in *Proceedings of the Third All-Union Conference on the Problem of the Physics of II-VI Compounds*, Vilna, 1972, Vol. 1, p. 165.
- <sup>5</sup>N. V. Baranova, A. S. Tomson, N. F. Astamonov, and A. V. Vanyukov, *Izv. Akad. Nauk. SSSR Neorg. Mater.* **12**, 2141 (1976).
- <sup>6</sup>H. R. Huff, H. R. Kraus, and B. H. Breazeal, in *IRIS Proceedings Symposium*, 1974.
- <sup>7</sup>H. F. Schaake, J. H. Tregilgas, J. D. Beck, M. A. Kinch, and B. E. Gnade, *J. Vac. Sci. Technol. A* **3**, 143 (1985).
- <sup>8</sup>F. A. Zaitov, G. M. Shalyapina, L. M. Shalyapina, and O. V. Mukhins, *Sov. Phys. Solid State* **16**, 774 (1974).
- <sup>9</sup>D. Shaw, *Philos. Mag. A* **53**(5), 727 (1986).
- <sup>10</sup>A. V. Gorshkov, F. A. Zaitov, S. B. Shangin, G. M. Shalyapina, I. N. Petrov, and I. S. Asaturova, *Sov. Phys. Solid State* **26**(10), 1787 (1984).
- <sup>11</sup>F. A. Kroger, *The Chemistry of Imperfect Crystals*, 2nd ed. (North-Holland, Amsterdam, 1974), Vol. 2, Chaps. 14-16.
- <sup>12</sup>M. F. S. Tang and D. A. Stevenson, *J. Vac. Sci. Technol. A* **6**, 2650 (1988).
- <sup>13</sup>R. F. Brebrick, *J. Phys. Chem. Solids* **40**, 177 (1979).
- <sup>14</sup>T. Tung, L. Golonka, and R. F. Brebrick, *J. Electrochem.* **128**, 451 (1981).
- <sup>15</sup>B. Goldstein, *Rev. Sci. Instrum.* **28**, 289 (1957).
- <sup>16</sup>M. F. S. Tang, Ph. D. thesis, Stanford University, 1987.
- <sup>17</sup>Kobayashi, O. F. San Key, and J. D. Dow, *Phys. Rev. B* **25**, 6367 (1982).
- <sup>18</sup>C. A. Swarta, M. S. Daw, and T. C. McGill, *J. Vac. Sci. Technol. A* **1**, 198 (1982).
- <sup>19</sup>C. L. Wang, S. Wu, and D. S. Pan, *J. Vac. Sci. Technol. A* **1**, 1631 (1983).
- <sup>20</sup>S. S. Chern and F. A. Kroger, *J. Solid State Chem.* **14**, 44 (1975).
- <sup>21</sup>K. C. Hass and D. Vanderbilt, *J. Vac. Sci. Technol. A* **5**, 3019 (1987).
- <sup>22</sup>A. B. Chen and A. Sher, *Phys. Rev. B* **32**, 3695 (1985).
- <sup>23</sup>R. Kikuchi and H. Sato, *J. Chem. Phys.* **51**, 161 (1969).
- <sup>24</sup>R. Kikuchi, *J. Chem. Phys.* **53**, 2702 (1970).
- <sup>25</sup>M. F. S. Tang and D. A. Stevenson (to be published).
- <sup>26</sup>J. Fleming, Ph.D. thesis, Stanford University, 1986.
- <sup>27</sup>J. L. Martins and A. Zunger, *Phys. Rev. B* **30**, 6217 (1984).

# Diffusion studies in the $\text{Hg}_{1-x}\text{Cd}_x\text{Te}$ system

Mei-Fan S. Tang and David A. Stevenson  
Stanford University, Stanford, California 94305

(Received 11 December 1987; accepted 17 February 1988)

An overview of diffusion studies in the  $\text{Hg}_{1-x}\text{Cd}_x\text{Te}$  system is presented which includes experimental studies of component self-diffusion and interdiffusion, a theory of the relationship between self-diffusion and interdiffusion coefficients for pseudobinary systems, and proposed diffusion mechanisms. The diffusion mechanisms are proposed for self-diffusion in  $x = 0.2$  material. The mechanism for interdiffusion behavior and the relationship between self-diffusion and interdiffusion coefficients are used to extrapolate experimental information to lower temperatures and to predict the stability of junctions and superlattices.

## I. INTRODUCTION

A major concern in the processing and use of mercury cadmium telluride (MCT) is its stability, since defects and components move about during the processing and the operation of devices. To quantify these features requires an experimental and theoretical knowledge of diffusion. Knowledge of diffusion mechanisms not only allows the prediction of concentration profiles in specific cases, but also provides a basis for controlling the diffusion behavior. In this section, we will introduce the self-diffusion, interdiffusion, thermodynamics of diffusion, and the scope of the present work.

The tracer diffusion technique, which determines the self-diffusion coefficient ( $D^*$ ) under isoconcentration conditions, is a powerful tool for determining the defect structure. There are convenient radiotracers for all three components. However, the information in the literature for self-diffusion is limited in its interpretation,<sup>1-4</sup> since the ambient vapor pressure is not clearly specified in most studies and there is considerable disparity in the values of  $D^*$  from different studies, which may differ by as much as two or three orders of magnitude.<sup>1,3</sup> Different diffusion coefficients are often used without being clearly defined, and the relationship between self-diffusion and interdiffusion is not established. Confronted by the numerous ambiguities in the literature, we review the fundamental definitions and relationships for diffusion in pseudobinary systems.

The interdiffusion behavior in the  $\text{HgTe-CdTe}$  system determines the sharpness of junctions in epitaxial layers and in superlattices and is a driving force for isothermal vapor phase epitaxy.<sup>5</sup> It also determines the rate of homogenization of nonuniform material and the intermixing of capping layers. Interdiffusion has been investigated principally using an improved Boltzmann-Matano analysis.<sup>6</sup> Several interdiffusion studies have been reported with generally good agreement.<sup>7-11</sup> The studies indicate that over the temperature range most commonly studied (700–450 °C), interdiffusion is relatively insensitive to the ambient component partial pressures, but there is a strong dependence on composition (CdTe mole fraction,  $x$ ). There are limited interdiffusion data at lower temperatures which are relevant to superlattice growth by molecular-beam epitaxy or metal organic chemical vapor deposition. Extrapolation of high-temperature interdiffusion data down to low temperatures<sup>12</sup> led to predictions of diffusion behavior which differ from the results of

x-ray studies of annealed superlattices.<sup>13</sup> For example, the latter studies indicate a lower activation energy of 0.7 eV, which is lower than  $\approx 2$  eV value determined from the high-temperature studies. One goal of the present study is to determine the interdiffusion behavior of  $\text{HgTe-CdTe}$  junctions for temperatures lower than 450 °C, and to analyze the mechanism for interdiffusion.

The classical relations between the interdiffusion coefficient ( $D$ ) and the component  $D^*$  values derived for binary systems do not explain the behavior in the present ternary system. We give equations for pseudobinary systems from fundamental diffusion theory, then consider the limiting forms appropriate for the MCT system. A defect model consistent with interdiffusion behavior is proposed, and is consistent with the defect model developed from the observed tracer diffusion behavior. The derived relationship provides the basis for predicting the stability of junctions and superlattices from the tracer diffusion data.

In this paper, we present the following: (i) a summary of our self-diffusion results, emphasizing the relative diffusion rates of metal and nonmetal species, the multiple diffusion mechanisms for the metal species in this system, and a possible explanation involving cluster formation in this alloy; (ii) the theoretical expression for relating the self-diffusion and the interdiffusion coefficients for pseudobinary systems, emphasizing the relevant limiting forms for the MCT system; and (iii) the highlights of the previously reported results on interdiffusion studies, and the associated defect mechanisms for interdiffusion based on (i) and (ii).

## II. RESULTS

### A. Component self-diffusion studies

Tracer self-diffusion coefficients describe the diffusion species in the absence of driving forces which make species move with a preferred direction. The values of  $D^*$  for the three components ( $D_{\text{Hg}}^*$ ,  $D_{\text{Cd}}^*$ , and  $D_{\text{Te}}^*$ ) are determined by using tracer sources with homogeneous samples and by analyzing the concentration profiles developed for specific boundary conditions. Analysis using the relevant principles of defect chemistry for this pseudobinary system provides the basis for establishing defect models. The dependence of  $D^*$  on mercury partial pressure ( $P_{\text{Hg}}$ ) and the temperature ( $T$ ) was determined from 350 to 500 °C to establish the

dominant mobile defects.<sup>14</sup> The highlights of the observed behavior and the proposed models follow.

There are two branches in the tracer diffusion profiles for both Hg and Cd [associated with the fast (*f*) and slow (*s*) components], whereas there is only one branch for Te. The fast component of Hg shows a dependence on  $P_{\text{Hg}}$ . The slope of a plot of  $\log D_{\text{Hg}}^*(f)$  vs  $\log P_{\text{Hg}}$  for a given temperature (called a diffusion isotherm) varies from  $-1$  to  $+1$  as the stoichiometry changes from the Te-rich conditions to the Hg-rich conditions. The slow component of  $D_{\text{Hg}}^*$  and the two components of Cd are essentially independent of  $P_{\text{Hg}}$  (Fig. 1), whereas  $D_{\text{Te}}^*$  shows a  $P_{\text{Hg}}^{-1}$  dependence.

Based on the observed diffusion isotherms, the following are proposed as the dominant mobile defects: interstitials for Te ( $\text{Te}_i$ ); metal vacancies ( $V$ ) at the Te-rich region and metal interstitials ( $I$ ) at the Hg-rich region for the fast mercury component. Both vacancies and interstitials are probably involved for the cadmium and the slow component of

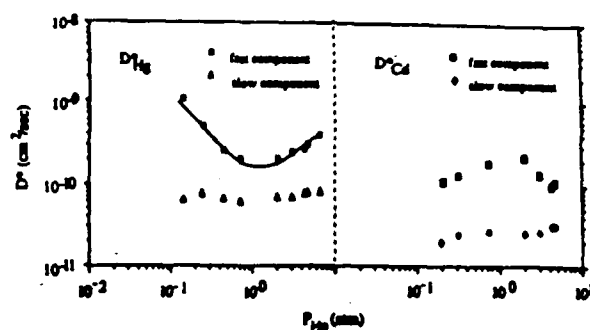


FIG. 1. Comparison between  $D$  and  $D^*$  at  $500^\circ\text{C}$ .  $D(x=0.2) = (2-3) \times 10^{-11} \text{ cm}^2/\text{s}$ .

mercury diffusion and cause these diffusion coefficients [ $D_{\text{Cd}}^*$ ,  $D_{\text{Hg}}^*(s)$ ] to be essentially independent of Hg partial pressure, as is discussed below. The dependencies of the component diffusion coefficients on  $T$  and  $P_{\text{Hg}}$  are given by

$$\begin{aligned} D_{\text{Hg},V}^* &= 4.87 \times 10^4 \exp(-2.10 \text{ eV}/kT) P_{\text{Hg}}^{-1}, & \text{at } P_{\text{Hg}} = 0.1 \text{ atm} & \quad (\text{cm}^2/\text{s}); \\ D_{\text{Hg},I}^* &= 5.5 \times 10^{-7} \exp(-0.61 \text{ eV}/kT) P_{\text{Hg}}, & \text{at } P_{\text{Hg}} = 1 \text{ atm} & \quad (\text{cm}^2/\text{s}); \\ D_{\text{Hg},s}^* &= 6.07 \exp(-1.70 \text{ eV}/kT) & & \quad (\text{cm}^2/\text{s}); \\ D_{\text{Cd},f}^* &= 38.4 \exp(-1.70 \text{ eV}/kT) & & \quad (\text{cm}^2/\text{s}); \\ D_{\text{Cd},s}^* &= 1.48 \exp(-1.65 \text{ eV}/kT) & & \quad (\text{cm}^2/\text{s}); \\ D_{\text{Te}}^* &= 88.6 \exp(-2.15 \text{ eV}/kT) P_{\text{Hg}}^{-1}, & \text{at } P_{\text{Hg}} = 1 \text{ atm} & \quad (\text{cm}^2/\text{s}). \end{aligned}$$

The relative diffusion rates of the metal and nonmetal species over the whole stoichiometric region are displayed on a plot of  $D^*$  vs  $1/T$  (Fig. 2) (similar to the pressure-temperature diagram). The Te component diffuses at least two orders of magnitude more slowly than the fast component of Hg for all stoichiometric conditions, and only approaches the value of the slow components of the metal species at Te saturation. The defects associated for metal diffusion are believed to be doubly charged.<sup>14</sup>

## B. Interdiffusion studies

In previous papers, we have characterized the interdiffusion coefficient as a function of  $T$ , stoichiometry ( $P_{\text{Hg}}$ ), and  $X$  for HgTe/CdTe couples.<sup>15,16</sup> At higher temperatures ( $T > 450^\circ\text{C}$ ),  $D$  depends strongly on  $X$  and is insensitive to  $P_{\text{Hg}}$ , whereas for  $T < 450^\circ\text{C}$ ,  $D$  is less dependent on  $X$  and  $T$ , and more dependent on  $P_{\text{Hg}}$ . These trends are more pronounced at higher  $X$  values. The dependence of  $D$  on  $X$  and  $T$  is explained by defect models and information on defect formation energies and the relationship between  $D$  and  $D^*$ . For the interdiffusion a dual mechanism is proposed, namely, both vacancies and interstitials are involved, with increasing importance of interstitials at higher  $X$  values and at lower temperatures.

## C. Theoretical relationships between $D$ and $D^*$ for pseudobinary systems

The classical relations derived for binary systems relating  $D$  values to the component  $D^*$  values do not explain the behavior in the present ternary system. Using the classical

Darken equation with  $D_{\text{Hg}}^*(f)$  and either  $D_{\text{Cd}}^*$  value, assuming the thermodynamic factor ([T.F.]) equals one, gives interdiffusion coefficients one decade higher than the observed experimental value (Fig. 1). We define diffusion coefficients based on the reference frame for composition profiles and the driving force causing atomic jumps in preferred directions. The equations for a pseudobinary system are derived from fundamental diffusion theory using thermodynamic driving forces and relations. Details of the deri-

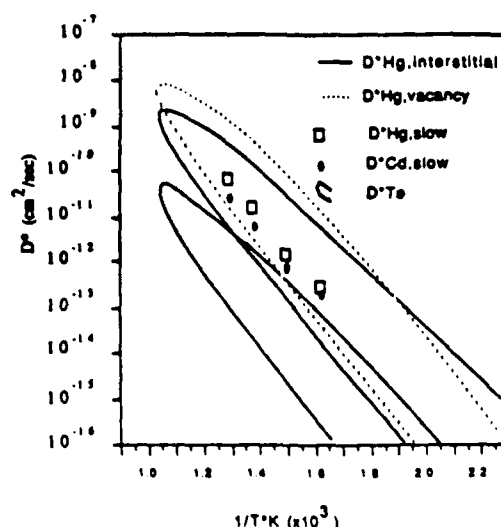


FIG. 2. Tracer diffusion coefficients of Hg (fast and slow components), Cd (slow component), and Te vs temperature for the whole stoichiometric region for  $x = 0.2$  MCT.

variations are provided elsewhere.<sup>17,18</sup> The classic Darken-type equation is only valid for diffusion under a driving force which arises from a regular (neutral) chemical potential gradient, whereas our derivation is extended to include additional constraints that arise from the relative diffusion rates of the nonmetal and the metal diffusing species, in combination with the constraints of electroneutrality and stoichiometry. The resulting relation is given in Eq. (1):

$$D = \{D_{\text{Cd}}^* D_{\text{Hg}}^* + D_{\text{Te}}^* [XD_{\text{Hg}}^* + (1-X)D_{\text{Cd}}^*]\} [\text{T.F.}] / [(1-X)D_{\text{Hg}}^* + XD_{\text{Cd}}^* + D_{\text{Te}}^*] \quad (1)$$

The thermodynamic factor is given by

$$[\text{T.F.}] = 1 + \partial \ln \gamma_{\text{HgTe}} / \partial \ln N_{\text{HgTe}} \\ = 1 + \partial \ln \gamma_{\text{CdTe}} / \partial \ln N_{\text{CdTe}};$$

$N_i$  is the mole fraction.

For specific conditions, depending on the relative diffusion rates of the metal and nonmetal species, Eq. (1) can be simplified into two forms for relatively fast diffusion of the metal species or the nonmetal species, Eqs. (2) and (3), respectively:

$$D = [(1-X)D_{\text{Cd}}^* + XD_{\text{Hg}}^*] [\text{T.F.}] \quad (2)$$

$$D = \{D_{\text{Cd}}^* D_{\text{Hg}}^* / [(1-X)D_{\text{Hg}}^* + XD_{\text{Cd}}^*]\} [\text{T.F.}] \quad (3)$$

These equations are valid for all pseudobinary systems. The limiting form of Eq. (2) is a Darken-type equation, with  $[\text{T.F.}]$  expressed for a pseudobinary system. The limiting form of Eq. (3) is consistent with the experimental data of tracer and interdiffusion results for the present system with  $[\text{T.F.}] = 1$  (Fig. 1). The details of these limiting cases and their applications for the understanding of interdiffusion behavior and predicting the stability of the superlattices are discussed below.

### III. DISCUSSION

#### A. Component self-diffusion mechanism

We first address the question whether the multiple branches in the tracer concentration profiles represent true self-diffusion. An identical question is whether there are multiple independent solutions to Fick's second law if there are defects in equilibrium. Generally, if there are no diffusion short circuits and if thermodynamic equilibrium is maintained, there should be only one solution. Since the diffusion isotherm implies the involvement of vacancies and interstitials in different regions, a mechanism involving both vacancies and interstitials is appropriate for explaining the fast and slow components for the Hg tracer diffusion. Diffusion may occur by a vacancy-interstitial dual mechanism proceeding either in parallel or in series, depending on the availability and mobility of the defects. The fast component of the Hg diffusion is associated with the Hg atom motion with the  $V$ - and  $I$ -associated diffusion mechanisms in parallel, with the faster component dominant. Therefore, it is detected as a vacancy mechanism under Te-rich conditions and as an interstitial mechanism under Hg-rich conditions. The Hg atoms may also diffuse with the dual mechanism proceeding in series; interstitials jump into vacant sites and

then into interstitial sites, with the slower of these steps rate limiting. Since each process involves more than a single type of defect, an independent solution may exist for independent defect motion that could be associated with two or more "independent" diffusion channels. In the MCT system, this phenomenon could be related to an ordering phenomenon that would establish two separate diffusion networks with different diffusion properties. There are experimental indications for this type of ordering,<sup>19</sup> and Hass *et al.*<sup>20</sup> have shown that the correlation effect in this system is stronger than previously predicted.<sup>21</sup>

The vacancy mechanism is straightforward; however, the mechanism involving interstitials may proceed either with the interstitials jumping from one interstitial site to another interstitial site or with the interstitials "displacing" the adjacent atom in a normal lattice site into another interstitial site. The latter is called an interstitialcy, or a "kick-out" mechanism. Both the interstitial and the interstitialcy mechanisms involve the interstitials in the diffusion process and have the same Hg vapor pressure dependence of the tracer diffusion coefficient. Since the sizes of the cations (Hg and Cd) and nonmetal species (Te) are comparable, the cations are more likely to diffuse by the interstitialcy mechanism in the zincblende crystal structure. We assume that the interstitials occupy the octahedral sites of the fcc lattice, and these interstitial sites form a fcc lattice.

For  $x = 0.2$  MCT material, the metal vacancy is the dominant metal defect species at higher temperatures. As temperature decreases, interstitials become increasingly important. When the concentrations of the available vacancy and interstitial and their mobility products are high, the vacancy and interstitialcy mechanism proceed simultaneously with the faster component dominant. This is the  $V$ - $I$  in parallel process. When vacancies are less available, or there is configurational constraint (i.e., in an ordered network), the interstitialcy mechanism helps the diffusing atom to reach the next available vacancy. By an interstitialcy mechanism, the atom sitting in an interstitial site has a higher probability to displace one of the six nearest atoms in the normal lattice site into one of the six nearest interstitial sites which has a vacancy available on the nearest neighbor. This is the basis for the  $V$ - $I$  in-series process.

For a  $V$ - $I$  in-series process described above, the resulting diffusion coefficient is a harmonic average of the  $V$  and  $I$  diffusion coefficients<sup>22,23</sup>:  $1/D_s = 1/2 [1/D_V^* + 1/D_I^*]$ .  $D_s$  denotes that the resulting diffusion coefficient is limited by the slower mechanism of the two. From  $D_{\text{Hg}}^*(f)$  values which are composed of  $D_V^*$  and  $D_I^*$ , we can calculate  $D_s$ . The calculated  $D_s$  values agree very well with our experimental values for  $D_{\text{Hg}}^*(s)$ . The independence of the  $D_{\text{Hg}}^*(s)$  on  $P_{\text{Hg}}$  arises from the opposite dependence of  $D_V^*$  and  $D_I^*$  on  $P_{\text{Hg}}$ . The changing importance of the defect species explains the difference between our experimental values and the calculated  $D_s$  at the two stoichiometric limits, where the  $V$ - $I$  in-series process involves some degree of parallel process for dual mechanism. For  $T < 450^\circ\text{C}$ , the  $D_{\text{Hg}}^*(s)$  values increase slightly with the increasing Hg overpressure, which is consistent with the increasing importance of interstitials.

To explain the fact that the fast and slow components for

the Cd diffusion coefficient have a similar Hg pressure dependence as the slow component for the Hg diffusion coefficient and to obtain further insight into this  $V-I$  in-series mechanism, we consider the relationship between the diffusion of the two cations, namely, the correlation factor ( $f_i$ ) for the metal species. The path-probability method,<sup>22-24</sup> which has been analyzed to develop the correlation formula for vacancy diffusion in regular binary systems, is used to obtain the formula for the metal diffusion in a pseudobinary system with the  $V-I$  in-series mechanism. It is observed that  $D_{\text{Cd}}^*(f) \approx 2.5D_{\text{Cd}}^*(s)$  at higher temperatures ( $T > 450^\circ\text{C}$ ), with the fast and slow components having the same  $V-I$  in-series mechanism. The fast component is assumed to correspond to Cd diffusing in the phase with a random arrangement in metal, and the slower diffusing component corresponding to those taking the "most probable" path in the ordered phase with  $f_{\text{Cd}}^* = 0.4$ . Since the calculated correlation factor for Hg is close to 1, only one Hg diffusion component associated with the  $V-I$  in-series process is detected experimentally, in contrast to Cd. The main diffusion process for Hg in the "random phase" is  $V-I$  in-parallel process, while the main diffusion process for Hg in the "ordered phase" is  $V-I$  in-series process due to the preferred configuration of the nearest metal ions.

The correlation factor in the alloy is not only a function of crystal symmetry, but also a function of the temperature and the composition of the alloy. The different behavior of the tracer diffusion coefficient in different temperature regions can be explained by the temperature dependence of the correlation factor, and the increased importance of the interstitials as the temperature decreases. Based on our proposed mechanism, we can predict the behavior of the tracer diffusion of cations in alloys of other compositions.<sup>14</sup>

### B. Relationship between $D$ and $D_i^*$

For pseudobinary systems, the relationship between  $D$  and  $D_i$  is the same as for a binary system and is described by the Darken equation. There can be driving forces in addition to chemical potential gradients and these forces may influence the cation interdiffusion in pseudobinary systems. The relationships between  $D_i$  and  $D_i^*$  and  $D$  and  $D_i^*$  are complicated by the diffusion of a common anion. The physical interpretations for the two limiting cases are given here. When doubly charged ions are the dominant diffusion species, the constraint of electroneutrality establishes a relationship between  $D_i$  and  $D_i^*$  which can be simplified depending on the relative diffusivities of the anions to the cations. If the anion moves relatively more rapidly than the cations, then the Hg and Cd move as if  $\text{HgTe}$  and  $\text{CdTe}$  neutral particles are diffusing and the electroneutrality and the stoichiometry are always maintained. The formula for interdiffusion is similar to the Darken-type equation for a binary system [Eq. (2)]. However, if Te moves more slowly than the faster diffusing cation, an electrical field will develop which will slow down the faster species and speed up the slower species: the cation diffusion fluxes are coupled. The intrinsic diffusion rate of two cations are equal and the interdiffusion rate will be dominated by the slower cation. When diffusion occurs at elevated temperatures where the material is intrinsic, an

electric field cannot be sustained, and the interdiffusion should proceed as a neutral case. If local defect equilibrium is not maintained, however, the conservation of lattice sites requires the flux of cations to be equal, and one obtains the same relationships for  $D$  and the  $D_i^*$  as for the case of the slowly moving anion (Te) in the extrinsic state. This is consistent with our experimental data. The lack of local equilibrium is also confirmed by marker experiments.<sup>25</sup>

### C. Interdiffusion mechanism

The interdiffusion may be analyzed using the relationship between  $D$  and  $D_i^*$  and the defect model established from the self-diffusion studies. The interdiffusion behavior for regions of different temperature and Hg overpressure is explained assuming that interdiffusion is dominated by the dual mechanism for the metal sublattice which proceeds in series with the fast Hg diffusion mechanism ( $V-I$  in parallel) slowed to maintain stoichiometry.

### IV. CONCLUSION

The component tracer diffusion coefficients for the MCT ( $x = 0.2$ ) pseudobinary system have been studied under well-defined diffusion ambients. The diffusion mechanism is established based on an analysis of the dependence of the self-diffusion coefficient on the Hg overpressure utilizing the principles of defect chemistry for MCT. In  $x = 0.2$  MCT, Te diffuses by interstitials, and moves more slowly than either metal species under all stoichiometric conditions. Both Hg and Cd diffuse by a dual, vacancy-interstitial mechanism. The existence of the multiple branches in the tracer concentration profile may be an indication of the existence of an ordered phase. Depending on the adjacent vacancy availability, Hg diffuses by either  $V-I$  in parallel or in series, with the faster mechanism dominating in the parallel diffusion path, and the slower mechanism dominating in the later, and the slower mechanism is presumed to be the only mechanism for Hg diffusion possible in the ordered phase due to the preferred configuration of the nearest neighbors on the metal sublattice. The concentration of Cd ( $x = 0.2$ ) is less than that of Hg, and there are fewer vacancies adjacent to Cd, therefore Cd moves dominantly by  $V-I$  in-series process. The two Cd diffusion coefficients might arise from the Cd diffusing in different networks, with the alloy being randomly distributed in one network and ordered in the other. The behavior of the cation tracer diffusion coefficients at lower temperatures ( $T < 450^\circ\text{C}$ ) is consistent with a more important role for the interstitial species.

The relationship between interdiffusion coefficient and the component intrinsic diffusion coefficients and tracer diffusion coefficients are derived for pseudobinary systems using  $\text{Hg}_{1-x}\text{Cd}_x\text{Te}$  as an example. The principles are applicable for all pseudobinary systems, and provide a basis for predicting low-temperature stability of junctions and superlattices from the diffusion data.

Based on the experimental results of self-diffusion, interdiffusion, and the equation interrelating the two for the MCT pseudobinary system, we propose a mechanism for interdiffusion. For MCT in the intrinsic region, the relatively slow diffusion rate of Te adds a constraint to the lattice

stoichiometry; to maintain stoichiometry, the diffusion fluxes of metals are coupled such that the slow diffusing metal species are rate limiting. The lower temperature behavior of interdiffusion is also consistent with an increased importance of interstitials.

#### ACKNOWLEDGMENTS

We thank Professor H. Schmalzried of the University of Hannover, Professor D. Shaw of Hull University, Dr. M. Brown of Grumman Corporate Research Center, and Dr. K. Zanio of Ford Aerospace and Communications Corporation for helpful discussions. This work is supported by DARPA through ONR, Contract No. N000-14-84K-0423.

- <sup>1</sup>A. V. Gorahkov, F. A. Zaitov, S. B. Shangin, G. M. Shalyapina, I. N. Petrov, and I. S. Asaturova, *Sov. Phys. Solid State* **26**, 10, 1787 (1984).  
<sup>2</sup>M. Brown and A. P. W. Willoughby, *J. Cryst. Growth* **59**, 27 (1982).  
<sup>3</sup>J. S. Chen, F. A. Kroger, and W. L. Ahlgren, in *Extended Abstract, U. S. Workshop on the Physics and Chemistry of Mercury Cadmium Telluride*, 1984, p. 109.  
<sup>4</sup>D. Shaw, *Philos. Mag. A* **53**, 5, 727 (1986).

- <sup>5</sup>J. Fleming and D. A. Stevenson, *J. Cryst. Growth* **82**, 621 (1987).  
<sup>6</sup>F. J. A. der Broeder, *Scr. Metall.* **3**, 321 (1969).  
<sup>7</sup>H. Rodot and J. Henoc, *C. R. Acad. Sci.* **256**, 1954 (1963).  
<sup>8</sup>F. Bailly, G. Cohen-Solal, and Y. Marfaing, *C. R. Acad. Sci.* **277**, 103 (1963).  
<sup>9</sup>F. Bailly, *C. R. Acad. Sci.* **262**, 635 (1966).  
<sup>10</sup>L. Svob and Y. Marfaing, *J. Appl. Phys.* **46**, 4251 (1975).  
<sup>11</sup>V. Leute, H. M. Schmidtke, W. Stratmann, and W. Winking, *Sov. Phys. Status Solidi A* **67**, 183 (1981).  
<sup>12</sup>K. Zanio and T. Massopust, *J. Electron. Mater.* **15**, 103 (1986).  
<sup>13</sup>J.-L. Staudenmann, R. D. Knox, and J.-P. Faurie, *J. Vac. Sci. Technol. A* **5**, 3161 (1987).  
<sup>14</sup>M. F. S. Tang and D. A. Stevenson (to be published).  
<sup>15</sup>M. F. S. Tang and D. A. Stevenson, *J. Vac. Sci. Technol. A* **5**, 3124 (1987).  
<sup>16</sup>M. F. S. Tang and D. A. Stevenson, *Appl. Phys. Lett.* **50**, 1272 (1987).  
<sup>17</sup>M. F. S. Tang and D. A. Stevenson (to be published).  
<sup>18</sup>G. B. Stephenson, *Scr. Metall.* **20**, 4, 465 (1986).  
<sup>19</sup>D. Zamir, K. Beshah, P. Becla, P. A. Wolff, R. G. Griffin *et al.*, *J. Vac. Sci. Technol. A* **6**, 2612 (1988) (these proceedings).  
<sup>20</sup>K. C. Haas and D. Vanderbilt, *J. Vac. Sci. Technol. A* **5**, 3019 (1987).  
<sup>21</sup>A. B. Chen and A. Sher, *Phys. Rev. B* **32**, 3695 (1985).  
<sup>22</sup>R. Kikuchi and H. Sato, *J. Chem. Phys.* **51**, 161 (1969).  
<sup>23</sup>R. Kikuchi, *J. Chem. Phys.* **53**, 2702 (1970).  
<sup>24</sup>H. Sato and R. Kikuchi, *Phys. Rev.* **28**, 2 (1983).  
<sup>25</sup>M. F. S. Tang and D. A. Stevenson (to be published).

## Appendix K:

### The Relationship Between Component Self-diffusion Coefficients and Interdiffusion Coefficient for Pseudobinary Systems

Department of Materials Science and Engineering

Mei-Fan Sung Tang and David A. Stevenson

Stanford University, Stanford, CA 94305

#### Abstract

A general relationship between the interdiffusion ( $D$ ) and component self-diffusion coefficients ( $D_i^*$ ) for pseudobinary systems is derived using the basic definitions of the diffusion coefficients and the constraints appropriate for pseudobinary systems. The  $\text{Hg}_{1-x}\text{Cd}_x\text{Te}$  (MCT) system is used as an example of such a system. The relationship between  $D$  and the intrinsic chemical diffusion coefficient ( $D_i$ ) is the same as for a binary system and is described by the Darken equation. In pseudobinary systems there are relevant diffusion driving forces in addition to neutral chemical potential gradients and the relationships between  $D_i$  and  $D_i^*$  and  $D$  and  $D_i^*$  are complicated by the diffusion of a common non-metal species. The physical meaning of the resulting equation is explained by the limiting behavior of the general equation. A Darken-type equation is obtained when there is only a neutral chemical potential gradient for metal diffusion species such as the case of a common non-metal species moving much faster than the metal species. However, when the common non-metal species diffuses more slowly than the metal components, the resulting interdiffusion coefficient is related to the  $D_i^*$  by a Nernst-Planck-type equation, since the electroneutrality and/or the conservation of lattice sites requires the flux of metals to be coupled. The slow movement of the common non-metal species plays the same role as lack of attainment of vacancy equilibrium in binary systems. Our experimental results of the  $D$  and  $D_i^*$  values in the MCT system support our theoretical analysis.



## I. Introduction

Interdiffusion in quasi-binary systems is of interest because it influences the sharpness of the junctions in epitaxial films and superlattices. Specific examples of such systems are HgTe/CdTe and GaAs/AlAs heterojunctions and superlattices. Interdiffusion has been analyzed for binary crystal systems<sup>1-4</sup> and amorphous systems<sup>4</sup> for the case of two species diffusing at different rates. However, there is no formal analysis of the corresponding diffusion in the pseudobinary systems, where two sublattices are involved<sup>5</sup>. The interdiffusion behavior in some systems, such as the HgTe/CdTe (MCT) system is further complicated by the existence of multiple mechanisms for the diffusion of the metal species. Without an explicit relationship between the interdiffusion and component self-diffusion for pseudobinary systems, one can not predict the stability of junctions in such systems from component diffusion data. In this paper, we derive a general relationship between the interdiffusion ( $D$ ) and component self-diffusion coefficients ( $D^*_i$ ) for pseudobinary systems using the basic definitions of the diffusion coefficients and the constraints appropriate for pseudobinary systems. We discuss the physical meaning of the resulting equation by examining the limiting behavior of the general equation, and compare with experimental results. Although we use the MCT system as a specific example, the results apply quite generally for all pseudobinary systems.

## II. Derivation

### A. Definitions of Diffusion Coefficients

Fick's first law defines a diffusion coefficient  $D$  for planar diffusion by the equation:

$$J_i = -D_i(\partial C_i / \partial x) \quad (1)$$

where  $J_i$  is the flux of the  $i$  species and  $C_i$  is the concentration. The fluxes and diffusion coefficients are measured with respect to driving forces and reference frames. The term "driving force" ( $F$ ) is related to any gradient that induces species to move in a preferred direction, rather than random motion.

The flux of species  $i$  is given by the velocity-concentration product:

$$J_i = C_i v_i F \quad (2)$$

where, in a linear theory,  $v_{iF}$  is proportional to the force, which arises from any potential gradient (The subscript F emphasizes the velocities arise from a driving force.) Since the partial molar Gibbs free energy ( $G_i$ ), the extended chemical potential, includes all of the possible potentials, the general equation for  $v_{iF}$  is expressed in terms of the gradient of  $G_i$ :

$$v_i = -\beta_i (\partial G_i / \partial x), \quad (3)$$

where  $\beta_i$  is the mobility, and

$$J_i = -L_i (\partial G_i / \partial x) \quad (4)$$

with

$$L_i = \beta_i C_i. \quad (5)$$

where  $L_i$  is designated as the phenomenological transport coefficient.

A simple application of equation (1) is for diffusion of a tracer isotope (in very dilute concentrations) in an otherwise homogeneous crystal with no driving forces. The only factor that produces a net flow of tracer atoms is the tracer concentration gradient. The corresponding diffusion coefficient is designated as  $D^*$  and is called the tracer diffusion coefficient.

A basic diffusion equation can be written as:

$$J_i = -D_i^* (\partial C_i / \partial x) + C_i v_{iF} \quad (6)$$

The term  $-D_i^* (\partial C_i / \partial x)$  arises because there are more atoms of the diffusing species on one side of the reference plane than on the other, but there is no preferred jump direction. This term is the same as the single term for tracer diffusion. The term  $C_i v_{iF}$  arises from the preferred jump direction of individual atoms due to a driving force which provides an average drift velocity  $v_{iF}$ .

The intrinsic diffusion coefficient, normally designated as  $D_i$ , is the diffusion coefficient arising from driving forces which are proportional to the concentration gradient. One such driving force arises from a gradient in the mixing enthalpy and the excess entropy in a nonideal solid solution. In this case,  $D_i$  is equal to  $D_i^*$  times a thermodynamic factor  $[1 + (\partial \ln \gamma_i / \partial \ln C_i)]$ . This relation is obtained from the basic definition of the chemical potential of the species (Eq. 4), and the basic diffusion equation (6). The intrinsic diffusion coefficient corresponds to the lattice plane reference frame. The diffusion coefficients with

the same driving force but referred to any reference frame different from the lattice planes are called chemical diffusion coefficients, even when the driving force includes other possible forces.

When two species move in opposite directions of respective chemical potential gradients, the two species intermix, with the rate of mixing dependent on the diffusion rates of both species. When two species interdiffuse with unequal intrinsic diffusion coefficients, there is a net atom flux across any lattice plane in the diffusion zone causing the crystal to swell on one side of the diffusion plane and shrink on the other side. Each lattice plane in the diffusion zone thus acquires a velocity  $v_k$  with respect to the laboratory frame (L), which is a reference plane fixed at one end of the crystal under conditions that no interdiffusion occurs at the end of crystal (semi-infinite boundary conditions).

The flux of species i measured with respect to L,  ${}_L J_i$ , is related to the flux measured with respect to the lattice in the diffusion zone,  $J_i$ , by the following expression:

$${}_L J_i = J_i + C_i v_k \quad (7)$$

From the definition of the intrinsic diffusion coefficient, equation (7) can be written as:

$${}_L J_i = -D_i (\partial C_i / \partial x) + C_i v_k \quad (8)$$

The interdiffusion coefficient is defined as a chemical diffusion coefficient referred to the L frame:

$${}_L J_i = -D (\partial C_i / \partial x) \quad (9)$$

The interdiffusion coefficients are in general different from the intrinsic diffusion coefficients.

#### B. The relationship between D and $D^*_i$

A relationship between the two measurable quantities, D and  $D^*_i$ , is derived through relationships to the intrinsic diffusion coefficients ( $D_i$ ). In the following section,  $D_i$  will be designated as the intrinsic diffusion coefficient only.

##### (a) The relationship between $D_i$ and $D^*_i$

The following relationship is obtained from the basic diffusion equations and the definition of diffusion coefficients.

$$D^*_i = L_i RT / C_i \quad (10)$$

This relationship is generally valid for all driving forces. On the other hand, the relationship between  $D_i$  and  $D_i^*$ , given in Eq.(11)

$$D_i^* = D_i (1 + \partial \ln \gamma_i / \partial \ln C_i)^{-1} \quad (11)$$

is valid only for the regular neutral chemical potential gradients. And

$$\partial \ln \gamma_i / \partial \ln C_i = \partial \ln \gamma_i / \partial \ln N_i$$

where  $N_i$  is the mole fraction of species  $i$ , under the constant molar volume condition.

(b) The relationship between  $D$  and  $D_i$

(i) For a binary system, the "Darken equation" relates  $D$  and  $D_i$  as follows:

$$D = (N_A D_B + N_B D_A) \quad (12)$$

This can be derived from the flux equations for A and B with the following constraints : conservation of atoms,  $L^J_A + L^J_B = 0$ ;  $N_A + N_B = 1$ ; and  $(\partial N_A / \partial x) = - (\partial N_B / \partial x)$ .

(ii) For a pseudobinary system such as  $Hg_{1-X}Cd_XTe$ , where  $X = N_j$ , is the mole fraction of CdTe in 1 mole of  $Hg_{1-X}Cd_XTe$  and

$$N_{Hg} + N_{Cd} = N_{Te} = 1, N_{Hg} = N_{HgTe} \text{ and } N_{Cd} = N_{CdTe}$$

The Darken equation relating  $D$  to  $D_i$ ,  $D = (N_{Hg} D_{Cd} + N_{Cd} D_{Hg})$ , can be derived as follows. The interdiffusion coefficient corresponding to the diffusion flux equation is referenced to the laboratory frame:

$$L^J_{Hg} = - L^{D_{Hg}} (\partial C_{Hg} / \partial x)$$

where, according to the above definitions,  $L^{D_{Hg}}$  is the interdiffusion coefficient ( $D$ ).

By the conservation of lattice sites, the net flux of diffusing species is zero everywhere in the crystal, with the fluxes referenced to the lattice frame ( $l$ ), which is the appropriate reference frame for intrinsic diffusion coefficients:

$$l^J_{Hg} + l^J_{Cd} + l^J_{Te} = 0 \quad (13)$$

Selecting the common anion as the reference, then the lattice velocity  $v_l$  can be written as

$$v_l = l^J_{Te} V_m \quad (14)$$

where  $V_m$  is the molar volume and

$$L^J_i = l^J_i + C_i v_l \quad (15)$$

An expression for the Hg flux is obtained by combining (13), (14) and (15):

$$L^J_{Hg} = - D_{Hg} (\partial C_{Hg} / \partial x) + C_{Hg} (D_{Hg} - D_{Cd}) (\partial C_{Hg} / \partial x) V_m$$

$$= [(N_{\text{Hg}}-1) D_{\text{Hg}} - N_{\text{Hg}} D_{\text{Cd}}] (\partial C_{\text{Hg}}/\partial x) \quad (16)$$

Since  $C_{\text{Hg}} V_m = N_{\text{Hg}}$  and  $N_{\text{Hg}} + N_{\text{Cd}} = 1$

$$\begin{aligned} L J_{\text{Hg}} &= -[N_{\text{Cd}} D_{\text{Hg}} + N_{\text{Hg}} D_{\text{Cd}}] \partial C_{\text{Hg}}/\partial x \\ &= -D \partial C_{\text{Hg}}/\partial x \end{aligned}$$

$$D = [N_{\text{Cd}} D_{\text{Hg}} + N_{\text{Hg}} D_{\text{Cd}}] \quad (17)$$

Therefore, the interdiffusion coefficient and the metal intrinsic diffusion coefficients are related by the Darken equation when the anion sublattice is chosen as the reference.

(c) The relationship between  $D$  and  $D_i^*$

(i) For a binary (AB) system with only chemical potential gradients, a Darken type equation is obtained by combining the Gibbs - Duhem Equation for binary systems ( $N_A d\mu_A + N_B d\mu_B = 0$ ) with the relationship between  $D_i$  and  $D_i^*$ , and the Darken Eq.(Eq.12)

$$\begin{aligned} D &= (N_A D_B + N_B D_A) \\ &= (N_A D_B^* + N_B D_A^*) (1 + \partial \ln \gamma_A / \partial \ln N_A) \end{aligned} \quad (18)$$

with the quantity  $(1 + \partial \ln \gamma_A / \partial \ln N_A) = (1 + \partial \ln \gamma_B / \partial \ln N_B)$ ,<sup>1</sup> designated as the thermodynamic factor ([T.F.]). Equation (18) is usually called the Darken equation. In order to differentiate other types of relationships between  $D$  and  $D_i^*$ , we refer to Eq.(18) as a "Darken- type equation", and use "Darken equation" to designate Eq.(12) which describes the relationship between  $D$  and  $D_i$ .

If two ionic species of the same charge interdiffuse with different rates, there is an initial transient period during which a diffusion potential develops, which establishes a zero net ion flux. In this case the driving force for the preferred motion can be shown to be proportional to the concentration gradient. One can derive the following relationship between  $D_i$  and  $D^*$  from the fundamental diffusion equations and definitions:

$D_A = (D_A^* D_B^*) / (N_A D_A^* + N_B D_B^*)$ , and interdiffusion coefficients equal to the intrinsic diffusion coefficient of each ions:

$$D = D_A = D_B = (D_A^* D_B^*) / (N_A D_A^* + N_B D_B^*) \quad (19)$$

This equation is a Nernst-Planck type of equation<sup>6</sup>.

(ii) We derive the relevant relationship between diffusion coefficients for pseudobinary systems using MCT as an example. Depending on the relative mobility of the common atom

(such as Te in HgTe-CdTe), there may be additional constraints of electroneutrality (for charged species) along with a Gibbs-Duhem equation of a different form from that for a binary system. We, therefore, derive the relationship between  $D_i$  and  $D^*_i$  through the relationship between  $L_i$  and  $D^*_i$  (Eq.10) which is generally applicable and then relate  $D$  and  $D^*_i$  with the Darken equation. This is presented in the following steps:

1<sup>0</sup>: The Gibbs -Duhem Eqn.(G. D. E.) for a pseudobinary system can be written as:

$$C_{\text{HgTe}} d\mu_{\text{HgTe}} + C_{\text{CdTe}} d\mu_{\text{CdTe}} = 0 \quad (20)$$

which is equivalent to

$$C_{\text{Hg}} d\mu_{\text{HgTe}} + C_{\text{Cd}} d\mu_{\text{CdTe}} = 0 \quad (21)$$

Since  $N_{\text{HgTe}} + N_{\text{CdTe}} = 1$ , we obtain:

$$\partial \ln \gamma_{\text{HgTe}} / \partial \ln N_{\text{HgTe}} = \partial \ln \gamma_{\text{CdTe}} / \partial \ln N_{\text{CdTe}} \quad (22)$$

2<sup>0</sup>: If the major diffusing species are charged species (e.g. doubly ionized ions), then the flux Eqs. for all the components are:

$$J_i = -L_i (\partial \eta_i / \partial x) \quad (i=\text{Hg}, \text{Cd}, \text{Te})$$

where  $\eta_i$  is the electrochemical potential,  $\eta_i = \mu_i + q_i F_a \phi$ ,  $q_i$  is the charge on the diffusing species,  $F_a$  is the Faraday constant, and  $\phi$  is the electric field.

3<sup>0</sup>: The electroneutrality condition (E. N.C.) requires that  $\sum q_i J_i = 0$ . Combining all the fluxes equations in 2<sup>0</sup> with the electroneutrality equations (E. N. E.) leads to the following:

$$m_{\text{Hg}} (\partial \eta_{\text{Hg}}^{+2} / \partial x) + m_{\text{Cd}} (\partial \eta_{\text{Cd}}^{+2} / \partial x) - m_{\text{Te}} (\partial \eta_{\text{Te}}^{-2} / \partial x) = 0 \quad (23)$$

where we define  $m_i = L_i / \sum L_i$  as the relative transport coefficient, with  $\sum m_i = 1$ .

$$4^0: \text{Hg}^{+2} + \text{Te}^{-2} = \text{HgTe} ; \quad d\mu_{\text{HgTe}} = d\mu_{\text{Hg}}^{+2} + d\mu_{\text{Te}}^{-2}$$

$$\text{Cd}^{+2} + \text{Te}^{-2} = \text{CdTe} ; \quad d\mu_{\text{CdTe}} = d\mu_{\text{Cd}}^{+2} + d\mu_{\text{Te}}^{-2}$$

$$5^0: d\mu_{\text{HgTe}} = d\mu_{\text{Hg}}^{+2} + (2F_a \phi) + d\mu_{\text{Te}}^{-2} + (-2)(F_a \phi)$$

$$= d\eta_{\text{Hg}}^{+2} + d\eta_{\text{Te}}^{-2}, \text{ and similarly}$$

$$d\mu_{\text{CdTe}} = d\eta_{\text{Cd}}^{+2} + d\eta_{\text{Te}}^{-2}$$

6<sup>o</sup>: Combining 5<sup>o</sup> with Eq.(21) and 4<sup>o</sup> :

$$\partial \eta_{\text{Hg}}^{+2} / \partial x = [m_{\text{Cd}}(C_{\text{Te}}/C_{\text{Cd}}) + m_{\text{Te}}] \partial \mu_{\text{HgTe}} / \partial x \quad (24)$$

7<sup>o</sup>: For a  $\text{Hg}_{1-x}\text{Cd}_x\text{Te}$  solid solution :

$$\begin{aligned} \partial \mu_{\text{HgTe}} / \partial x &= RT \partial (\ln \gamma_{\text{HgTe}} N_{\text{HgTe}}) / \partial x \\ &= RT [\text{T.F.}] (\partial C_{\text{Hg}} / \partial x) / C_{\text{Hg}} \end{aligned} \quad (25)$$

with the thermodynamic factor ([T.F.]) defined as :

$$\begin{aligned} [\text{T.F.}] &= 1 + (\partial \ln \gamma_{\text{HgTe}} / \partial \ln N_{\text{HgTe}}) \\ &= 1 + (\partial \ln \gamma_{\text{CdTe}} / \partial \ln N_{\text{CdTe}}), \text{ according to Eq.(22)} \end{aligned} \quad (26)$$

8<sup>o</sup>: Combining (24) with (25), and substituting into the flux Eqs. in 2<sup>o</sup>

$$\begin{aligned} J_{\text{Hg}} &= -L_{\text{Hg}} \partial \eta_{\text{Hg}}^{+2} / \partial x \\ &= -RT [m_{\text{Cd}} (L_{\text{Hg}}/C_{\text{Hg}}) (C_{\text{Te}}/C_{\text{Cd}}) + m_{\text{Te}} (L_{\text{Hg}}/C_{\text{Hg}})] [\text{T.F.}] \partial C_{\text{Hg}} / \partial x \\ &= -D_{\text{Hg}} (\partial C_{\text{Hg}} / \partial x) \end{aligned} \quad (27)$$

According to the definition,  $D_{\text{Hg}}$  is the intrinsic diffusion coefficient.

$$9^{\circ}: D_{\text{Hg}} = RT (L_{\text{Hg}}/C_{\text{Hg}}) [m_{\text{Cd}} (C_{\text{Te}}/C_{\text{Cd}}) + m_{\text{Te}}] [\text{T.F.}]$$

Since  $m_{\text{Te}} = 1 - m_{\text{Hg}} - m_{\text{Cd}}$  and  $C_{\text{Te}} - C_{\text{Cd}} = C_{\text{Hg}}$ :

$$D_{\text{Hg}} = RT L_{\text{Hg}} [ (1/C_{\text{Hg}}) + (m_{\text{Cd}}/C_{\text{Cd}} - m_{\text{Hg}}/C_{\text{Hg}}) ] [\text{T.F.}] \quad (28)$$

$$\text{Similarly, } D_{\text{Cd}} = RT L_{\text{Cd}} [ (1/C_{\text{Cd}}) + (m_{\text{Hg}}/C_{\text{Hg}} - m_{\text{Cd}}/C_{\text{Cd}}) ] [\text{T.F.}] \quad (29)$$

10<sup>o</sup>: Since Eq.(10),  $L_i = D^*_i C_i / RT$ , is valid in general

$$D_{\text{Hg}} = D^*_{\text{Hg}} [1 + m_{\text{Cd}}(C_{\text{Hg}}/C_{\text{Cd}}) - m_{\text{Hg}}] [\text{T.F.}] \quad (30)$$

$$D_{\text{Cd}} = D^*_{\text{Cd}} [1 + m_{\text{Hg}}(C_{\text{Cd}}/C_{\text{Hg}}) - m_{\text{Cd}}] [\text{T.F.}] \quad (31)$$

11<sup>o</sup>: Substituting (Eq.30) into (Eq.17):  $D = (C_{\text{Hg}} D_{\text{Cd}} + C_{\text{Cd}} D_{\text{Hg}}) V_m$

$$\begin{aligned} D &= \{ C_{\text{Cd}} D^*_{\text{Hg}} [1 + m_{\text{Cd}}(C_{\text{Hg}}/C_{\text{Cd}}) - m_{\text{Hg}}] + \\ &\quad C_{\text{Hg}} D^*_{\text{Cd}} [1 + m_{\text{Hg}}(C_{\text{Cd}}/C_{\text{Hg}}) - m_{\text{Cd}}] \} [\text{T.F.}] V_m \end{aligned}$$

$$= [C_{Cd} D^*_{Hg} + C_{Hg} D^*_{Cd} + D^*_{Hg} m_{Cd} C_{Hg} - D^*_{Hg} C_{Cd} m_{Hg} + D^*_{Cd} C_{Cd} m_{Hg} - D^*_{Cd} C_{Hg} m_{Cd}] [T.F.] V_m \quad (32)$$

12<sup>o</sup>: Using  $X = C_{CdTe} V_m$  and  $C_{Te} V_m = (C_{CdTe} + C_{HgTe}) V_m = 1$  with

$1-X = C_{HgTe} V_m$ , (32) becomes:

$$D = [X D^*_{Hg} + (1-X) D^*_{Cd} + (D^*_{Hg} / \Sigma L_i) (L_{Cd} C_{Hg} - L_{Hg} C_{Cd}) + (D^*_{Cd} / \Sigma L_i) (L_{Hg} C_{Cd} - L_{Cd} C_{Hg})] [T.F.] \\ = [X D^*_{Hg} + (1-X) D^*_{Cd} - X(1-X) (D^*_{Hg} - D^*_{Cd})^2] [T.F.] (1/ V_m RT \Sigma L_i) \quad (33)$$

13<sup>o</sup>: With  $RT V_m \Sigma L_i = V_m RT (L_{Hg} + L_{Cd} + L_{Te})$

$$= V_m RT (D^*_{Hg} C_{Hg} / RT + D^*_{Cd} C_{Cd} / RT + D^*_{Te} C_{Te} / RT) \\ = (1-X) D^*_{Hg} + X D^*_{Cd} + D^*_{Te} \quad (34)$$

then,

$$D = (D^*_{Hg} D^*_{Cd} + D^*_{Te} [X D^*_{Hg} + (1-X) D^*_{Cd}]) [T.F.] / [(1-X) D^*_{Hg} + X D^*_{Cd} + D^*_{Te}] \quad (35)$$

### III. Discussion

The relationship between  $D$  and  $D^*_i$ , equation (35), is derived for a pseudobinary system using MCT as an example. We assume that the mobile species are ions, and derive the relevant equations for extrinsic conditions. In this section, we discuss the results by analyzing the limiting forms of the equation and the physical interpretation. We also consider the relevant equations for intrinsic conditions.

(a) When the major diffusion species are ionized

Equation (35) is for a pseudobinary system involving the transport of ionic species with the same electric charge and is complicated by simultaneous anion diffusion. However, the equation can be simplified to two limiting forms depending on the relative diffusivity of the cations and anions.



(i) Case 1: Anions diffuse much more slowly than cations:

If  $D_{Te}^*$  is smaller than either  $D_{Cd}^*$  or  $D_{Hg}^*$ , Eq.(35) can be simplified by neglecting  $D_{Te}^*$ , or the electroneutrality equation (23) may be simplified as follows:

$$m_{Hg} \partial \eta_{Hg}^{+2} / \partial x + m_{Cd} \partial \eta_{Cd}^{+2} / \partial x = 0 \quad (36)$$

By algebraic rearrangement, we obtain the following expression:

$$D = \{ D_{Cd}^* D_{Hg}^* / [X D_{Cd}^* + (1-X) D_{Hg}^*] \} [T.F.] \quad (37)$$

and

$$D = D_{Hg} = D_{Cd}$$

The interdiffusion rate is dominated by the slower cation, and it is a Nernst-Planck type of equation.

(ii) Case 2: The anion moves faster than both cations:

If  $D_{Te}^*$  is larger than  $D_{Cd}^*$  and  $D_{Hg}^*$ , then we obtain a Darken-type of equation either directly from Eq.(35), or using  $m_{Te} \approx 1$  in the derivation:

$$D_{Hg} = D_{Hg}^* [T.F.]$$

$$D_{Cd} = D_{Cd}^* [T.F.]$$

and

$$D = [(1-X) D_{Cd}^* + X D_{Hg}^*] [T.F.] \quad (38)$$

When the diffusion species are ionized species with the same charge, it follows from the above discussion that if the common anion moves more slowly than either cation, an electric field is built up in the same manner that a diffusion potential is established for a single binary case. A force arises to balance the diffusion of the two ions and the diffusion flux of the cations are coupled. This is equivalent to stating that the electroneutrality condition requires that  $|j_{Hg}| = |j_{Cd}|$  and the interdiffusion rate is dominated by the slower cation. If the anion moves faster than either cation, the interdiffusion coefficient is an algebraic average of the two cations, similar to diffusion in a binary system in the presence of neutral chemical potential gradient only; the chemical diffusion coefficient of each cation is the same value as the tracer diffusion coefficient times the [T.F.]. The anion can always keep pace with the cations and the electroneutrality condition can be accommodated even if the cation species diffuse at different rates. One may consider this case as diffusion of HgTe and CdTe species, and the Gibbs-Duhem equation can be written for HgTe-CdTe binary system. The

resulting interdiffusion equation is therefore the Darken-type of equation with a thermodynamic factor expressed in terms of a binary (Eq.26).

(b) Interdiffusion under intrinsic electronic conditions

At diffusion temperatures of interest,  $\text{Hg}_{1-X}\text{Cd}_X\text{Te}$  is intrinsic, and thermally generated electrons and holes are the dominant electrical species. The electric field, which arises from the different diffusivity of the cations, is not sustained, and the electroneutrality condition is no longer a criterion and neutral chemical potential gradients are the driving forces. A general relationship can be derived based on the same principles except that instead of the electroneutrality constraint requiring that the total flux of species must be zero, one may invoke the conservation of lattice sites as a constraint. The resulting equation is:

$$D = \{D^*_{\text{Hg}}D^*_{\text{Cd}} - D^*_{\text{Te}}[XD^*_{\text{Hg}} + (1-X)D^*_{\text{Cd}}][T.F.]\} / [(1-X)D^*_{\text{Hg}} + XD^*_{\text{Cd}} - D^*_{\text{Te}}] \quad (39)$$

The limiting forms of this equation for relative values of diffusion rates of metal to non-metal species provides a basis for a physical interpretation of this equation.

We obtain the same limiting form for the Eq.(39); a Nernst-Planck type when  $D^*_{\text{Te}} \ll D^*_{\text{Hg}}$  and  $D^*_{\text{Cd}}$ , and a Darken-type when  $D^*_{\text{Te}} \gg D^*_{\text{Hg}}$  and  $D^*_{\text{Cd}}$ . Since electric field is not sustained for intrinsic electronic disorder, it would appear to be that the Te diffusion rate should not have influence on the interdiffusion rate, and the diffusion behavior should be like a pure binary system with a chemical potential gradient, with a Darken-type equation governing. However, for a binary system, there is an implicit assumption in the development of the Darken equation, that there is the internal thermodynamic equilibrium. The local defects (vacancies)- which are responsible for diffusion- attain local equilibrium, and these defects are produced or removed at the sites of the repeatable growth. A different approach has been taken by Stephenson<sup>4</sup> to show that if the local defect is not achieved, the resultant interdiffusion would be the Nernst-Planck type, and the derivation for binary system involves the third component, the vacancies, in the flux equations. In pseudobinary systems, if we require the net flux to be zero everywhere, it is identical to considering local defect equilibrium for binary systems. The common non-metal lattice in the pseudobinary systems plays the same role as the local defects in binary systems. When the non-metal

moves much more slowly than the metal species, the constraint of conservation of lattice sites has the same effect as failure to attain the local defect equilibrium in the binary systems; this requires the flux of two metals to be coupled and a Nernst-Planck type equation is the result.

In a previous paper<sup>7</sup>, we have shown that Hg diffuses simultaneously by two mechanisms in MCT. Hg diffuses much faster than Cd, and Te diffuses more slowly than either of the two metal species. In the intrinsic region, the tracer diffusion coefficients of the fast component of Hg and Cd, which are the true self-diffusion coefficients, can be related to the interdiffusion coefficient by the Nernst-Planck type equation only.

#### IV. Summary

The relationships between the interdiffusion coefficient and the component intrinsic diffusion coefficients and the tracer diffusion coefficients are derived for pseudobinary systems, using  $\text{Hg}_{1-x}\text{Cd}_x\text{Te}$  as an example. The relationship between  $D$  and  $D_i$  is described by the Darken equation, and is the same as for a binary system. Driving forces other than neutral chemical potential gradients influence the cation interdiffusion in pseudobinary systems; the relationships between  $D_i$  and  $D^*_i$  and  $D$  and  $D^*_i$  are complicated by the diffusion of a common anion. When doubly charged ions are the dominant diffusion species, the constraint of electroneutrality establishes a relationship between  $D_i$  and  $D^*_i$  which can be simplified depending on the relative diffusivities of the anions to the cations. If the anion moves relatively faster than the cations, then the Hg and Cd move as if HgTe and CdTe neutral particles are diffusing and the electroneutrality and the stoichiometry are always maintained, and the formula for interdiffusion is the Darken-type equation. However, if Te moves more slowly than the faster diffusing cation, there will be an electrical field built up which will slow down the faster species; the cation diffusion fluxes are coupled. The intrinsic diffusion rates of two cations are equal and the interdiffusion rate will be dominated by the slower cation. When diffusion occurs at temperatures where the material is intrinsic, an electric field is not sustained, and one might expect the interdiffusion behavior to be governed by the regular binary interdiffusion with only a chemical potential gradient. However, a Darken-type equation does not apply for a ternary system when the common

non-metal species diffuses more slowly than the metals since the conservation of lattice sites requires the flux of metals to be coupled. The resulting interdiffusion coefficient is related to the  $D^*_i$  by a Nernst-Planck-type relation. The slow movement of the common non-metal species plays the same role as lack of attainment of vacancy equilibrium in binary systems. All the limiting forms for pseudobinary systems are governed by the same relation as for binary systems, except for a different thermodynamic factor which arises from a different form of the Gibbs-Duhem Equation.

#### V. Acknowledgements

We thank Professors H. Schmalzreid of the University of Hannover and D.M. Barnett of Stanford University, and Dr. G.B. Stephenson of IBM Thomas J. Watson Research Center for their helpful discussions. This work is supported by DARPA through ONR, Contract No. N000-14-84K-0423.

#### VI. References

1. L.S. Darken, Trans. Am. Inst. Min, Met. Eng. 175, 184, (1948)
2. W. Nernst, Z. Phys. Chem. 2, 613, (1888)
3. M. Planck, Ann. Physik (Wiedemann), 39, 161, (1890)
4. G.B. Stephenson, Scripta Metallurgica. 20, 465, (1986)
5. H. Schmalzreid, Monographs in Modern Chemistry, Vol. 12, Solid State Reactions (1981)
6. J. R. Manning, Diffusion Kinetics for Atoms in Crystal, (1968)
7. M-F. S. Tang and D. A. Stevenson, J. Vac. Sci. Technol. A6(4), 2650, (1988)